1969

The limitations of infrared image detectors in astronomy

H. J. Fraser
Wollongong University College

THE UNIVERSITY OF NEW SOUTH WALES

WOLLONGONG UNIVERSITY COLLEGE

THE LIMITATIONS OF INFRARED IMAGE DETECTORS IN ASTRONOMY

THESIS PRESENTED FOR THE DEGREE OF MASTER OF SCIENCE

H.J. Fraser

Department of Physics

1969

898379

CONTENTS.

LITERATURE SURVEY.

This literature survey has been added to the thesis on the recommendation of the examiners.

---

1. Comparison of image tubes with the photographic plate in the visible region.

The photographic plate has long been the main tool used for astronomical observations despite its relatively low detection efficiency and nonlinearity.

The relative advantages of speed and linearity which image tubes, based upon the photoelectric effect, possess over photographic plates, were first pointed out by Lallemand (1936). Since then much effort has been expended in the development and applications of a variety of image tubes.

Comparison of image tubes with the photographic plate is given by Livingstone (1967). Whereas the nonlinearity of the photographic process is a severe limitation, the photoelectric effect is linear over a range of the order of 10^{14} which allows accurate calibration and precise photometry with image tubes. A comparison of speed may be made by noting that the detective quantum efficiency, as defined by Jones (1959), of Kodak 103a-0 emulsion is

0.005 (Marchant and Millikan (1965)), whereas the responsive quantum efficiency of an S20 photocathode at 400 n.m. is 0.45 (Livingstone (1967)). Image tubes are in direct competition with the photographic plate in the visible region, and Livingstone reaches the conclusion that photography gives higher positional accuracy and long term geometrical stability when compared with image tubes, although the former is wasteful of light and otherwise imperfect for photometric purposes. Image tubes are used mainly where photometry or speed with moderate resolution is required, and greater distortion of the image can be tolerated.

2. Types of image tubes and some illustrative applications.

The Lallemand tube is considered first because it is founded upon the most simple physical processes. This tube consists of a photocathode from which electrons are accelerated to about 40kV and focussed on a photographic plate situated within the same vacuum chamber. This type of tube was used by Walker et. al.(1965) to obtain better time resolution of spectrum variables in a study of A E Aquarii.

The Lallemand tube has a wide linear range between input light intensity and optical density of the emulsion, and Aller and Walker (1965) make full use of this photometric capability in a study of line intensities in planetary nebulae.

Another type of image tube is the R.C.A. cascade tube which was developed specifically for astronomical purposes (Baum et. al. (1964)). This tube accelerates electrons from a photocathode through an accelerating potential of 10 kV to strike a phosphor-photocathode sandwich membrane. Photo-electrons from the second photocathode are accelerated through a similar potential difference to strike a P11 phosphor output screen. This tube has been used by Wilson et. al. (1965) for relative photometric measurements at 670 n.m. in a large number of stars. In this application it has a speed advantage over photography.

A third type of image tube is the Transmission Secondary Emission (T.S.E.) tube. Tube type PD829D made by English Electric is a T.S.E. device, and this tube is described by Ruggles and Slark (1964). Electrons from the photocathode of the PD829D are accelerated through a potential difference of 4.5 kV to strike a thin potassium chloride surface supported by an electron transparent aluminium membrane. Each primary electron produces about five secondary electrons which are accelerated through a potential difference of 4.5 kV to the next membrane. Five such dynodes produce an electron gain of about 3000. The final image appears in the fluorescense of a P11 phosphor. Total light gain with an overall accelerating potential of 36 kV is 5×10^5, which

is sufficient for scintillations due to individual photoelectrons to be easily recorded. This tube is most useful at very low light levels, but it suffers from a light dependent background. This background appears to be caused by light scattering and optical feedback within the tube (Iredale et. al. (1964)).

A distinct class of image tubes consists of the signal generating types of which the image orthicon, the image isocon, and the vidicon are representative.

Weimer (1960) gives a detailed review of these tubes. The first two of these are based upon a photocathode for the primary detection process. They do not appear to have any fundamental advantage over modern image tubes, which have the same type of photocathode, although the signal generating tubes have the advantage of electrical signal output for remote transmission where this is required.

The image orthicon has been used for rapid but low precision photometry of stars (Barkos and Rymer (1964), Livingstone (1967)).

The visible spectrum vidicon was used in unmanned space flights (Malling and Allen (1966), Allen (1966)) because of its simple rugged construction and because it is relatively unaffected by internal scattered light and stray magnetic fields.

3. Imaging devices for the infra-red region, potentialities and applications.

The potentialities and applications of the vidicon, image tubes with S1 cathodes, and photography for infra-red astronomy are discussed in this section. The vidicon is based upon photoconductivity for its primary detection process, and this fact suggests that the vidicon may have a fundamental advantage over the photographic plate or image tubes with S1 cathodes, particularly in the infra-red, because from a fundamental viewpoint the detection efficiency of a photoconductor is much higher than that of a photoemitter in the infra-red region (refer Rose (1963)). Furthermore, Sommers (1963) shows that there is a formal possibility of obtaining photoconductive gain in a vidicon, although no such gain has yet been achieved in commercial vidicons.

The potentialities of the vidicon for astronomical use are discussed by Gebel (1962), and his paper emphasises that amplifier noise is the most significant limitation to the vidicon. Gebel gives little specific data for operation in the infra-red region, and the present author considers that the approximations he has made in estimating circuit noise are invalid. Because of the importance of circuit noise in the overall performance of the vidicon this thesis examines associated valve and transistor circuits in some detail to determine the practical limitations of the vidicon with

specific circuits and operating conditions.

In so far as infra-red astronomical applications are concerned, experience to date has shown that the image tubes with S1 cathodes are far superior in speed to the infra-red plate (see for example Fredrick (1961), Firor and Zirin (1962), Zirin and Dietz (1963)). The infra-red vidicon has been used to advantage by Kuprevich (1963) for observations of the moon at 1600 n.m., an application where it is not in competition with either the photographic plate or the image tubes. However, there appears to be no other reported application of the infra-red vidicon to astronomical work.

The S1 photocathode is useful to about 1200 n.m., whereas the infra-red vidicon is sensitive out to 2000 n.m., so that if the infra-red vidicon is to be competitive with the S1 cathode, it should be so in the vicinity of 1100 n.m., which is within the useable spectrum for both devices.

Zirin and Dietz (1963) found that the 1083 n.m. line of He I yields unique information on the solar chromosphere. This application at 1083 n.m. is essentially one where low contrast scenes are involved and it is at a wavelength where the infra-red vidicon may be able to compete with the image tubes. For these reasons it is this application which is considered in this thesis.

The scene to be detected in this application is generally of low contrast (of the order of two per cent), and it is

found that, when there is sufficient light input to enable detection at this low contrast, the photon statistical noise is much greater than the thermal emission noise of practical image tubes (refer Ch. 4). This simplifies the discussion because the thermal emission noise may then be neglected.

Although this argument ignores spurious light flashes due to such factors as voltage breakdown and optical feedback within image tubes, it does allow comparison of devices on a more fundamental basis. The practical performance of image tubes is under constant development and improvement, so that it is important to make comparisons on the basis of fundamental limitations.

4. The vidicon and its spatial resolution compared with image tubes.

The vidicon was first introduced commercially in 1950 (Weimer et. al. (1950), (1951)), and further details of its operation and performance are given by Redington (1958) and by Weimer (1960). Infra-red vidicons have been reported by Morton and Forgue (1959), Heimann and Kunze (1962), and Hovi et. al. (1969).

Langmuir (1937) determined the limit of resolution due to low velocity scanning beams which is also applicable to the vidicon, and he shows that the limit due to the finite dimensions of the beams alone should be greater than 10000 lines per inch. A more serious limitation of resolution is due to

the potential distribution of the target bending the scanning beam (see Weimer (1960)), and this gives a limit of the order of 600 to 1000 lines per inch.

Krittman (1963) and Lubszynski and Wardley (1963) also discuss the resolution of vidicons. Krittman's paper analyses the limit of resolution due to finite target thickness which causes deflection of the scanning beam .

Lubszynski and Wardley show that connecting a separate target mesh to a potential which is positive with respect to the wall anode decreases these beam bending effects and improves the resolution.

The resolution of the vidicons used in the present work was measured and found to be approximately 750 lines per inch at the target (see Ch. 4). In comparison the typical resolution of image tubes is also about 750 lines per inch, as reported by Ruggles and Slark (1964), Fredrick and Hall (1962), Randall (1966) and Emberson and Long (1969).

5. Image evaluation.

There has been a significant trend over the last decade to apply modulation transfer functions to the evaluation of imaging systems. One advantage of this technique is the ease in which modulation transfer functions of the elements of an imaging system may be combined to

obtain the modulation transfer function of the complete system. The concepts involved are treated by Fellgett and Linefoot (1955), Dunham (1960) and McGee (1961).
A characterisation and analysis of a complete facsimile system using modulation transfer functions is given by Rindfleisch and Willingham (1966) whose work has been used in this thesis to illustrate that an equivalent analysis can be made on the electrical signals and noise in the video output of a television camera.

The measurement of the real part of the modulation transfer function or the transfer modulation response on the video output channel of a television camera is described in Chapter 4 of the thesis. Although this measurement does not include the kinescope output, this is not considered a serious limitation because phosphor screens have beeen reported by McGee et. al. (1966) with typical resolutions of 2500 lines per inch, which is much greater than the resolution of the vidicon.

6. Vidicon Circuit Noise.

The main noise source of a vidicon camera is due to the electronic devices associated with the video amplifier, and it is necessary to be able to calculate the signal to noise ratio of various amplifier configurations under different operating conditions. These calculations are most easily accomplished by using Peterson's theorem (Montgomery (1952))

to obtain a uniform characterisation of noisy networks and by substituting the magnitude of the noise sources as given by North (1940) and Van der Ziel (1954) for the valve, and by Van der Ziel (1962) for the field effect transistor. This procedure is fully discussed in Chapter 2 of this thesis.

An early analysis of the signal to noise ratio of a television camera is given by DeVore and Iams (1940), and their results are directly applicable to the vidicon with a valve amplifier.

De Haan (1960) gives an equivalent expression for a valve amplifier. His paper also covers signal to noise ratios of other image devices due to photon statistical noise, as well as circuit device noise.

Elad and Nakamura (1967) showed that field effect transistors could be operated down to 78 K for silicon and 4 K for germanium with improved gain and reduced noise due to the lower temperature. It became obvious from this work that a significant improvement in signal to noise ratio could be obtained by using cooled field effect transistors (F.E.T.'s) instead of valves in the video amplifier. Elad and Nakamura (1967) demonstrated this improvement in amplifiers used with semiconductor gamma ray detectors with bandwidths of about 1 M Hz, but the present author is unaware of any published use of cooled F.E.T.'s in wide band vidicon cameras.

This topic is treated in this thesis by applying the general approach to the noise problem presented in Chapter 2.

BIBLIOGRAPHY FOR LITERATURE SURVEY.

Allen, J. 1966, Adv. Electronics Electron Phys. 22B, 849.

Aller, L.H. and Walker, M.F. 1965, Astrophys. J. 141, 1318

Bakos, G.A. and Rymer, K.R. 1964, Astron. J. 69, 531.

Baum, W.A., Hall, J.S., Marton, L.L. and Tuve, M.A. 1964, Cannegie Inst. Wash. Year Book (1955 - 1965).

De Haan, E.F. 1960, Adv. Electronics Electron Phys. (Academic Press) 12, 291.

Dunham, T.J., 1960, J. Opt. Soc. Aus. 50, 1129.

Elad, E. and Nakamura, M. 1967, University of California, Lawrence Radiation Lab. Report U.C.R.L.17818.

" " " " 1967, I.E.E.E. Transactions on Nuclear Science, N.S. 14, 1, 523.

Emberson, D.L. and Long, B.E. 1969, Adv. Electronics Electron Phys. (Academic Press), 28A, 119.

Fellgett, P.B. and Linefoot, E.H. 1955, Phil. Trans. A247, 369.

Firor, J. and Zirin, H. 1962, Astrophys. J. 135, 122.

Fredrick, L.W. 1961, Lowell Obs. Bull. 5, 149.

Fredrick, L.W. and Hall, J.S. 1962, Adv. Electronics Electron Phys. (Academic Press), 16, 403.

Gebel, R.K.H. , 1962, Adv. Electronics Electron Phys. (Academic Press), 16, 451.

Heimann and Kunze, 1962, Adv. Electronics Electron Phys. (Academic Press) 16, 217.

Hovi, H. Tsuji, S., and Kiucha, Y. 1969, Adv. Electronics Electron Phys. (Academic Press) 28A, 253.

Iredale, P., Hinder, G.W., and Ryden, D.J. 1964, I.E.E.E. Trans. Nucl. Sci. NS-11, 139.

Jones, R.C. 1959, Adv. Electronics Electron Phys. 11, 87.

Kapany, N.S. and Capellaro, D.F. 1961, J. Opt. Soc. Am. 51, 23.

Krittman, I.M. 1963. I.E.E.E. Trans. on Electron Devices ED10, 6, 404.

Kuprevich, N.F. 1963, Astron. Zh. 40, 889.

Lallemand, A. 1936, Compt. Rend. 203, 243.

Langmuir, D.B. 1937, Proc. I.R.E. 25, 977.

Livingstone, W.C. 1967, Adv. Electronics Electron Phys. (Academic Press) 23, 347.

Lubszynski, H.G. and Wardley, J. 1963, I.E.E. Conference Report Series No. 5.

McGee, J.D. 1961, Rept. Progr. Phys. 24. 169.

McGee, J.D., Airey, R.W. and Aslam, M. 1966, Adv. Electronics Electron Phys. (Academic Press) 22A, 571.

Malling, L.R. and Allen, J. 1966, Adv. Electronics Electron Phys. 22B, 835.

Marchant, J.C. and Millikan, A.G. 1965, J. Opt. Soc. Am. 55, 907.

Montgomery, H.C. 1952, Proc. I.R.E. 40, 1461.

Morton, G.A. and Forgue, S.V. 1959, Proc. I.R.E. 47, 1607.

North, D.O. 1940, R.C.A. Review, 4, 441.

Randall, R.P. 1966, Adv. Electronics Electron Phys. (Academic Press) 22A, 87.

Redington, R.W. 1958, J. Appl. Phys. 29, 189.

Rindfleisch, T. and Willingham, D. 1966, Adv. Electronics Electron Phys. (Academic Press), 22A, 341.

Rose, A. 1963, Concepts in Photoconductivity and Allied Problems (John Wiley).

Rothe, H. and Dalke, W. 1956, Proc. I.R.E. 44, 811.

Ruggles, P.C. and Slark , N.A. 1964, I.E.E.E. Trans. Nucl. Sci. NS-11, 100.

Sommers, H.J. 1963, J. Appl. Phys. 10, 2923.

Van der Ziel, A. 1954, Noise (Prentice-Hall).

Van der Ziel, A. 1962, Proc. I.R.E. 3, 461.

Walker, M.F. 1965, Sky and Telescope 29, 23.

Weimer, P.K. 1960, Adv. Electronics Electron Phys. 13, 387.

Weimer, P.K., Forgue, S.V. and Goodrich, R.R. 1950,
Electronics 23, 70.

Weimer, P.K., Forgue, S.V., and Goodrich, R.R. 1951,
R.C.A. Review 12, 306.

Wilson, O., Baum, W.A., Ford, W.K., and Purgathofer, A., 1965,
Publ. Astron. Soc. Pacific. 77, 359.

Zirin, H. and Dietz, R.D. 1963, Astrophys. J. 138, 664.

SUMMARY

This thesis describes an investigation into the limiting performance of infrared imaging detectors which are suitable for short exposure low contrast solar observations at 1083 nm. The investigation centres around the limiting performance of image tubes with S_1 cathodes and the limiting performance of the infrared vidicon.

A theoretical treatment is given which describes the limitations due to photon noise and circuit noise. Experimental measurements of the light equivalent noise input of an infrared vidicon, a visible spectrum vidicon and a single stage image converter are described. These experimental values are substituted into the expressions derived to predict the performance of the devices ; including the performance of the vidicon with cooled amplifiers and slow scanning speeds.

The results show that image tubes with S_1 cathodes are the more suitable devices although the light flux required by the vidicon can approach within a factor of ten the light flux required by image tubes for low contrast scenes if a cooled field effect transistor amplifier is used.

Chapter 1

INTRODUCTION

1.1 The Nature of the Problem

1.2 General Characterization of Imaging Systems

1.3 Outline of the Thesis

1.1 The Nature of the Problem

Imaging detectors which are sensitive in the infrared region are of great interest to astronomers. The limiting performance expected of these detectors is the subject of this thesis. The task of comparing the performance of imaging detectors is made difficult by the variation in the types of measurements required by astronomers and by the large number and complexity of available image tubes. Furthermore, such infrared devices are under continuous development.

Obviously there is no device which is best for all applications. Each practical device is a compromise between many factors, such as speed, resolution, image distortion, dynamic range (i.e. range of useful input signals), linearity etc. If an investigation of the relative merits of image devices is to be fruitful, it should be directed towards a particular application.

The application considered in this work is the observation with high spatial resolution of the infrared absorption line of wavelength 1083 nm arising from highly excited HeI in the Sun's chromosphere. Observations of this HeI infrared absorption line ($2^3S \rightarrow 2^3P$ transition) averaged over large areas of the solar chromosphere have shown the relative line depth (contrast) to be about one per cent. Hence there is a particular interest in imaging

devices suitable for observing low contrast objects in the infrared. There is no doubt that in plage regions, and elsewhere on the disc where temperatures are very high, the He 1083 nm line depth is much greater than one per cent. However, a great deal of valuable information (particularly as to the nature of "spicules") can be provided by an infrared image detector capable of matching the spatial resolution of the best solar telescopes (say 1 second of arc) for objects of low contrast of the order of two per cent.

Some such observations have been made with infrared-sensitive photographic film by Tandberg-Hanssen, Curtis and Watson (1959) and with image tubes based upon photoemission from an S_1 type cathode by Fisher (1964) and by Firor and Ziron (1962) who report a speed gain of 30 times over an infrared sensitive plate which was exposed for 30 minutes.

The properties required of the imaging detector for the application discussed above are high resolution, large dynamic range and fast response. These properties are desirable because modern solar telescopes have high real angle resolution, the scene contrast is generally small due to low absorption of the He 1083 nm line, and possible dynamic changes in He 1083 nm emission and in

atmospheric turbulence ("seeing conditions") necessitate fast speed of response.

It is convenient to divide image detectors suitable for astronomical observations in the infrared region into three categories, depending upon the basic mechanism of the initial detection process, as follows:-

(a) Direct infrared-sensitive photographic plate.

(b) Image tubes based upon the phenomenum of photo-conductivity.

(c) Image tubes based upon photo emission from an S_1 type cathode.

It is clear (see for example Firor and Zirin (1962)) that where speed of response is important the infrared photographic film cannot compete with S_1 type image tubes at 1083 nm. It remains to be seen which of the image tubes in either categories (b) and (c) can simultaneously best satisfy the requirements of high resolution, large dynamic range and fast response.

The vidicon is an image tube based upon photoconductivity (category (b) above) for the initial detection process and the potentialities of vidicons for astronomical use have been discussed by Gebel (1962). However, he gives little specific data for operation in the infrared region around 1083 nm and the present author considers

that the approximations made by Gebel in calculating vidicon circuit noise level are invalid. It is proposed to investigate the infrared-sensitive vidicon in greater detail in this thesis. It is also proposed to examine various types of amplifier which give better performance than the valve amplifier. The problem to be resolved is the determination, for the vidicon and for the image tube with S_1 cathode, of the amount of light flux required from the object to produce an acceptable image of a low contrast scene. The lower limit of contrast which can be detected by the vidicon is also to be determined.

This work relies heavily on many results of circuit and electronic device noise theory and therefore a comprehensive but concise account of this theory is given in Chapter 2. This general noise theory is presented to show how the limitations of vidicon performance depend upon the physical properties of the components of the amplifier and upon the operating temperature and it allows ready extension to other operating conditions not specifically treated in this thesis.

1.2 General Characterization of Imaging Systems

A complete imaging system may contain many complex elements, all of which degrade the image resolution in one way or another. For example, the optical telescope, image tube and the photographic plate each represent elements of a system which process the light signal from the object and finally present a degraded image to the eye.

It is desirable to formulate a unified treatment of the whole system such that resolution and signal to noise performance may be discussed in general terms without resorting to detailed description of any one device.

Such a formulation based upon linear system analysis has been given by Rindfleisch and Willingham (1966). These authors assume linearity, which means that the system must satisfy the principle of superposition; that is, the output response due to one input is independent of other inputs. More precisely a system is linear if, and only if

$$H(\alpha x_1 + \beta x_2) = \alpha H x_1 + \beta H x_2$$

where α, β are any constants,

x_1, x_2 are any input signals

and H is such that the relation $y = Hx$ means that y is

the response of the system to the input x. Obviously the type of system under discussion is nonlinear for large signals, but the assumption of linearity is valid for low contrast scenes.

The other assumption made is that a sine wave spatial input brightness distribution will result in a sine wave spatial output brightness distribution of the same spatial frequency. The output signal, S, may be expressed as an inverse Fourier transform:-

$$S = \alpha I_0 \int_{-\infty}^{\infty} dk_x \int_{-\infty}^{\infty} dk_y G(k_x,k_y) H(k_x,k_y) B_s(k_x,k_y)$$

where

$B_s(k_x,k_y)$ = Fourier transform of the spatially varying brightness distribution,

k_x,k_y = spatial frequency components,

G = transfer function of the system,

H = transfer function of the eye,

I_0 = uniform intensity level of output,

and α = gain of system for low spatial frequencies.

In this context, transfer function means the Fourier transform of the response to a unit impulse or Dirac delta function.

If the random brightness of the system (system noise) is evenly distributed over all spatial frequencies with a

constant mean square brightness N_o per unit spatial frequency then the r.m.s. brightness output distribution $N_{r.m.s.}$ is given by

$$N_{r.m.s.} = I_o \cdot N_o^{\frac{1}{2}} \cdot \left[\int_{-\infty}^{\infty} dk_x \int_{-\infty}^{\infty} H^2(k_x, k_y) dk_y \right]^{\frac{1}{2}}$$

From these relations the signal to r.m.s. noise ratio can be found and minimised by varying the spatial frequency response of the system or of the observer to amplify those spatial frequencies which are in the scene and to attenuate those spatial frequencies which contribute noise but little signal information. These techniques are a standard application of linear systems analysis (for a full discussion refer to Schwartz and Friedland (1965)).

An equivalent analysis can be made in terms of the electrical signal and random electrical noise in the video channel of a television camera. In this case the spatial frequency components above would be replaced by real frequencies in hertz and N_o would become the mean square noise current per unit bandwidth (1 Hz).

In either case N_o is commonly called the power spectral density in analogy to a random current i flowing through a resistance of 1 ohm dissipating N_o watts. Whether or not power is involved the term power spectral density

is used throughout this thesis to denote the mean square value of a random variable per unit interval of its corresponding independent variable.

In principle then, the small signal performance of an imaging system can be specified by measuring the overall spatial frequency response and the system noise. Such measurements have been made on a commercial vidicon camera and are described in Chapter 4.

1.3 Outline of the Thesis

The limitation of the infrared vidicon due to circuit noise is closely examined in this thesis and various types of amplifier are investigated to find the improvement possible by operation at low temperatures or at slow scanning rates.

A full discussion of circuit and device noise theory is given in Chapter 2 because the author considers it better to present full arguments in support of the work rather than to quote many isolated references.

Measurements have been taken of the light equivalent noise input for a G.M.B.H. type 2000 infrared vidicon, an R.C.A. type 7735 A visible spectrum vidicon and an R.C.A. type 6914-A image converter. Spatial frequency responses of the vidicons have also been measured. The experimental methods and results are described in Chapter 4.

Chapter 3 develops the theory of the limitations of imaging photon detectors due to photon noise or circuit noise. The minimum detectable contrast due to the limited dynamic range of the vidicon is also discussed. The experimentally determined quantities of Chapter 4 are substituted into the theoretical equations of Chapter

3 in order to find the light flux required by each detector for a given scene contrast. The results are presented in graphical form in Fig. 3.4 which shows the limiting performance of these devices and the bounds of performance for other image tubes.

The arguments used in this thesis involve only the gross characteristics of the commercial devices. No attempt is made to discuss the detailed mechanisms of operation and possible improved designs and methods of construction. For those interested in these detailed mechanisms, Rose (1963) gives a very readable account of photoconductivity with descriptions of various trap and recombination models which account for the observed light intensity response characteristics of photoconductors. The response of photoconducting imaging devices with floating electrodes (including the vidicon) is discussed by Sommers (1963) who gives formal conditions required of the photoconductor to obtain a gain on read-out. However, no photoconductive gain has been achieved in commercial vidicons. The resolution of vidicon tubes is discussed by Krittman (1963) and by Lubszynski and Wardley (1963).

Other scanned T.V. image tubes such as the image orthicon are not treated here. Although they are capable

of operating at lower light levels than the vidicon, they are unsuitable for low contrast scenes due to high beam current noise in the small signal region. Further details of these and other imaging devices may be found in the review papers of Weimer (1960) and Livingstone (1967).

Chapter 2

CIRCUIT THEORY OF NOISY NETWORKS AND PHYSICAL SOURCES OF ELECTRICAL NOISE

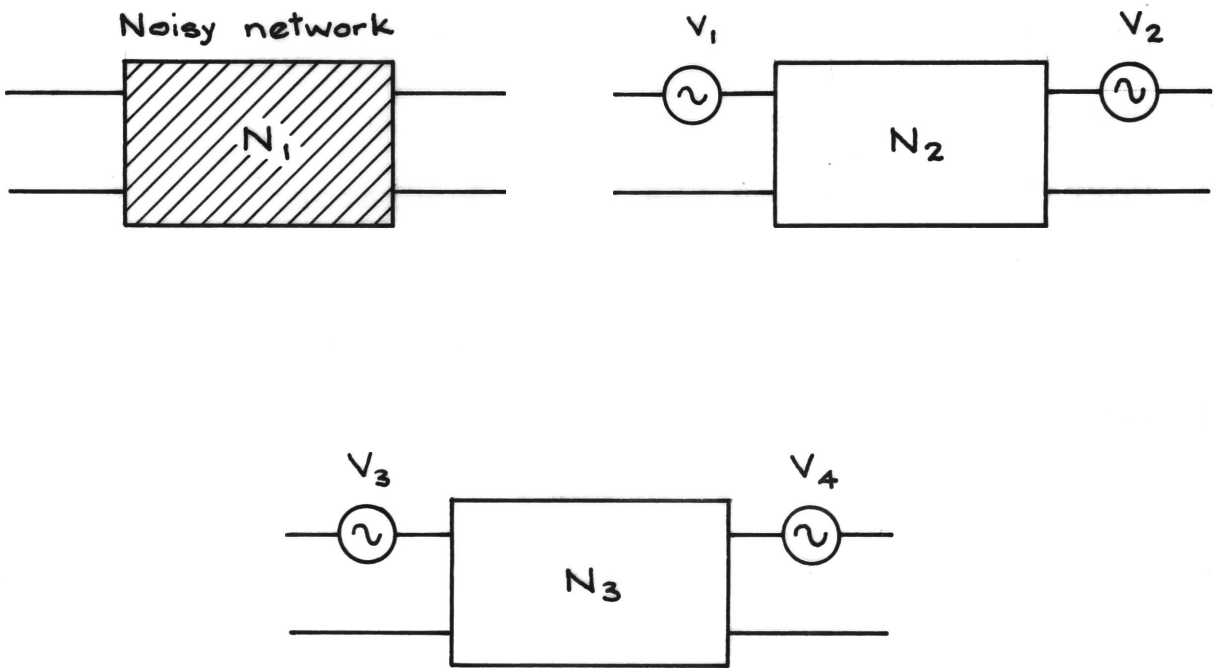

FIG. 2·1 EQUIVALENT NOISE CIRCUITS

2.1 Circuit Theory of Noisy Two Port Networks

In this part of the work it is proposed to treat the circuit theory of noisy two port networks, physical sources of noise, and the application of circuit theory to the problem of selecting the optimum driving impedance to obtain best signal to noise ratio. The effect of feedback on noise performance of a circuit will also be discussed.

2.1.1 Peterson's theorem

Peterson's theorem (Montgomery, 1952) states that the performance of a noisy linear two port network may be described completely by the addition of two noise generators to a noise free network which is otherwise equivalent. Montgomery gives a simple proof for the case where the two noise generators are voltage generators (of zero impedance) in series with the input and output respectively.

Montgomery considers three linear networks N_1, N_2, N_3 (see Fig. 2.1) which have identical transmission properties in both directions for external signals. The networks N_2 and N_3 are noise free. Voltage generators v_1, and v_2 give open circuit voltages at the input and output terminals identical to N_1. Therefore by Thevenin's theorem N_1 and N_2 must supply identical currents to the same terminating

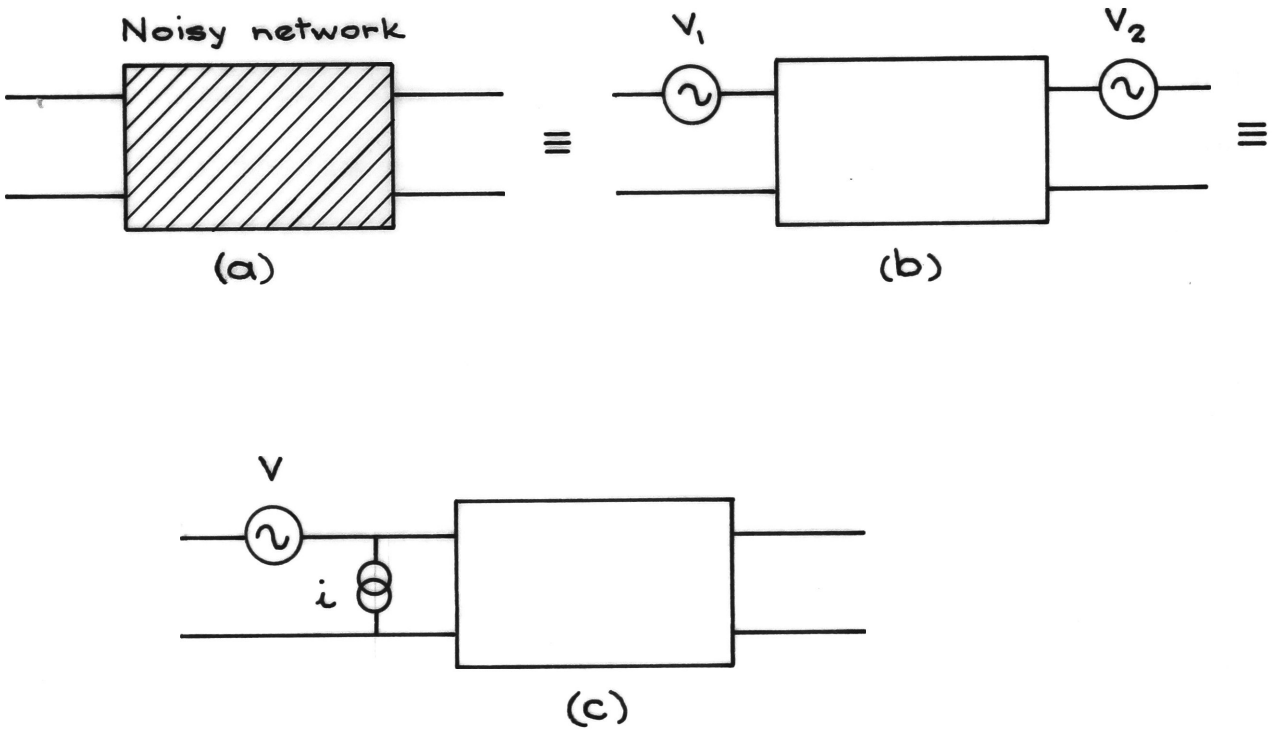

FIG. 2·2 STANDARD FORMS OF EQUIVALENT NOISE CIRCUIT

impedances. Voltage generators v_3 and v_4 are made statistically equivalent to v_1 and v_2; hence they must supply statistically equivalent currents to the same terminating impedances as does N_2. It follows that N_3 and N_1 must supply statistically equivalent currents to the same terminating impedances and therefore the noise performance is equivalent. This proves the theorem for this case.

The extension of the two voltage generator form of the theorem to an equivalent voltage generator and a current generator (of infinite impedance) at the input as shown in Fig. 2.2 is easily derived by standard network theory using mesh equations to show their equivalence. (See for example Rothe and Dalke 1956). Further theory relevant to the noise equivalent circuit of Fig. 2.2(c) is developed below, because this is the most important case in practical applications.

2.1.2 Correlation between the noise generators

In general the noise sources v and i of Fig. 2.2(c) will be partly correlated. Rothe and Dalke (1956) express this correlation by

$$v = v_u + iZ_{cor} \,. \tag{2.1}$$

$$i = i_u + vY_{cor} \,. \tag{2.2}$$

Sec. 2.1

It can be seen from equation (2.1) that the noise voltage is divided into two parts. The first part v_u is not correlated with the current generator and the second part iZ_{cor} is fully correlated with the current generator. Similarly from equation (2.2) the noise current is divided into one part i_u not correlated with the voltage generator and the second part vY_{cor} which is fully correlated with the voltage generator. Clearly Z_{cor} and Y_{cor} must have the dimensions of impedance and admittance respectively.

2.1.3 Correlation coefficient

The correlation coefficient is commonly used as a measure of the correlation between two generators. By definition the correlation coefficient κ is equal to the normalized covariance

$$\kappa = \frac{\text{Cov.}(v,i)}{\sigma_v \sigma_i} \tag{2.3}$$

where σ_v, σ_i are the standard deviations of v and i. For noise sources with no mean value

$$\kappa = \overline{iv^*}/(\overline{|i|^2}.\overline{|v|^2})^{\frac{1}{2}} \tag{2.4}$$

where v^* is the complex conjugate of v.

Now

$$Z_{cor} = \kappa(\overline{v^2}/\overline{i^2})^{\frac{1}{2}}$$

$$\therefore Z_{cor} = \overline{iv^*}/\overline{|i|^2} \tag{2.5}$$

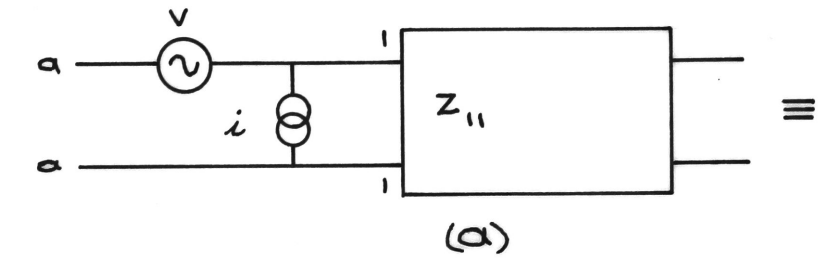

(a)

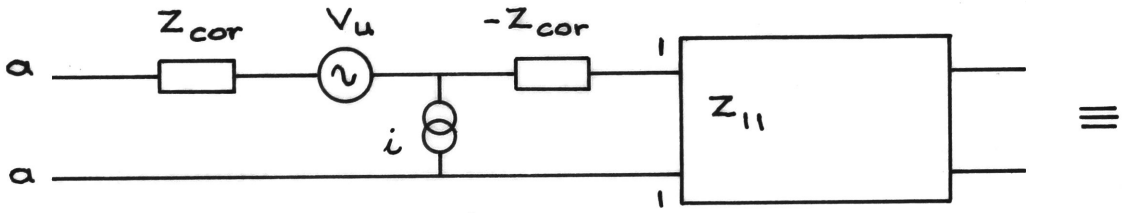

(b)

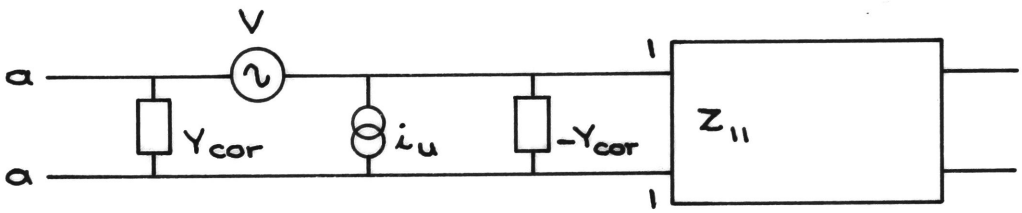

(c)

FIG. 2·3 EQUIVALENT NOISE CIRCUITS WITH UNCORRELATED SOURCES

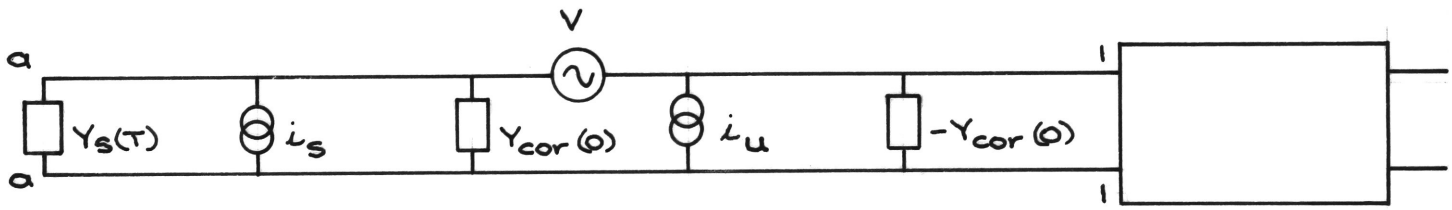

(a)

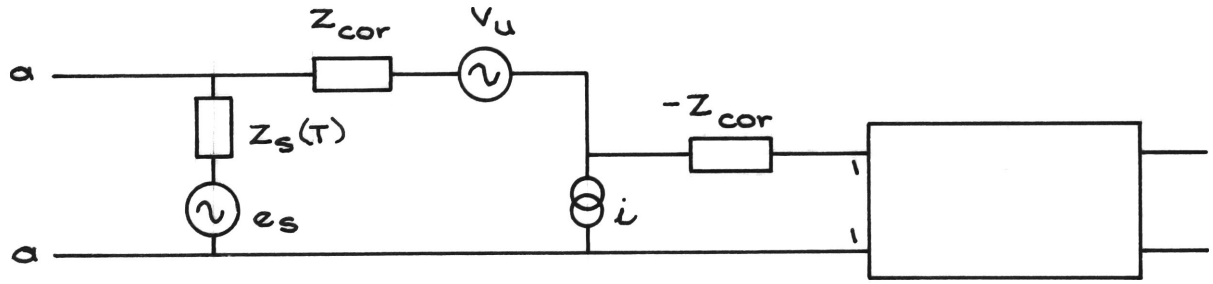

(b)

FIG. 2·4 NOISE CIRCUITS INCLUDING INPUT GENERATOR

Similarly

$$Y_{cor} = \kappa(\overline{i^2}/\overline{v^2})^{\frac{1}{2}} = \overline{i^* v}/\overline{|v|^2} \quad . \qquad (2.6)$$

where i^* is the complex conjugate of i.

2.1.4 Equivalent uncorrelated generator circuit

Using the equations (2.1), (2.2) to replace the partly correlated noise generators v and i of Fig. 2.2(c) results in the equivalent circuits of Fig. 2.3. These circuits are easily shown to be equivalent by calculating the input current to the terminals 1,1 for any general impedance termination at a,a. Note that Z_{cor} and Y_{cor} are noiseless.

Thus we now have two possible equivalent circuits, either Fig. 2.3(b) or Fig. 2.3(c) which have all noise sources located at the input to the noiseless network. The appropriate noise generators (v_u, i or v, i_u) are now totally uncorrelated.

2.1.5 Connection of an input signal

In normal operation a signal source is connected to the input of the noisy two port network. If the signal source has an internal impedance $Z_s = R_s + jX_s$ or admittance $Y_s = G_s + jB_s$ then the circuits of Fig. 2.3(b) and (c) become those of Fig. 2.4(a) and (b). In Fig. 2.4, (T) denotes the noise temperature of the source at the input, (due to R_s or G_s), which contributes an uncorrelated voltage e_s or current i_s at the positions shown.

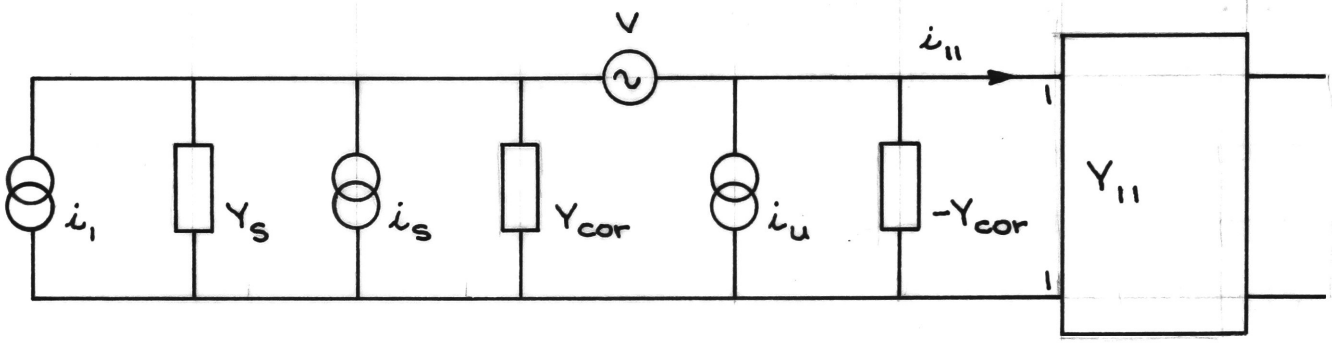

FIG. 2·5 EQUIVALENT NOISE CIRCUIT USED TO DERIVE SIGNAL TO NOISE PERFORMANCE

2.1.6 Measures of noise performance

The signal to noise performance of the circuits of Fig. 2.4 require some definition. The objective is to find a generator impedance $Z_{s(min)}$ which results in a minimum of the ratio P defined by

$$P = \frac{\text{total noise output power}}{\text{signal output power}} . \qquad (2.7)$$

The signal input amplitude may itself be a function of generator impedance. For example if a transformer is used at the input then $\overline{|e_s|^2} \propto R_s$ and $\overline{|e_{signal}|^2} \propto R_s$ where R_s is the transformed generator impedance looking back into the secondary winding of the input transformer. The signal power in equation (2.7) can be replaced by the noise power of R_s as these quantities are directly proportional in this case. Equation (2.7) then becomes

$$F = \frac{\text{total noise output power}}{\text{noise output power due to the thermal noise of } Z_s} . \qquad (2.8)$$

The usual definition of noise factor is given by equation (2.8). However, equation (2.7) is more general and it can be applied to a wider range of circuits than equation (2.8).

2.1.7 The problem of maximizing signal to noise power

Consider now the equivalent circuit of Fig. 2.5 where i_1 is a current generator in parallel with Y_s representing the input signal. The noise current of G_s is represented by the current generator i_s and Y_{11} is the admittance looking into the terminals 11 of the noiseless network.

Then

$$i_{11} = \frac{(i_1 + i_s + i_u)Y_{11}}{Y_s + Y_{11}} + \frac{v.Y_{11}(Y_s + Y_{cor})}{Y_s + Y_{11}} \quad . \qquad (2.9)$$

Because all terms are uncorrelated therefore

$$\overline{i_{11}^2} = \frac{(\overline{i_1^2} + \overline{i_s^2} + \overline{i_u^2})|Y_{11}|^2 + \overline{v^2}|Y_{11}(Y_s + Y_{cor})|^2}{|Y_s + Y_{11}|^2} \quad . (2.10)$$

Thus

$$P = \frac{\text{total noise power}}{\text{signal power}}$$

$$= \frac{(\overline{i_s^2} + \overline{i_u^2})|Y_{11}|^2 + \overline{v^2}|Y_{11}(Y_s + Y_{cor})|^2}{\overline{i_1^2}|Y_{11}|^2} \qquad (2.11)$$

$$= \frac{\overline{i_s^2} + \overline{i_u^2} + \overline{v^2}\left((G_s + G_{cor})^2 + (B_s + B_{cor})^2\right)}{\overline{i_1^2}} \quad . \qquad (2.12)$$

This expression will now be applied to three particular cases.

Case 1 Input voltage proportional to $\sqrt{R_s}$ or $i_s \propto \sqrt{G_s}$. This case covers circuits in which an impedance transformation can be made by an input transformer of variable turns ratio. Example: Radio communication circuits.

Case 2 Input voltage independent of input impedance (constant voltage source).

Examples: Photovoltaic cells, thermocouples.

Case 3 Input current independent of input impedance (con-

stant current source).

Examples: Nuclear Detectors, Photoemissive cells, Vidicons.

Case 1 Input voltage $e_1 \propto \sqrt{R_s}$ $(i_1 \propto \sqrt{G_s})$

For this case equation (2.12) becomes

$$P \propto \frac{4\ kTG_s + \overline{i_u^2} + \overline{v^2}\left((G_s + G_{cor})^2 + (B_s + B_{cor})^2\right)}{G_s} .$$

$$\therefore P \propto 4\ kT + \frac{\overline{i_u^2} + \overline{v^2}\left((G_s + G_{cor})^2 + (B_s + B_{cor})^2\right)}{G_s} . \quad (2.13)$$

One condition for a minimum of P is that

$$\frac{\partial P}{\partial B_s} = 0 \quad (2.14)$$

which requires that $B_s = -B_{cor}$. Substituting this into equation (2.13) gives

$$P_m \propto 4\ kT + \frac{\overline{i_u^2} + \overline{v^2}(G_s + G_{cor})^2}{G_s} .$$

The second condition for a minimum is that $\frac{\partial P_m}{\partial G_s} = 0$ which requires

$$2\ G_s.\overline{v^2}(G_s + G_{cor}) = \overline{i_u^2} + \overline{v^2}(G_s + G_{cor})^2 .$$

$$\therefore G_s = \left[\frac{\overline{i_u^2}}{\overline{v^2}} + G_{cor}^2\right]^{\frac{1}{2}} . \quad (2.15)$$

Case 2 Constant input voltage independent of input impedance

It is assumed that a transformer cannot be used; otherwise infinite signal to noise ratio could be obtained. The

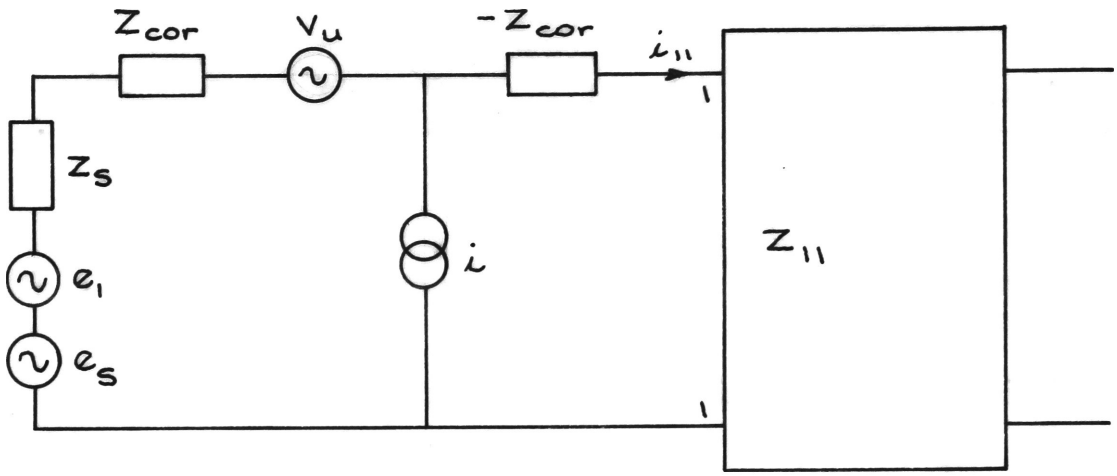

FIG. 2·6 EQUIVALENT NOISE CIRCUIT WITH CONSTANT VOLTAGE INPUT

most appropriate circuit for this case is given in Fig. 2.6 (cf. Fig. 2.4b).

Here $$i_{11} = \frac{e_s}{Z_s + Z_{11}} + \frac{e_1}{Z_s + Z_{11}} + \frac{v_u}{Z_s + Z_{11}} + \frac{i(Z_{cor} + Z_s)}{Z_s + Z_{11}} . \tag{2.16}$$

$$\therefore \quad P = \frac{\text{total noise power}}{\text{signal power}}$$

$$= \frac{\overline{e_s^2} + \overline{v_u^2} + \overline{i^2}\left((R_s + R_{cor})^2 + (X_s + X_{cor})^2\right)}{\overline{e^2}}$$

$$\text{or} \quad P \propto 4\,kTR_s + \overline{v_u^2} + \overline{i^2}\left((R_s + R_{cor})^2 + (X_s + X_{cor})^2\right). \tag{2.17}$$

$\frac{\partial P}{\partial X_s} = 0$ for $X_s = -X_{cor}$, and substituting this in equation (2.17) gives

$$P_m \propto 4\,kTR_s + \overline{v_u^2} + \overline{i^2}(R_s + R_{cor})^2.$$

This is minimum for $\frac{\partial P_m}{\partial R_s} = 0$, that is when

$$R_s = -R_{cor} - \frac{2kT}{\overline{i^2}} . \tag{2.18}$$

Because R_s is restricted to non negative values and because R_{cor} is positive or zero for the cases considered, therefore P is minimum when R_s is zero. That is, there is no advantage gained by inserting any resistive component of Z_s in series with the input generator.

Sec. 2.1

Case 3 Constant current generator

From equation (2.12)

$$P = \frac{\overline{i_s^2} + \overline{i_u^2} + \overline{v^2}\left((G_s + G_{cor})^2 + (B_s + B_{cor})^2\right)}{i_1^2} . \quad (2.19)$$

For i_1 constant

$$P \propto 4\,kTG_s + \overline{i_u^2} + \overline{v^2}\left((G_s + G_{cor})^2 + (B_s + B_{cor})^2\right).$$

From the condition $\frac{\partial P}{\partial B_s} = 0$ we have

$$B_s = -B_{cor}.$$

From the condition $\frac{\partial P}{\partial G_s} = 0$ we have

$$G_s = -G_{cor} - \frac{2kT}{\overline{v^2}} . \quad (2.20)$$

From these equations it is seen that for G_{cor} positive or zero any conductance shunting the source decreases the signal to noise ratio.

2.1.8 General remarks

In the following work it is assumed that the signal to noise performance of cascaded amplifiers is determined by the first stage only and that the gain of this stage is much greater than unity when the generator impedance is at optimum value. These assumptions avoid analytical complexity in applying the extended noise factor of Friss

(1944) and the difficult general theory of Haus and Adler (1959) and yet they apply to many practical situations. It should be remembered however that Haus and Adler (1959) have shown that any arbitrarily large gain may be obtained by cascading amplifiers of low gain with the same overall signal to noise performance as that of a single stage. It remains to discuss the effects of negative feedback on the signal to noise performance of a single amplifier of high gain.

It is a well known result that usually the effect of feedback does not alter the signal to noise performance (except for the added thermal noise of the feedback components) nor the value of the optimum generator impedance required for best signal to noise ratio. The conditions under which these results are true are discussed in the next section.

2.1.9 Effects of negative feedback in signal to noise performance

Bogner (1965) shows that the noise performance of an amplifier and its optimum generator impedance are substantially unaffected by negative feedback.

However, the feedback components generally add a small component of thermal noise to the input and hence best noise performance is obtained without feedback on the

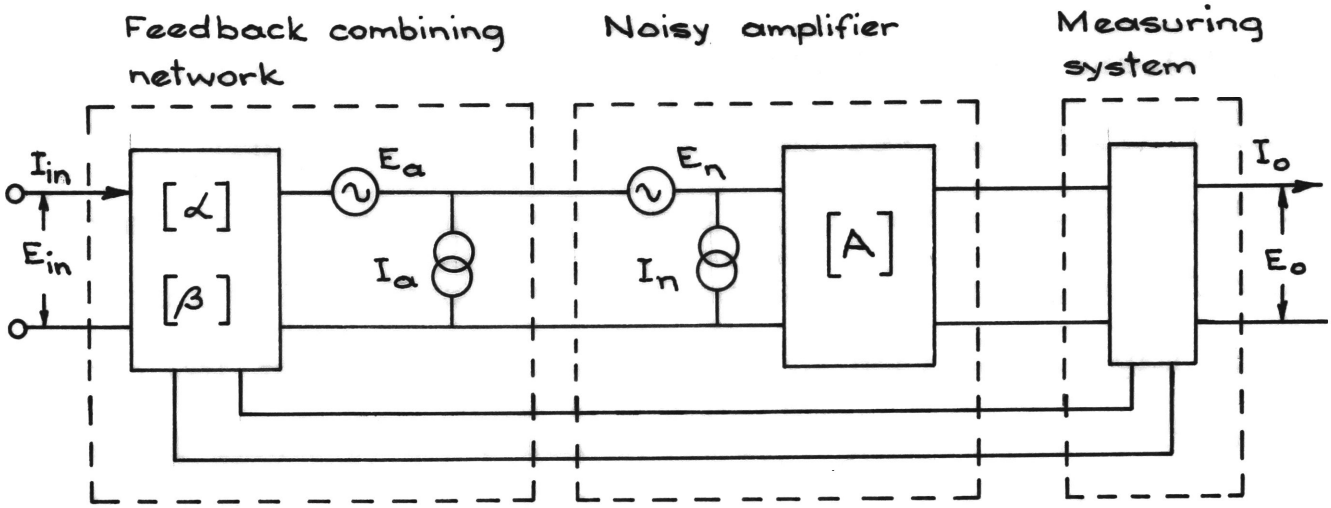

FIG. 2·7 CIRCUIT OF FEEDBACK AMPLIFIER

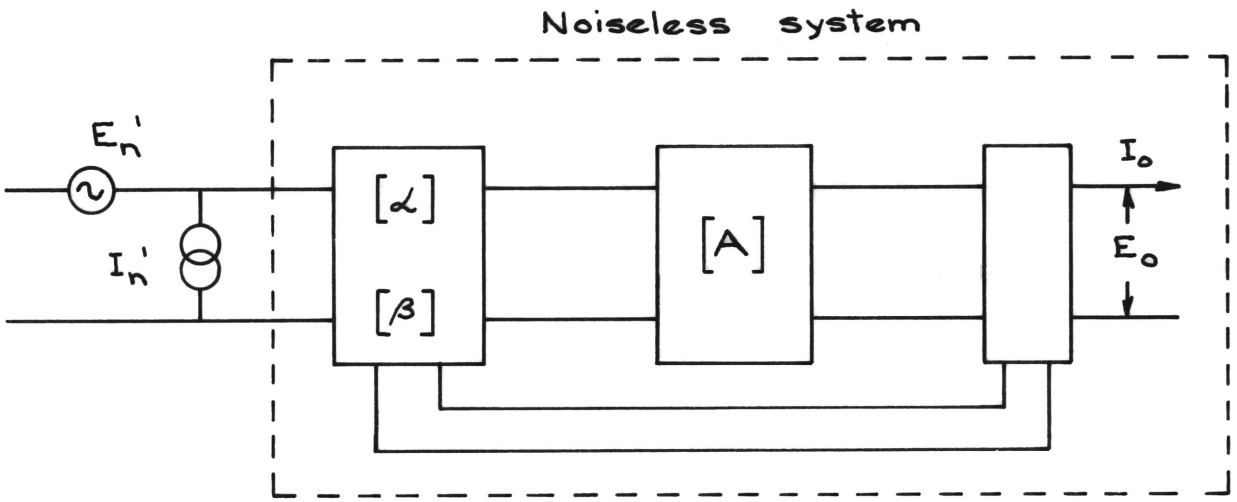

FIG. 2·8 NOISE EQUIVALENT CIRCUIT OF FEEDBACK AMPLIFIER

first stage. Nevertheless other considerations such as gain stability, input impedance or required bandwidth may still require the use of feedback on the first stage.

An outline of Bogner's proof is given here. Feed forward through the system is ignored. Fig. 2.7 shows the generalized circuit of a feedback amplifier.

The matrices $[\alpha]$, $[\beta]$ represent the feedback combining network which combines part of the output I_0, E_0 with the input I_{in}, E_{in}, while E_a, I_a represent the noise contributed by the feedback combining network.

From Fig. 2.7

$$\begin{bmatrix} E_0 \\ I_0 \end{bmatrix} = [A] \begin{bmatrix} E_1 + E_n \\ I_1 + I_n \end{bmatrix} \tag{2.21}$$

where

$$\begin{bmatrix} E_1 \\ I_1 \end{bmatrix} = [\alpha] \begin{bmatrix} E_{in} \\ I_{in} \end{bmatrix} + [\beta] \begin{bmatrix} E_0 \\ I_0 \end{bmatrix} + \begin{bmatrix} E_a \\ I_a \end{bmatrix} \tag{2.22}$$

and E_{in} and I_{in} are input signals.

Substituting for $\begin{bmatrix} E_1 \\ I_1 \end{bmatrix}$ in equation (2.21) gives

$$\begin{bmatrix} E_0 \\ I_0 \end{bmatrix} = [A] \left\{ [\alpha] \begin{bmatrix} E_{in} \\ I_{in} \end{bmatrix} + [\beta] \begin{bmatrix} E_0 \\ I_0 \end{bmatrix} + \begin{bmatrix} E_n \\ I_n \end{bmatrix} + \begin{bmatrix} E_a \\ I_a \end{bmatrix} \right\} . \tag{2.23}$$

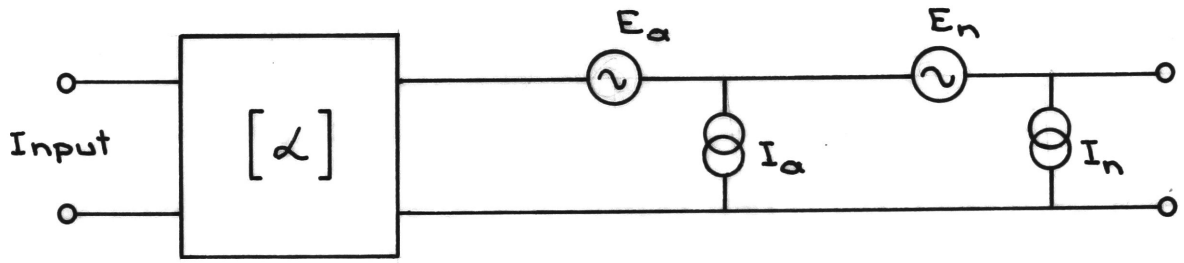

FIG. 2·9 ALTERNATIVE NOISE CIRCUIT FOR FEEDBACK AMPLIFIER

Sec. 2.1

The equivalent system of Fig. 2.8 is described by the equation

$$\begin{bmatrix} E_0 \\ I_0 \end{bmatrix} = [A]\left\{ [\alpha] \begin{bmatrix} E_{in} \\ I_{in} \end{bmatrix} + [\alpha] \begin{bmatrix} E'_n \\ I'_n \end{bmatrix} + [\beta] \begin{bmatrix} E_0 \\ I_0 \end{bmatrix} \right\} \qquad (2.24)$$

for input signals E_{in} and I_{in}. Equating equation (2.23) to equation (2.24) gives

$$[\alpha] \begin{bmatrix} E'_n \\ I'_n \end{bmatrix} = \begin{bmatrix} E_n \\ I_n \end{bmatrix} + \begin{bmatrix} E_a \\ I_a \end{bmatrix} . \qquad (2.25)$$

Equation (2.25) shows that these equivalent noise generators are independent of $[\beta]$ and therefore independent of feedback.

The noise generators E'_n, I'_n of Fig. 2.8 may be compared directly with the input signals E_{in}, I_{in}. However, it is often more convenient to consider that both signal and noise are transformed by $[\alpha]$. This is illustrated in Fig. 2.9 and is equivalent to comparing the transformed signal with the original noise generators of Fig. 2.7.

2.2 Physical Sources of Noise

The circuit theory of noisy networks is given in the previous section (2.1) in terms of equivalent noise voltage and noise current generators at the input of a noiseless network. It is the purpose of this section (2.2) to describe the physical origin and magnitude of these equivalent noise generators for valve, transistor and field effect transistor amplifiers.

2.2.1 Types of noise

Shot noise Shot noise is caused by a series of short independent events such as single electrons or discrete groups of charges applied to a circuit. Each event may be assumed to deliver an impulse of current with constant power spectral density, W_0. The power spectral density is given by

$$W_x(\omega) = \int_{\infty}^{\infty} r_x(u) e^{-j\omega u}\, du.$$

The autocorrelation function r_x for the impulse is

$$r_x = W_0 \delta(t)$$

where $\delta(t)$ is the delta function. The power spectral density as measured in the laboratory is

$$W_x(\omega) = 2W_0 = 2\bar{n}\, q^2 \qquad (2.26)$$

where $\bar{n}$ is the average number of events per unit time

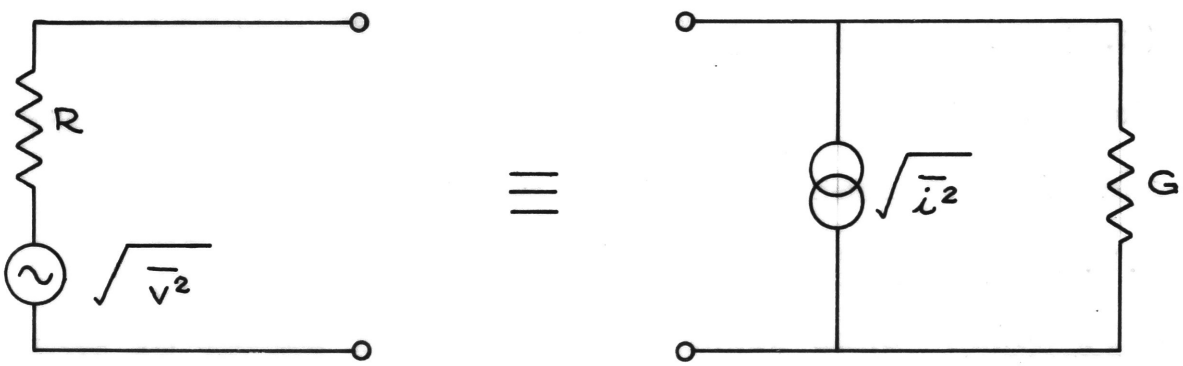

FIG. 2·10 THERMAL NOISE GENERATORS

and q is the charge per event.

$$\therefore W_x = 2 I_0 q \qquad (2.27)$$

where I_0 $(=\bar{n}q)$ is the average current. It follows that the shot noise current i_s is given by

$$\overline{i_s^2} = 2 I_0 q df.$$

The power spectral density of the shot noise at the output of a linear system is given by

$$W_y(\omega) = 2 I_0 q . |H|^2 \qquad (2.28)$$

where H is the transfer function of the linear system.

Thermal noise Thermal or Johnson noise occurs when there is a large concentration of charge carriers and is due to the random thermal motions of the charges. For a resistance in thermal equilibrium with its surroundings at temperature T degrees Kelvin the available open circuit noise voltage is given by one form of Nyquists theorem as

$$\overline{v^2} = 4 kTR\, df \qquad (2.29)$$

where df = the frequency interval in Hz

k = Boltzmans constant = $1.38 \times 10^{-23} J^0 K^{-1}$

T = temperature, K.

Equivalent circuits are shown in Fig. 2.10.

From Fig. 2.10 $\overline{i^2} = 4 kTG\, df$ where $G = \frac{1}{R}$. If this

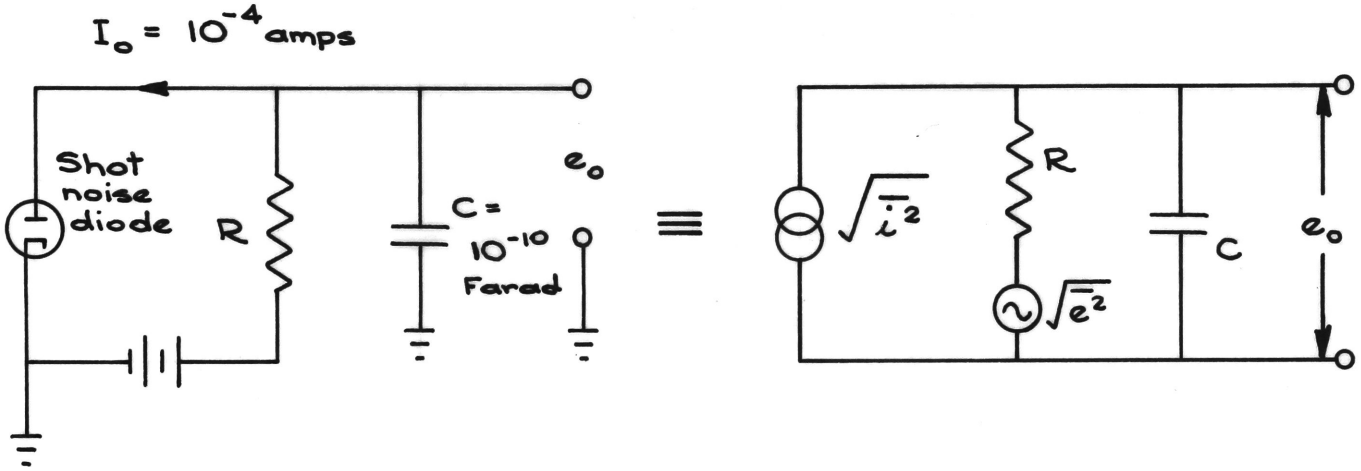

FIG. 2·11 NOISE DIODE AND EQUIVALENT CIRCUIT

noise source is applied to a circuit with a transfer function H the noise output is given by

$$W_y(\omega) = 4\ kTRdf|H|^2 . \qquad (2.30)$$

Flicker Noise Flicker noise occurs in devices through which a d.c. current is flowing. There is no satisfactory theory for the effect which has a frequency spectrum approximately proportional to $\frac{1}{f}$ and is therefore sometimes called $\frac{1}{f}$ noise. It appears true that as manufacturing techniques improve the flicker noise of all devices tends to be relegated to progressively lower frequencies.

Generation-Recombination noise In addition to the resistive thermal noise of semiconductors further noise occurs due to fluctuations in the number of charge carriers present due to random trapping or release of charge carriers.

Other sources of noise will be discussed for particular devices as they are considered below.

Example The example illustrated in Fig. 2.11 will serve to clarify the previous remarks.

The shot noise current $\overline{i_s^2} = 2\ I_0 qdf$. This current flows into the impedance (R in parallel with C) to generate part (e_s) of the output voltage. The transfer function H_1 in this case is therefore

Sec. 2.2

$$H_1 = Z = \frac{R \cdot \frac{1}{j\omega C}}{R + \frac{1}{j\omega C}} .$$

$$\therefore \overline{e_s^2} = 2 I_0 q df . |Z|^2$$

$$= 2 I_0 q . \frac{R^2}{1 + \omega^2 C^2 R^2} df . \qquad (2.31)$$

The total shot noise integrated over all frequencies is then

$$\overline{e_{s(T)}^2} = \frac{2 I_0 q R^2}{2\pi} \int_0^\infty \frac{1}{1 + \omega^2 C^2 R^2} . d\omega$$

$$= \frac{2 I_0 q R^2}{2\pi} . \frac{\pi}{2RC} = \frac{I_0 q R}{2C}$$

$$= \frac{10^{-4} \times 1.6 \times 10^{-19} \times 10^3}{2 \times 10^{-10}} = 80 \times 10^{-12} V^2 .$$

The thermal noise voltage $\overline{e^2} = 4 kTRdf$ is applied to the series circuit R in series with C. The thermal noise output voltage is that developed across C and the transfer function to be used here is

$$H_2 = \frac{\frac{1}{j\omega C}}{R + \frac{1}{j\omega C}} .$$

It should be noted that this differs from the parallel circuit transfer function used to calculate the shot noise.

Sec. 2.2

$$\therefore \quad \overline{e_t^2} = 4\ kTRdf.|H_2|^2$$

$$= 4\ kTR.\frac{1}{1 + R^2\omega^2C^2} \cdot df. \qquad (2.32)$$

The total thermal noise integrated over all frequencies is then

$$\overline{e^2_{t(T)}} = \frac{4kTR}{2\pi}\int_0^\infty \frac{1}{1 + \omega^2R^2C^2} \cdot d\omega$$

$$= \frac{4kTR}{2\pi} \cdot \frac{\pi}{2RC} = \frac{kT}{C}$$

$$= \frac{1.38 \times 10^{-23} \times 300}{10^{-10}} = 4 \times 10^{-11}V^2 \quad \text{for } T = 300\ ^oK.$$

Because the shot noise and thermal noise are totally uncorrelated

$$\overline{e^2_{0(T)}} = \overline{e^2_{s(T)}} + \overline{e^2_{t(T)}} \cdot$$

$$\therefore \overline{e^2_{0(T)}}^{\frac{1}{2}} = \sqrt{12 \times 10^{-11}} = 1.1 \times 10^{-6}V(\text{rms}) \cdot$$

In some cases we are not so much concerned with the total noise as with the noise at a particular frequency. The power spectral densities for the shot and thermal noise of this example are given by equations (2.31) and (2.32). It is seen that for this case they both have

the same frequency dependence due to the common term $\frac{1}{1 + \omega^2 R^2 C^2}$.

2.2.2 Noise in thermionic valves

(i) Noise in a space charge limited diode

Space charge reduces shot noise below its normal value by acting as a velocity dependent gate which smoothes the fluctuations due to variable emission velocities. The space charge noise power spectral density is expressed as

$$\overline{i_{sc}^2} = \overline{i_s^2} \cdot \Gamma^2 = 2 I_0 e \Gamma^2 \qquad (2.33)$$

where Γ^2 represents the smoothing factor. North (1940) shows that for anode currents well below saturation

$$\Gamma^2 = \frac{9(1 - \frac{\pi}{4}) kT_k}{e(V_a - V_m)}$$

where k = Boltzmans constant

e = electron charge

V_a = anode volts

V_m = minimum potential in space charge

and T_k = cathode temperature.

Neglecting V_m

$$\Gamma^2 = \frac{9(1 - \frac{\pi}{4}) kT_k}{eV_a} . \qquad (2.34)$$

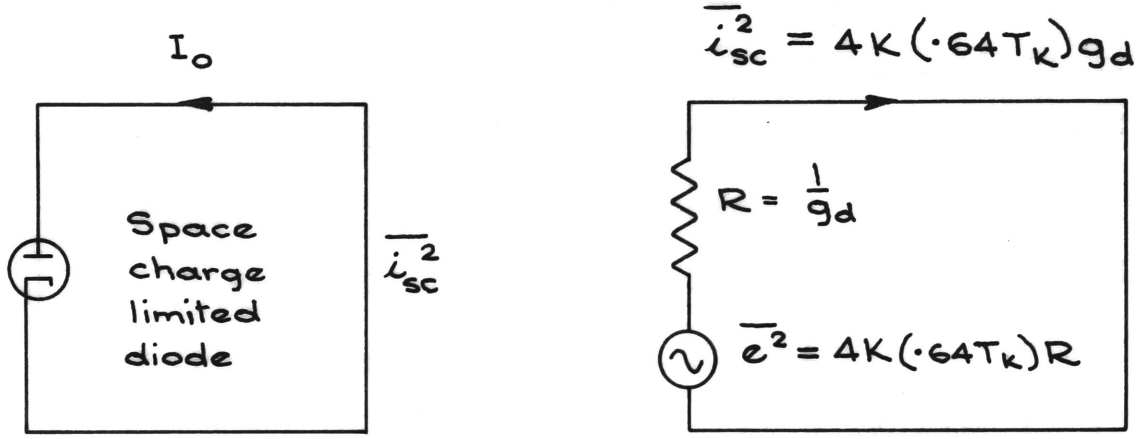

FIG. 2·12 NOISE GENERATOR OF SPACE CHARGE LIMITED DIODE

Sec. 2.2

$\therefore$ from equation (2.33)

$$\overline{i_{sc}^2} = \frac{2I_0 .9(1 - \frac{\pi}{4}).k.T_k}{V_a} . \qquad (2.35)$$

Introducing the diode conductance,

$$g_d = \frac{dI_0}{dV_a} = \frac{3}{2}\frac{I_0}{V_a}$$

equation (2.35) becomes

$$\overline{i_{sc}^2} = 4\ kT_k.g_d.3(1 - \frac{\pi}{4})$$

$$= 4\ kg_d(0.64)T_k \quad . \qquad (2.36)$$

The mean square noise current is thus the same as the thermal noise available from a conductance g_d operating at a temperature of 0.64 T_k. This equivalence is shown in Fig. 2.12. Although diodes are not used as low noise amplifiers the theory applies to the triode with little modification.

(ii) Space charge limited triode

Shot noise It follows from the theory of the space charge limited diode that the suppressed shot noise for the triode is given by

$$\overline{i_s^2} = 4k(0.64)T_k\ G_m\ df \qquad (2.37)$$

Sec. 2.2

where $G_m = \left(\frac{\partial I_a}{\partial V_g}\right)_{V_a}$ is the mutual conductance. Referred to the grid of the valve this noise current would be equal to the full thermal noise voltage produced by an equivalent resistance $R_{eq}(S)$, i.e.

$$4\ kT\ R_{eq}(S)G_m^2 = \overline{i_{sc}^2} = 4\ k(0.64)T_k G_m\ .$$

$$\therefore\quad R_{eq}(S) = \frac{0.64\ T_k}{TG_m} \qquad (2.38a)$$

$$= 2.2/G_m \text{ for } T_k = 1000 \text{ K and } T = 290 \text{ K} \qquad (2.38b)$$

Flicker Noise A good low noise valve has a flicker noise current of approximately

$$\overline{i_f^2} = \frac{I_a^2 \times 10^{-13}}{f}\ A^2 Hz^{-1}\ . \qquad (2.39)$$

The equivalent noise resistance referred to the grid is

$$R_{eq}(f) = \frac{I_a^2 \times 10^{-13}}{f \times 4kT\ G_m^2}\ . \qquad (2.40)$$

Because $G_m \propto I_a^{\frac{1}{3}}$
It follows from equation (2.40) that

$$R_{eq}(f) \propto I_a^{\frac{4}{3}} \propto G_m^4 \qquad (2.41)$$

for a given valve structure.

The frequency at which flicker noise equals shot noise is given by

$$\frac{I_a^2 \times 10^{-13}}{f\ 4kT\ G_m^2} = \frac{2.2}{G_m} \quad . \tag{2.42}$$

$$\therefore \quad f = \frac{I_a^2 \times 10^{-13}}{2.2 \times 4kT\ G_m} \quad . \tag{2.43}$$

For example if I_a = 1mA, G_m = 1mAV^{-1} then f = 3 kHz while if I_a = 10 mA, G_m = 10 mAV^{-1} then f = 30 kHz.

Grid current noise The various components, i_g, of grid current, I_g, each contribute full shot noise.

$$\therefore \quad \overline{i^2} = 2q\sum i_g = 2qI_g \tag{2.44}$$

where I_g is the sum of the absolute values of the components. The grid voltage developed by this current flowing in a grid circuit resistance of R_g is

$$\overline{e_g^2} = 2qI_g\ R_g^2 \quad . \tag{2.45}$$

The equivalent thermal noise resistance R_{eq} is given by

$$4\ kT\ R_{eq} = 2qI_g\ R_g^2 \quad .$$

$$\therefore \quad R_{eq} = \frac{2qI_g\ R_g^2}{4kT} \quad . \tag{2.46}$$

Sec. 2.2

From equation (2.46) the grid current noise equals the thermal noise of R_g when

$$R_g = \frac{4kT}{2qI_g} \tag{2.47}$$

$$\simeq \frac{5 \times 10^{-2}}{I_g} \text{ for } T = 300 \text{ K} \tag{2.48}$$

$$= 500 \text{ k}\Omega \quad \text{for } I_g = 0.1\mu\text{A}.$$

It should be noted that grid currents in valves are not well defined and can change during the life of the valve. The only reasonable design approach is to use a maximum figure for grid current as specified by the manufacturer. An approximately limiting value of grid current due to soft x-ray emission is given by

$$I_g \simeq I_a \, (E_{g-p})^{\frac{3}{2}} \times 10^{-10}\text{A}.$$

We now summarize the arguments to this point for practical triodes at operating frequencies where transit time is negligible.

The shot noise equivalent thermal resistance $(\frac{2.2}{G_m})$ ranges from 2200Ω to 45Ω, at T ≃ 300 K.

The grid current noise is small compared with thermal noise for low grid circuit resistance (< 250 kΩ for $I_g < 10^{-7}$A).

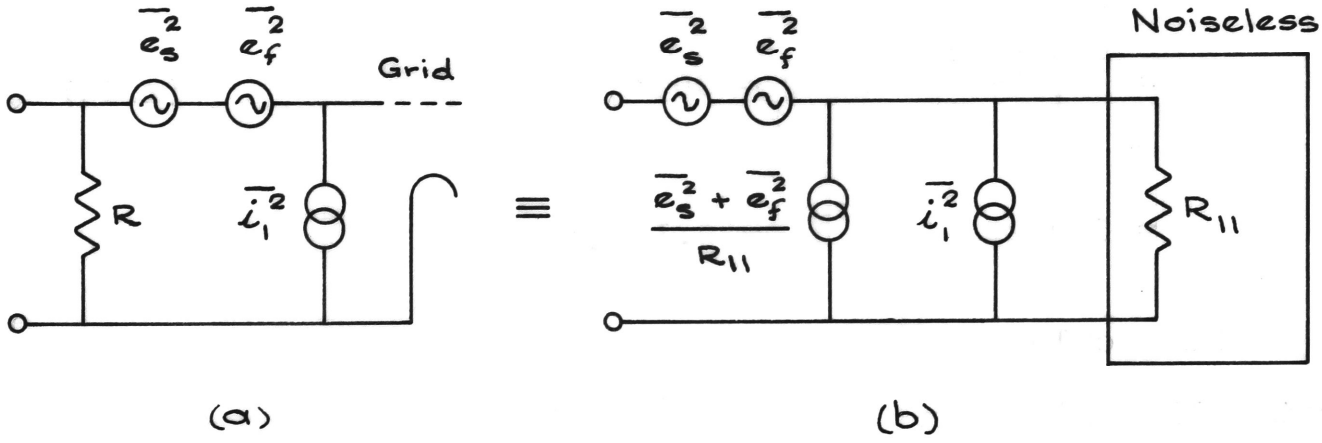

FIG. 2·13 NOISE GENERATORS OF SPACE CHARGE LIMITED TRIODE

The grid current noise should however be compared with shot noise in problems involving noise factor i.e. where the input signal $\propto \sqrt{R_g}$. When this is done grid current noise becomes significant at much lower grid resistances ($\simeq$ 10kΩ).

If low frequency amplification is required the flicker noise predominates and from equation (2.41) low plate current operation will give best results.

For frequencies above the flicker noise region the best valve is one which has high G_m and low I_g [from equations (2.38 and (2.45)]. Two typical examples are given in the following table.

Type	G_m (mAV^{-1})	I_a (mA)	I_g (A)
EC1000	14	14	10^{-8}
E810F	50	35	10^{-7}

The equivalent noise circuit of the triode is shown in Fig. 2.13(a) which applies at frequencies where the interelectrode and Miller effect capacitances are neglected. [Miller effect capacitance may be eliminated by "cascode" connection of two valves or two transistors as described by Cherry and Hooper (1968)]. Fig. 2.13(b) is the equivalent circuit in the general form of Fig. 2.2(c). R_{11} is the input resistance of the valve. In Fig. 2.13 the shot noise is given by $\overline{e_s^2} = 4kT\, R_{eq}(S)$ [where $R_{eq}(S)$ is given by equation (2.38)]. The flicker noise is given

by $\overline{e_f^2} = 4\ kT\ R_{eq}(f)$ where $R_{eq}(f)$ is given by equation (2.40). The grid current noise is given by

$$\overline{i_1^2} = 2qI_g \quad \text{[see equation (2.44)]}.$$

Neglecting flicker noise $\overline{e_f^2}$ of Fig. 2.13(b), it is seen that i_1 is the only component of current fully uncorrelated with the noise voltage generator e_s. The remaining component of current $\frac{e_s}{R_{11}}$ is fully correlated to the voltage generator e_s. From equation (2.2) it follows that $Y_{cor} = \frac{1}{R_{11}}$. The results of Section 2.1.7 can now be applied. If for example the input voltage is proportional to $\sqrt{R_s}$ then equation (2.15) shows that the minimum noise to signal ratio is obtained for

$$G_s = \sqrt{\frac{\overline{i_u^2}}{\overline{v^2}} + G_{cor}^2}\ .$$

From Fig. 2.13(b) $\overline{i_u^2} = \overline{i_1^2}$ and $\overline{v^2} = \overline{e_s^2}$ giving

$$G_s = \sqrt{\frac{\overline{i_1^2}}{\overline{e_s^2}} + G_{11}^2}\ . \qquad (2.49)$$

If $G_{11} = 0$ then on substituting $4kT\ R_{eq}(S)$ for $\overline{e_s^2}$ and $2qI_g$ for $\overline{i_1^2}$ from equation (2.44) in equation (2.49)

$$R_s = \sqrt{\frac{4kT\ R_{eq}(S)}{2qI_g}}\ .$$

Substituting for $R_{eq}(S)$ from equation (2.38a) we have

$$R_s = \sqrt{\frac{4k \times 640}{2qI_g G_m}} \quad \text{for } T_k = 1000 \text{ K}.$$

(iii) Multigrid valves

In addition to the suppressed shot noise of the anode current, partition noise occurs in a tetrode or pentode because an electron may be captured by the screen grid or it may pass to the anode or next grid. Obviously partition noise is reduced in grid aligned structures. For the pentode, Van der Ziel (1954) gives the additional partition noise as

$$\overline{i_p^2} = \frac{2qI_a I_2}{I_a + I_2} \quad \text{where } I_2 = \text{screen current}.$$

When $I_a >> I_2$ we have

$$\overline{i_p^2} \simeq 2qI_2 \tag{2.50}$$

which is the full shot noise of the screen current. If $R_{eq}(p)$ is the partition noise equivalent thermal resistance referred to the grid then

$$4kT\, R_{eq}(p)\, g_m^2 = 2qI_2 .$$

$$\therefore R_{eq}(p) = \frac{2qI_2}{4kT\, G_m^2} . \tag{2.51}$$

Sec. 2.2

The ratio M of $\dfrac{R_{eq}(p)}{R_{eq}(S)} = \dfrac{2qI_2}{4kT\ G_m \times 2.2}$

$$\text{i.e. } M \simeq 10\ \frac{I_2}{G_m} \text{ at } T = 300\ K .$$

If now we let $I_2 = 0.2\ I_a$ which is a reasonable practical value for non aligned structures, then

$$M \simeq \frac{2I_a}{G_m} \simeq 2$$

for $I_a = 10$ mA and $G_m = 10\ mAV^{-1}$.

In this example the partition noise is twice the suppressed shot noise and increases inversely as G_m.

(iv) High frequency valve noise

At higher frequencies the current generator $\dfrac{\overline{e_s^2} + \overline{e_f^2}}{R_{11}^2}$ of Fig. 2.13 must be increased to $\dfrac{\overline{e_s^2} + \overline{e_f^2}}{|Z_{11}|^2}$ where Z_{11} is the input impedance at the grid. For moderate frequencies and resistive plate load, Z_{11} consists of R_{11} in parallel with an input capacitance C_{in}.

$$\therefore \frac{\overline{e_s^2} + \overline{e_f^2}}{|Z_{11}|^2} = \frac{\overline{e_s^2} + \overline{e_f^2}}{R_{11}^2} (1 + R_{11}^2\omega^2C_{in}^2) \qquad (2.52)$$

(v) Higher frequency valve noise (transit time effects)

As the frequency increases the input conductance

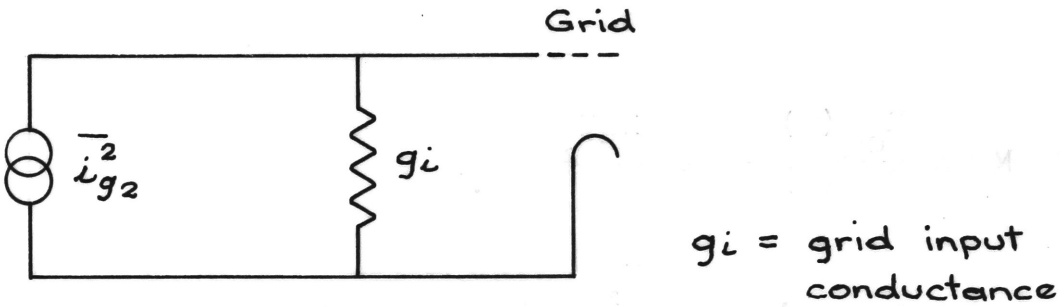

FIG. 2·14 VALVE NOISE GENERATOR DUE TO TRANSIT TIME EFFECTS

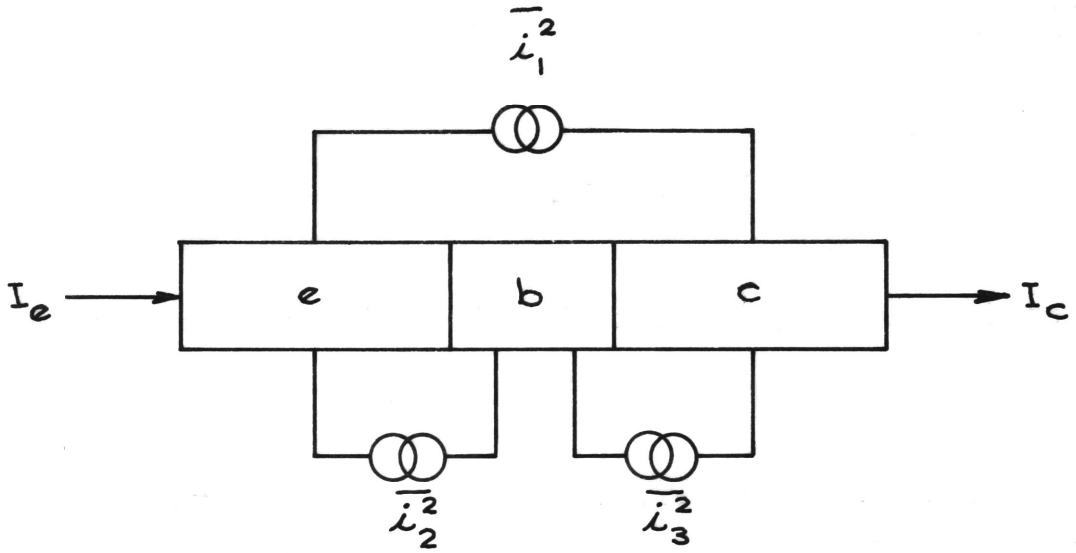

FIG. 2·15 NOISE GENERATORS OF TRANSISTORS

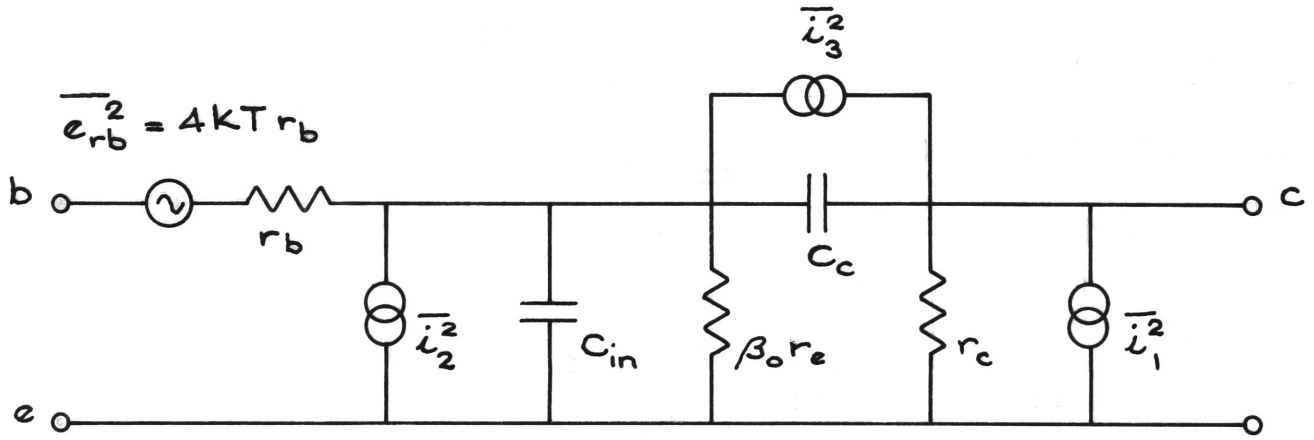

FIG. 2·16 EQUIVALENT NOISE CIRCUIT OF TRANSISTOR

increases and also a further noise source is added, due to induced currents flowing into the grid. This additional noise source is approximated by a noise current [refer Aldous (1961)] of

$$\overline{i_{g_2}^2} = 4kT_k \times 1.43\, g_i . \tag{2.53}$$

This is illustrated in Fig. 2.14.

2.2.3 Noise in junction transistors

The noise currents are those of the two diode junctions forming the transistor. [Refer to Van der Ziel (1958), Van der Ziel and Becking (1958)]. A noise model of the intrinsic transistor is shown in Fig. 2.15 where

I_e = emitter current,

I_c = collector current,

I_{c_0} = collector base leakage current,

$\bar{\alpha}$ = d.c. current gain,

I_b = base current.

We then have

$$\overline{i_1^2} = 2q\bar{\alpha}\, I_e = 2q\, I_c \text{ for } I_{c_0} \ll I_c \text{ and } \bar{\alpha} \simeq 1 \tag{2.54}$$

$$\overline{i_2^2} = 2q(I_b + I_{c_0}) \tag{2.55}$$

$$\overline{i_3^2} = 2q\, I_{c_0} . \tag{2.56}$$

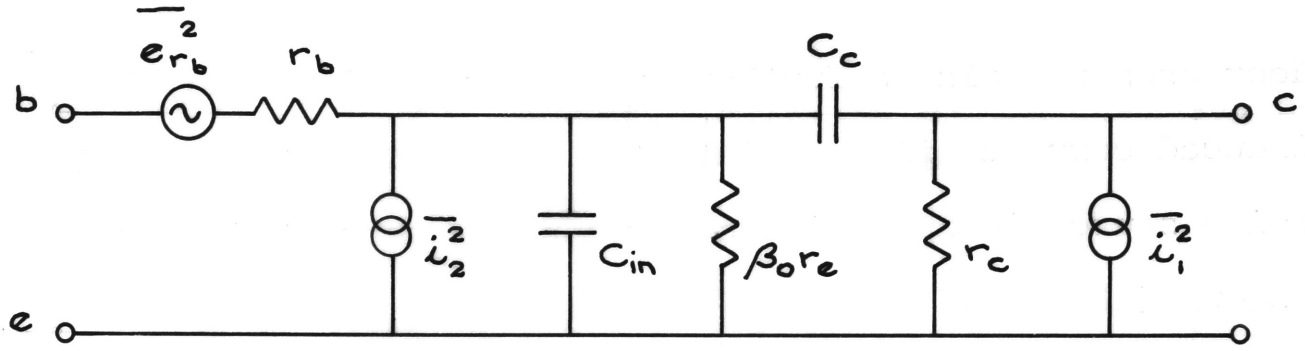

FIG. 2·17 TRANSISTOR NOISE CIRCUIT

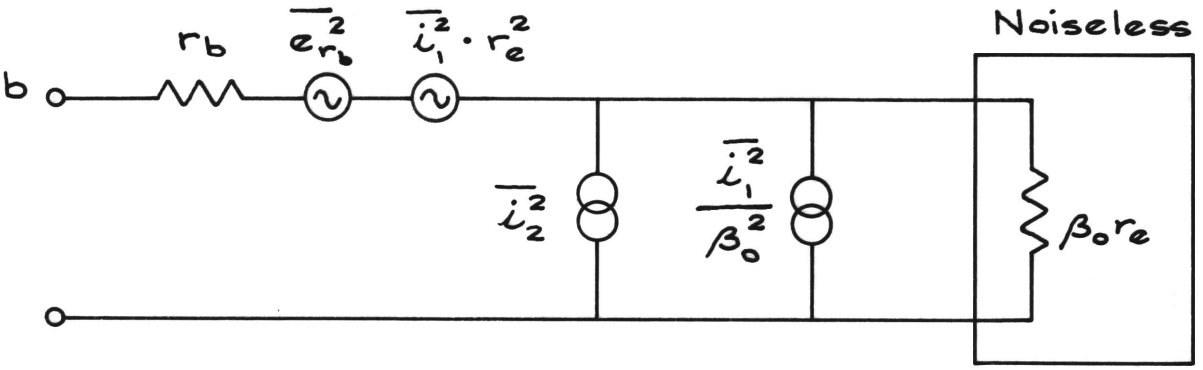

FIG. 2·18 TRANSISTOR NOISE CIRCUIT
IN STANDARD FORM

Sec. 2.2

The equivalent circuit including the extrinsic base resistance r_b is given in Fig. 2.16 (β_0 is the small signal low frequency common emitter current gain). Flicker noise generators are not included in Fig. 2.16. For silicon transistors the leakage term I_{c_0} may be neglected in equations (2.54), (2.55) and (2.56). The noise circuit (Fig. 2.16) for silicon transistors then becomes that of Fig. 2.17.

The equivalent noise circuit in the standard form of Fig. 2.2(c) is then as shown in Fig. 2.18. The capacitances have been omitted as we are not interested in the higher frequency noise performance at this stage. The generators shown indicate mean square values.

The combined voltage generator

$$\overline{e^2} \equiv \overline{e_{rb}^2} + \overline{i_1^2}\, r_e^2$$

$$= \overline{e_{rb}^2} + 2q\, I_c r_e^2 \qquad (2.57)$$

by substitution from equation (2.54).

The combined current generator

$$\overline{i^2} \equiv \overline{i_2^2} + \frac{\overline{i_1^2}}{\beta_0^2}$$

$$= 2qI_b + \frac{2qI_c}{\beta_0^2} \qquad (2.58)$$

by substitution from equations (2.54) and (2.55). The

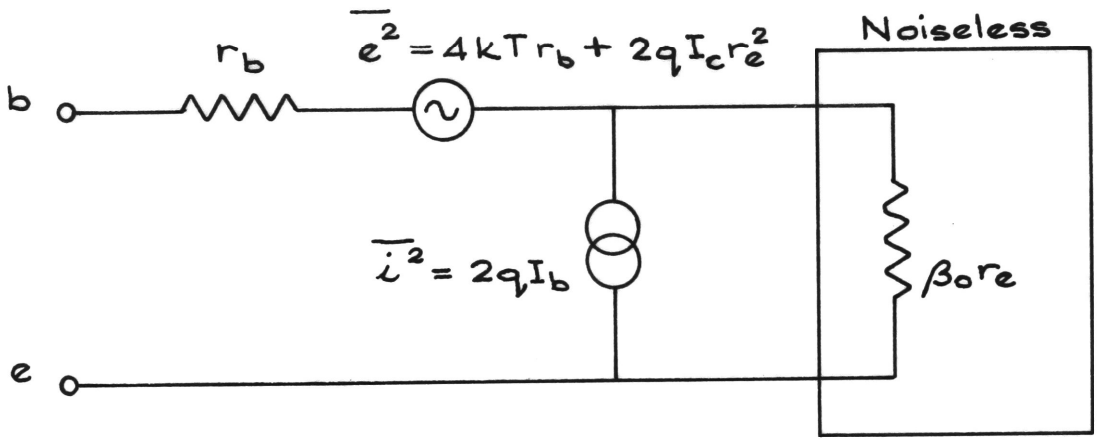

FIG. 2·19 SIMPLIFIED LOW FREQUENCY TRANSISTOR NOISE CIRCUIT

second term of equation (2.58) is much less than the first and it will be neglected.

The final low frequency noise equivalent circuit (neglecting flicker noise) is shown in Fig. 2.19. In contrast to valve equivalent circuits, the current source of transistor equivalent circuits is reasonably well defined and low noise equivalent circuits for transistors (excluding flicker noise) are more predictable than is the case for valves.

It is assumed that the generators of Fig. 2.19 are uncorrelated. This is a reasonable assumption because Crawford (1965) has shown that at low emitter currents the correlation coefficient K is given by $K = 1/\sqrt{\beta}$ which is small. The results of Section 2.1.7 can now be applied to Fig. 2.19. For example when the input signal voltage is proportional to $R_s^{\frac{1}{2}}$, minimum noise to signal ratio is obtained for the value of R_s corresponding to equation (2.15) viz.

$$R_s = \frac{1}{G_s} = \left(\frac{\overline{i_u^2}}{\overline{v^2}} + G_{cor}^2 \right)^{-\frac{1}{2}}$$

$$= \sqrt{\frac{\overline{v^2}}{\overline{i_u^2}}} \quad \text{because } G_{cor} = 0.$$

Sec. 2.2

The following values for $\overline{v^2}$, $\overline{i_u^2}$ taken from Fig. 2.19 are $\overline{v^2} = \overline{e^2} = 4kTr_b + 2qI_c r_e^2$ and $\overline{i_u^2} = \overline{i^2} = 2qI_b$. On substituting these values, we find that

$$R_s = \sqrt{\frac{4kTr_b + 2qI_c r_e^2}{2qI_b}}$$

$$= \sqrt{\frac{4kTr_b}{2qI_b} + \frac{I_c r_e^2}{I_b}} \quad .$$

If now we let $I_c/I_b \simeq \beta$, then

$$R_s = \sqrt{\frac{4kTr_b}{2qI_b} + \beta r_e^2} \quad .$$

$$\therefore \quad R_s \simeq r_e\sqrt{\beta}$$

because $\frac{4kTr_b}{2qI_b}$ is $<<$ βr_e^2 in the low noise region.

The noise factor F of the transistor follows from the definition of F given in equation (2.8) by substituting the thermal noise $4kTG_s$ for $\overline{i_1^2}$ and for $\overline{i_s^2}$ in equation (2.12). The result is given by

$$F = 1 + \frac{\overline{i_u^2} + \overline{v^2}\left((G_s + G_{cor})^2 + (B_s + B_{cor})^2\right)}{4kTG_s}.$$

Sec. 2.2

As the generators of Fig. 2.19 are uncorrelated $G_{cor} = B_{cor} = 0$. Furthermore, at the low frequencies considered $B_s = 0$.

$$\therefore \quad F = 1 + \frac{\overline{i_u^2} + \overline{v^2}\, G_s^2}{4kTG_s} .$$

Letting $R_s = 1/G_s$, we find that

$$F = 1 + \frac{\overline{i_u^2}\, R_s^2 + \overline{v^2}}{4kTR_s} . \qquad (2.61)$$

On substituting in equation (2.61) the following values for the generators as shown in Fig. 2.19

$$\overline{i_u^2} = \overline{i^2} = 2qI_b$$

and $$\overline{v^2} = \overline{e^2} = 4kTr_b + 2qI_c r_e^2$$

and also substituting for R_s its optimum value $R_s = r_e\sqrt{\beta}$ from equation (2.60) we find that equation (2.61) becomes

$$F_{min} = 1 + \frac{4kTr_b + 2qI_c r_e^2 + 2qI_b r_e^2 \beta}{4kTr_e\sqrt{\beta}} .$$

Substituting $\beta I_b = I_c$ gives

$$F_{min} = 1 + \frac{r_b}{r_e\sqrt{\beta}} + \frac{qI_c r_e}{kT\sqrt{\beta}} . \qquad (2.62)$$

Sec. 2.2

On substituting $r_e = \frac{kT}{qI_c}$, equation (2.62) becomes

$$F_{min} = 1 + \frac{r_b}{r_e\sqrt{\beta}} + \frac{1}{\sqrt{\beta}} . \qquad (2.63)$$

To obtain low noise operation the transistor must have high β and be operated at low current. Also r_b should be small.

To a first approximation the frequency response is given by

$$\omega_{(3db)} = \frac{\omega_\alpha}{\beta}$$

where ω_α = transistor α cut off frequency. Therefore the requirements of low noise operation limit the frequency response.

We now consider transistor noise at high frequencies. Since the input impedance of the transistor decreases with frequency the noise current generator $\frac{\overline{i_1^2}}{\beta_0^2}$ of Fig. 2.18 must be increased to maintain the noise $\overline{i_1^2}$ at the output. This current generator becomes

$$\overline{i^2} = \frac{\overline{i_1^2}\, r_e^2}{|Z_{in}|^2} \qquad (2.64)$$

where Z_{in} is the input impedance at the base (which is

a resistance βr_e in parallel with an input capacitance C_{in}, for resistive collector loads). The output generator $\frac{\overline{i_1^2}}{\beta_0^2}$ must therefore be increased by the factor

$$\frac{\beta^2 r_e^2}{Z_{in}^2} = 1 + \beta^2 r_e \, \omega^2 C_{in}^2 \, . \qquad (2.65)$$

If Miller feedback capacitance is neglected (e.g. "cascode" operation)

$$C_{in} = \frac{1}{\omega_1 r_e}$$

where ω_1 is the gain bandwidth product of the transistor and the above factor becomes equal to

$$\left[1 + \left(\frac{\beta\omega}{\omega_1}\right)^2\right]. \qquad (2.66)$$

The flicker noise of the best available transistors starts to become significant at about 1000 Hz.

2.2.4 Comparison of valves and transistors

The voltage noise source of the valve can be of the same order as the voltage noise source of the transistor for high G_m valves. This can be seen by comparing the valve noise voltage generator of equation (2.38b) with the transistor voltage noise generator $e^2 = 4kTr_b + 2qI_c r_e^2$ of Fig. 2.19.

The equivalent current noise source of a valve is

generally much less than the current noise source of the transistor. (Grid current is much less than base current). It follows, therefore, that the optimum source impedance required for minimum noise figure (signal input $\propto \sqrt{R_s}$) is higher for the valve than for the transistor.

For constant voltage inputs, where a transformer cannot be used, the valve and transistor can give the same performance if high G_m valves are used.

For constant current inputs the valve will give better performance than the transistor because its noise current is lower.

2.2.5 Noise in field effect transistors

In insulated gate F.E.T.'s the flicker noise predominates up to very high frequencies and these devices are not yet useful for low noise circuits. However, junction F.E.T.'s are relatively low noise devices and their noise characteristics will now be discussed.

(i) F.E.T. Thermal noise Van der Ziel (1962) shows that the limiting noise in an F.E.T. is due to thermal noise in the conducting channel. He states that a good approximation for the thermal noise of all types of F.E.T. is given by

$$\overline{i_t^2} = 4kT \times \frac{2}{3} g_m \, df \qquad (2.67)$$

where g_m = mutual conductance.

Sec. 2.2

(ii) F.E.T. Gate Current noise The gate current of a junction F.E.T. is the leakage current of the reverse biased diode forming the gate to channel control system. It therefore contributes full shot noise which is expressed by Van der Ziel (1962) as

$$\overline{i_g^2} = 2e(I_{g1} + I_{g2})df \qquad (2.68)$$

where

$-I_{g1}$ = current due to holes arriving at the gate and electrons leaving the gate.

I_{g2} = current due to holes leaving the gate and electrons arriving at the gate.

The nett gate current $I_g = -I_{g1} + I_{g2}$. Sevin (1965) states that the gate current of silicon junction F.E.T.'s is generally in the range 10^{-8} to 10^{-10}A. Data sheet figures for three types are given in Table 2.1.

Table 2.1 F.E.T. Characteristics

Type	Material	Typical g_m (mA/V)	I_g 25°C A	65°C	150°C
TIX m301	Germanium	10	6×10^{-6}		
2N4360	Silicon	4	1×10^{-9}	2×10^{-8}	
2N3823	Silicon	4	2×10^{-11} (Selected units 2×10^{-12}		3×10^{-8}

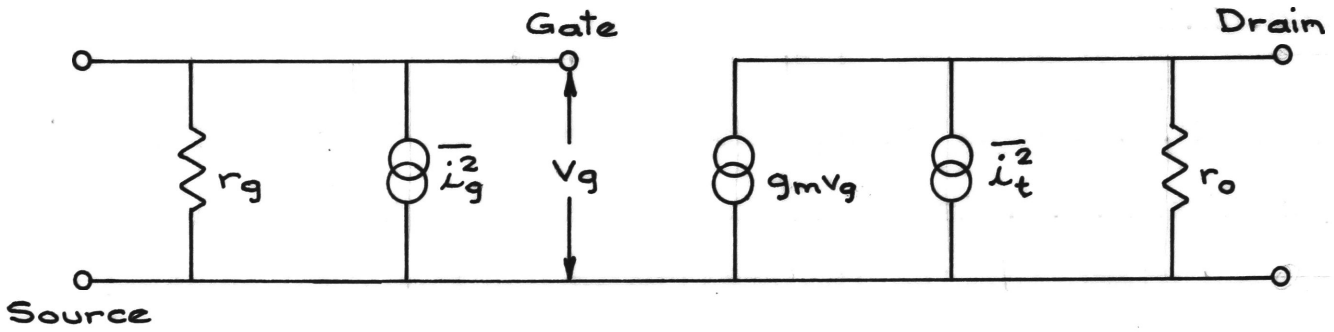

FIG. 2·20 NOISE GENERATORS OF FIELD EFFECT TRANSISTOR

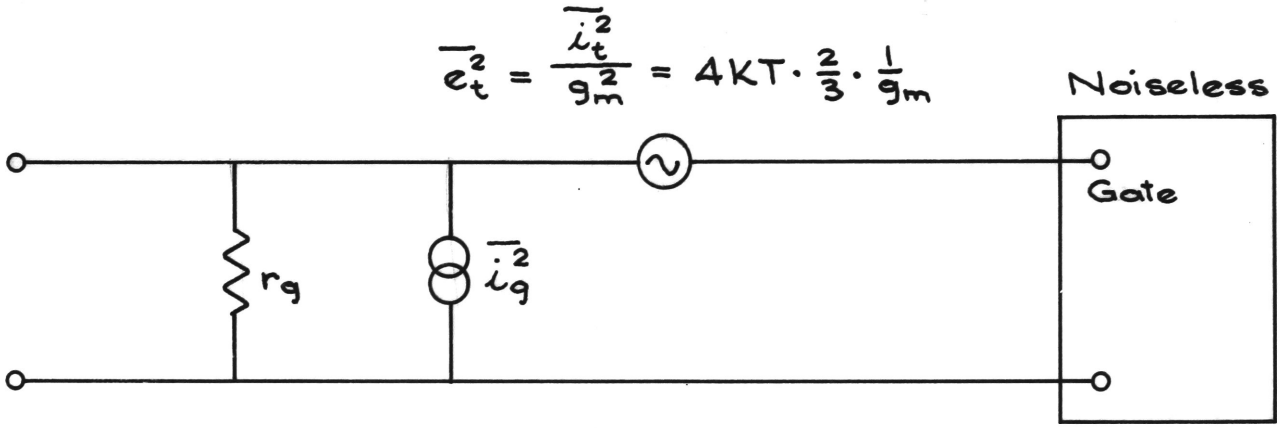

FIG. 2·21 EQUIVALENT NOISE CIRCUIT OF F.E.T.

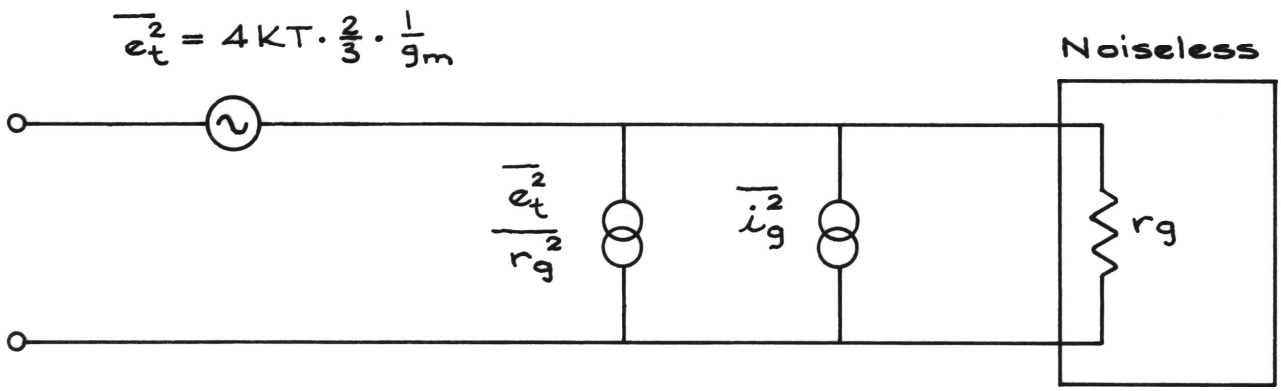

FIG. 2·22 NOISE CIRCUIT OF F.E.T. IN STANDARD FORM

The gate currents of the silicon devices are less than valve grid currents at normal ambient temperatures. One advantage of F.E.T.'s is that, unlike the valve, operation at low temperatures is possible with consequent reduction in both thermal and gate current noise.

(iii) Equivalent Circuit The low frequency equivalent circuit of the F.E.T. (neglecting flicker noise) is given in Fig. 2.20. The noise equivalent circuit with both noise generators at the input is given in Fig. 2.21.

The noise equivalent circuit in the standard form of Fig. 2.2(c) follows from Fig. 2.21 and is shown in Fig. 2.22. Note that there is full correlation between the current source $\frac{\overline{e_t^2}}{r_g^2}$ and the voltage source $\overline{e_t^2}$. For source impedances very much less than r_g the current source $\frac{\overline{e_t^2}}{r_g^2}$ may be neglected. The results of Section 2.1.7 can now be applied to Fig. 2.22. The problem is similar to that already worked out for the valve and transistor. Specifically when the appropriate values of noise generators for the F.E.T. are substituted into equation (2.15) the source impedance for a minimum noise figure is given by

Sec. 2.2

$$R_s = \sqrt{\frac{\overline{e_t^2}}{\overline{i_g^2} + e_t^2/r_g^2}} \qquad (2.69)$$

If $r_g \to \infty$ then

$$R_s = \sqrt{\frac{\overline{e_t^2}}{\overline{i_g^2}}}$$

$$= \sqrt{\frac{4kT\,\frac{0.66}{g_m}}{2eI_g'}} \qquad (2.70)$$

where I_g' is the sum of the absolute values of the components of gate current. If the typical values $g_m = 4mAV^{-1}$ and $I_g' = 2 \times 10^{-11}A$ are substituted in equation (2.70) we find $R_s \simeq 600\ k\Omega$.

Of the other categories of noise, flicker noise of good junction F.E.T.'s starts to become important at about 100 Hz while high frequency noise is discussed in the next paragraph.

As the frequency increases the input current generator $\frac{\overline{e_t^2}}{r_g^2}$ must be increased to supply the noise $\overline{i_t^2}$ at the output. The frequency effect sought

is one which increases the input noise generators to maintain the noise output current at i_t despite increasing frequency. It is seen that the only modification required to Fig. 2.22 is to change the current source from $\overline{e_t^2}/r_g^2$ to $\overline{e_t^2}/|Z_g|^2$ where Z_g is the input impedance at the gate. At intermediate frequencies with resistive drain load this input impedance is given by a capacitance C_{in} shunting the input gate resistance, in which case

$$\frac{\overline{e_t^2}}{|Z_g|^2} = \frac{\overline{e_t^2}}{r_g^2} (1 + r_g^2\omega^2 C_{in}^2) . \qquad (2.71)$$

2.2.6 Comparison of transistors, valves and F.E.T.'s

The equivalent input noise voltage generator can be of the same order for all devices at room temperature. Equivalent performance is therefore expected when fed from constant voltage sources. The equivalent input noise current generator decreases in the order transistor, valve, F.E.T. It follows that the optimum source impedance for minimum noise figure increases in the same order.

If fed from a current source the valve and F.E.T. give better performance than the transistor. The F.E.T. can be cooled to give lower noise than the valve.

Chapter 3

IMAGING PHOTON DETECTORS

Sec. 3.1

3.1 Introduction

The work described in this chapter is summarized in the following paragraphs.

Firstly an expression [equation (3.6)], describing the limitations of perfect linear photon detectors due to random detection processes is derived. This equation specifies a limit of detection due only to random photon noise where the detector is assumed to have an ideal contrast modulation response extending to any arbitrarily high spatial frequency. This limit is useful as it represents an upper bound to the performance of practical detectors and it is given in terms of resolution, scene contrast, integration time, detector quantum efficiency and total light flux available to the detector for a given signal to noise ratio.

For practical vidicon detectors an expression for the limiting detectable contrast at low spatial frequencies is determined by comparing the signal output from the vidicon for low spatial frequencies to the noise as deduced from the noise theory of Chapter 2. The performance at any spatial frequency can then be determined from the contrast modulation response of the device which has been found experimentally as described in Chapter 4.

Two numerical examples given at the end of Chapter 3

illustrate the procedure for determining the limiting performance of an infrared vidicon and a visible spectrum vidicon as a function of spatial frequency.

Noise current of the vidicon circuit with a valve amplifier is calculated using the theory developed in Chapter 2 and the experimentally measured parameters of the camera described in Chapter 4.

This is followed by the derivation of an expression for the signal current from the vidicon as a function of the change in stored charge on the vidicon target due to photoconductivity induced by the light input. The charge required to produce a signal current equal to three times the r.m.s. noise current is given by equation (3.21) for a linear vidicon and by equation (3.23) for a non-linear vidicon.

Expressions for the lower limit of detectable contrast, due to the limited charge storage of the vidicon target, are given by equation (3.25) and (3.26) for typical linear and non linear vidicons respectively. The implications of these expressions are discussed.

A comparative summary of performance is given for a perfect detector, the image converter, and the infra-red vidicon at 1083 nm and for the visible vidicon at 656 nm.

Finally the spatial frequency response and its connection with the flux-contrast relations are discussed.

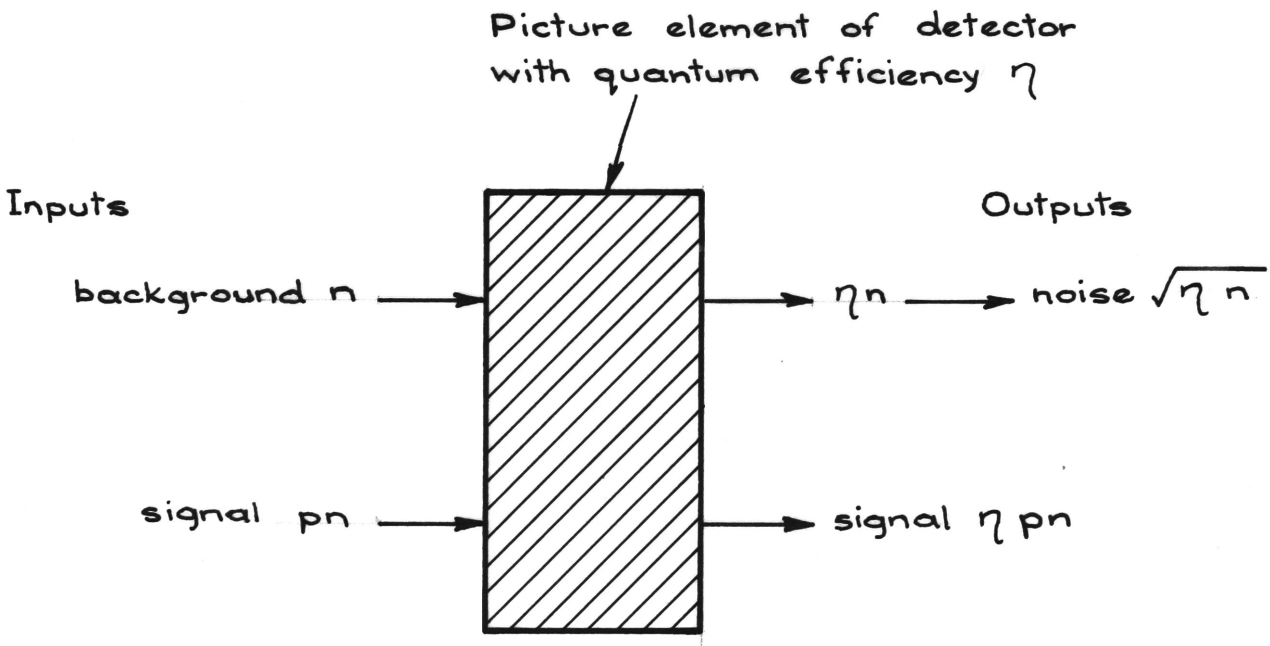

FIG. 3·1 IDEAL ELEMENTARY PHOTON DETECTOR

3.2 Fundamental Limitation of Linear Photon Detectors

Before considering other limitations imposed by the special physical characteristics of various photon detectors, the fundamental limitation due to the random nature of the detection process will be discussed. The signal obtained from the initial photon detector must be amplified to a useful level. In the ideal case, amplification should be effected by means such that photon noise exceeds circuit or device noise at all stages in the system.

The prime interest in this study is the detection of low contrast, low brightness scenes with limited integration time and with high resolution. Consider a scene which delivers a total number of n photons to each picture element of the detector area in the integration time t. Let one particular picture element in this scene receive an additional number of photons pn, (for low contrast p is small). It is required to detect this picture element against the background.

For simplicity assume that the input photon flux from the scene is constant. The situation is illustrated in Fig. 3.1. The background photons n give an output of ηn events where η is the quantum efficiency of the detector.

Sec. 3.2

Because of the random nature of photon detection, this output has an r.m.s. noise of $\sqrt{\eta n}$ events. The signal input pn gives a signal output of ηpn events. Therefore,

$$\frac{\text{Signal output}}{\text{Noise output}} = \frac{\eta pn}{\sqrt{\eta n}} = p\sqrt{\eta n}. \tag{3.1}$$

Schade (1962) has made measurements on the detectability of isolated objects displayed against uniform backgrounds and finds that a signal to noise ratio of three gives a detection probability of about eighty per cent. On substituting the value three for the signal to noise ratio equation (3.1) becomes

$$p^2 \eta n = 9 \tag{3.2}$$

$$\text{or} \quad n = 9/p^2\eta. \tag{3.3}$$

This expression gives the minimum number of photons required per picture element of the scene for reliable detection when the contrast is p. If the resolution obtained corresponds to a total of m picture elements and the total flux to the whole picture area of the detector is ϕ_T photons/second, it follows that

$$n = \phi_T t/m \tag{3.4}$$

where t is the integration time. Substituting for n

from equation (3.4) into equation (3.3) gives

$$\frac{\phi_T t}{m} = \frac{9}{p^2 \eta}$$

$$\text{i.e.} \quad \phi_T = \frac{9m}{p^2 \eta t} \quad . \tag{3.5}$$

It is seen from (3.5) that for a given flux (ϕ_T) high resolution requires long integration time. The integration time is usually limited by seeing conditions in astronomical applications or by the requirement to record fast changing dynamic scenes.

Now let t be fixed ($t = t_1$) by either of these conditions; then

$$\phi_T = \frac{9m}{p^2 \eta t_1} \quad . \tag{3.6}$$

For a linear detector limited by random photon noise only, this expression gives the minimum light flux required to detect reliably a scene of contrast p with resolution m, integration time t_1 and detector quantum efficiency η.

From equation (3.6) we have

$$\frac{m}{p^2} = \frac{\phi_T \eta t_1}{9} \quad . \tag{3.7}$$

It is seen from this equation that the performance of the ideal linear detector does not depend upon its area, as it is assumed that the total integrated flux can be read out in some manner such as to provide an output which is independent of flux density. For practical detectors there exist limitations to the area of the detector set by the following considerations.

(1) Optical efficiency and permissible abberation in coupling the flux from the scene to the detector.

(2) Noise level of the detector (Granularity of photographic films, electrical noise of tubes).

(3) Limiting resolution of the detector and readout mechanism.

(4) The nonlinearity of the output versus light intensity transfer characteristic of the detector.

In practice there will be an optimum area for the detector determined by the above factors. The equation (3.7) is useful in that it defines a limit which cannot be bettered by any practical detector. De Haan (1960) gives a more detailed analysis which includes input photon noise and various cascaded arrangements used to process the signal. He shows that in all cases the signal to noise ratio cannot be better than that determined solely by the quantum efficiency of the initial detector alone.

3.3 Signal to Noise Performance of the Vidicon

This discussion is related to the limiting performance of the vidicon and consequently a simple derivation of vidicon signal current is given which ignores factors of minor importance. The noise contributed by the vidicon is assumed to be only the shot noise of the dark current (typically 100 nA). Cooling of the vidicon as a means of decreasing the dark current is not considered due to probable increase in target lag. The other sources of noise are the vidicon load resistor and the video amplifier. Types of amplifier and operating conditions are discussed which best illustrate the limits of performance of conventional devices.

3.3.1 The vidicon and camera circuit

The vidicon is essentially a constant current source and it has been shown in Section 2.1.7 (Case 3) that any conductance shunting such a source decreases the signal to noise ratio. The conductance concerned is the conductance G_s of the vidicon load resistor R_s. A high value of R_s increases the signal to noise ratio but decreases the bandwidth of the input circuit.

The falling response of the input circuit due to a high value of R_s is compensated by shaping the amplifier

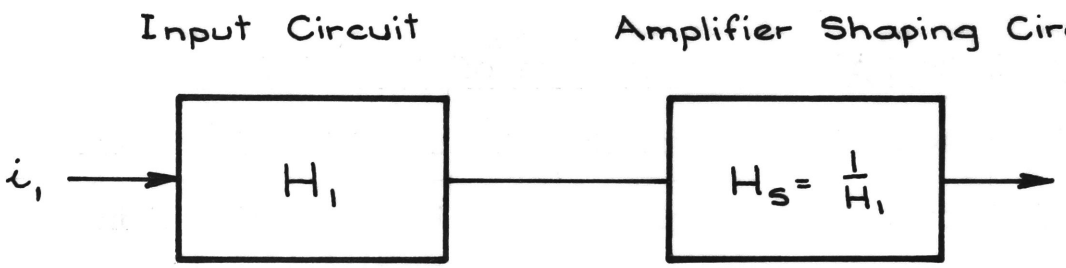

FIG. 3·2 BLOCK DIAGRAM OF CAMERA CIRCUIT

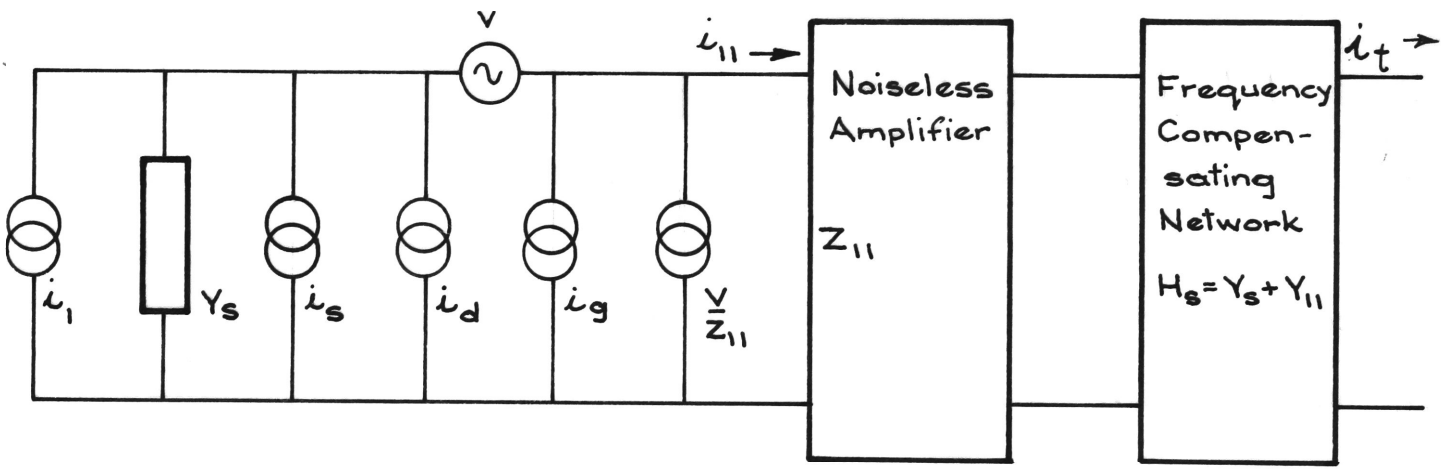

FIG. 3·3 EQUIVALENT NOISE CIRCUIT OF VIDICON AND AMPLIFIER

response so that a substantially flat frequency response is obtained over the bandwidth of 8 MHz, which is sufficient for a resolution of approximately 10^5 picture elements. A practical limit for the compensating increase in gain at high frequencies is about fifty times and this limits the maximum value of R_s to $R_s C_T = \frac{50}{\omega_1}$ where C_T = input circuit capacitance and ω_1 = maximum angular frequency.

Fig. 3.2 shows the signal input current i_1 entering the input circuit which has a transfer function H_1 followed by the amplifier shaping circuit with the inverse transfer function $H_s = \frac{1}{H_1}$ so that the overall transfer function H equals $H_1 \times \frac{1}{H_1} = 1$ and the system thus has a flat frequency response.

3.3.2 Noise of the vidicon circuit

The noise equivalent circuit of the vidicon and amplifier is shown in Fig. 3.3 in the standard form of Fig. 2.4.

From equation (2.10) of Section 2.1.7 the total noise current is given by

$$\overline{i_{11}^2} = \frac{\left(\overline{i_s^2} + \overline{i_d^2} + \overline{i_g^2}\right)|Y_{11}|^2}{|Y_s + Y_{11}|^2} + \frac{\overline{v^2}|Y_s + Ycor|^2 . |Y_{11}|^2}{|Y_s + Y_{11}|^2} \qquad (3.8)$$

where

i_1 = signal input current from vidicon,

Y_s = source admittance (resistive load of vidicon in parallel with total output capacitance of vidicon and input circuit),

i_s = thermal noise current of G_s,

i_d = noise current due to dark current (I_d) of vidicon,

i_g = uncorrelated part of amplifier noise current generator,

v = noise voltage of input circuit,

v/Z_{11} = correlated part of amplifier noise current generator,

Z_{11} = input impedance of the noiseless amplifier,

$Y_{11} = 1/Z_{11}$.

∴ The mean square noise voltage is given by

$$\overline{v_{11}^2} = \frac{\overline{i_{11}^2}}{|Y_{11}|^2} = \frac{\overline{i_s^2} + \overline{i_d^2} + \overline{i_g^2}}{|Y_s + Y_{11}|^2} + \frac{\overline{v^2}|Y_s + Ycor|^2}{|Y_s + Y_{11}|^2} \cdot \qquad (3.9)$$

Substituting $Y_s = G_s + j\omega C_s$,

$Y_{11} = j\omega C_{in}$, (neglect input conductance)

$Ycor = j\omega C_{in}$,

and $C_T = C_s + C_{in}$

gives

$$\overline{v_{11}^2} = \frac{\overline{i_d^2} + \overline{i_g^2} + \overline{i_s^2}}{G_s^2 + \omega^2 C_T^2} + \overline{v^2} \cdot \qquad (3.10)$$

Sec. 3.3

The output noise current i_t of the network of Fig. 3.3 follows by applying the general relation (Schwartz and Friedland (1965)).

$$\overline{i_t^2} = \frac{1}{2\pi}\int |H_s(\omega)|^2 \; W_x(\omega)\, d\omega$$

where $\overline{i_t^2}$ = mean square output response.

$H_s(\omega)$ = transfer function of system.

$W_x(\omega)$ = spectral power density of input noise = $\overline{v_{11}^2}$

$$\therefore \quad \overline{i_t^2} = \frac{1}{2\pi}\int_0^{\omega_1} \left[G_s^2 + \omega^2 C_T^2\right] \left[\frac{\overline{i_d^2} + \overline{i_g^2} + \overline{i_s^2}}{G_s^2 + \omega^2 C_T^2} + \overline{v^2}\right] d\omega \quad (3.11)$$

$$= \frac{1}{2\pi}\left[\overline{i_d^2} + \overline{i_g^2} + \overline{i_s^2} + \overline{v^2}G_s + \frac{\overline{v^2}C_T^2\omega^3}{3}\right]_0^{\omega_1} \quad (3.12)$$

$$= \overline{i_d^2} f_1 + \overline{i_g^2} f_1 + \overline{i_s^2} f_1 + \overline{v^2}G_s^2 f_1 + \frac{\overline{v^2}C_T^2(2\pi)^2 f_1^3}{3} \quad (3.13)$$

The values of the parameters of the vidicon camera used in the experimental work described in Chapter 4 are as follows:-

Vidicon dark current $i_d = 100$ nA

Vidicon load resistance $R_s = 0.13\ M\Omega$

Vidicon load conductance $G_s = (R_s)^{-1} = 7.7 \times 10^{-6}\Omega^{-1}$.

Sec. 3.3

Input Capacitance	$C_T = 25$ pF
Temperature	$T = 290$ K
Bandwidth	$f_1 = 8$ MHz
Mutual conductance of input valve	$g_m = 10^{-2}\Omega^{-1}$
Grid current of input valve	$I_s = 100$ nA .

Substituting these values into equation (3.13) and using equation (2.38) viz. $\overline{v^2} = 4kT_0 \times \frac{2.2}{g_m}$,the five terms of equation (3.13) become

(1) $\overline{i_d^2} f_1 = 2q I_d f_1 = 0.25 \times 10^{-18} A^2$

(2) $\overline{i_g^2} f_1 = 2q I_g f_1 = 0.25 \times 10^{-18} A^2$

(3) $\overline{i_s^2} f_1 = 4kTG_s f_1 = 1 \times 10^{-18} A^2$

(4) $\overline{v^2} G_s^2 f_1 = 4kT \times \frac{2.2}{g_m} . G_s^2 f_1 = 0.0017 \times 10^{-18} A^2$

(5) $\frac{\overline{v^2} C_T^2 (2\pi)^2}{3} . f_1^3 = \frac{4kT_0 \times 2.2}{3g_m} . C_T^2 (2\pi)^2 f_1^3 = 15 \times 10^{-18} A^2$.

The total mean square noise current obtained by adding these five terms is $\overline{i_t^2} = 16.5 \times 10^{-18} A^2$.

$$\therefore \quad i_t = 4.1 \text{ nA (rms)} . \qquad (3.14)$$

Inspection of the five noise terms shows that, at the bandwidth of 8 MHz, shot noise [term (5)] predominates. The bandwidth f' for which the shot noise contribution is equal to the sum of all the other noise terms is given by

Sec. 3.3

$15 \times \frac{f'^3}{8^3} = 1.5 \frac{f'}{8}$. That is f' = 2.5 MHz. The total noise at this bandwidth is

$$i'_t = 0.94 \text{ nA (rms)} \quad . \tag{3.15}$$

Now consider the effect of cooling the input resistor to 78 K to reduce the thermal noise [term (3)]. The bandwidth f'(78) at this temperature for which the shot noise equals the sum of all other terms is given by

$$15 \times \frac{(f'(78))^3}{8^3} = 0.77 \frac{f'(78)}{8} \quad .$$

That is f'(78) = 1.8 MHz. The total noise would then be given by

$$i'_t(78) = 0.6 \text{ nA (rms)} \tag{3.16}$$

It is seen that cooling the input resistor of a valve amplifier is worthwhile only for a narrow bandwidth system which would be well below the resolution capability of the vidicon.

These results are at variance with those of Gebel (1962), who neglects valve noise compared to thermal noise of the vidicon load resistor at 78 K for a bandwidth of 4 MHz. This approximation of Gebels conflicts with the noise theory presented in Chapter 2 of this thesis and it is not supported by the experimental results reported in Chapter 4.

3.3.3 Vidicon Output Signal

To derive the output signal from the vidicon at low spatial input frequencies, consider firstly the limiting case of zero spatial frequency where the whole target area is illuminated with a uniform flux density.

Let this illumination discharge the vidicon target by a total of Q_T coulombs in the scan time t_f. The output current from the target is in this case given by the steady value

$$i = \frac{Q_T}{t_f} \tag{3.17}$$

If the illumination is now slightly increased and the total discharge of the target increases to $Q_T + \Delta Q_T$ the target output current becomes the steady value

$$i' = \frac{Q_T + \Delta Q_T}{t_f}$$

Therefore in order to detect the change in illumination we must detect the difference between these currents which corresponds to detecting signal current given by

$$i_l = i' - i = \frac{\Delta Q_T}{t_f} \tag{3.18}$$

Equation (3.18) holds at all spatial frequencies for which the contrast modulation response has not decreased from its value at low spatial frequency.

To illustrate this point assume that a small area a has the higher illumination and the rest of the target area A has a slightly lower illumination. Let the discharge over A be Q_T coulombs during the total scan time t_f and the discharge over a be $Q_T \cdot (\frac{a}{A}) + dq$ in the time taken to scan area a, that is $t_f \cdot \frac{a}{A}$. The signal current corresponding to the difference in target current for these two areas is given by

$$i = \frac{Q_T \cdot (\frac{a}{A}) + dq}{t_f \cdot (\frac{a}{A})} - \frac{Q_T}{t_f} = \frac{dq \cdot (\frac{A}{a})}{t_f} = \frac{\Delta Q_T}{t_f} \qquad (3.18\ a)$$

where ΔQ_T would be the total change in target charge if the whole area A had the increased illumination.

3.3.4 Vidicon transfer characteristics

The relation between the output response of a vidicon and the input light flux to it is called the vidicon transfer characteristic.

The form of this relation depends upon the particular interactions occuring between the input light and the photoconductor which are determined by the input light intensity and the distribution of electronic trap and recombination centres within the photoconductor. Although a wide range of transfer characteristics is formally

possible commercially available vidicons fall into two classes.

At normal input light levels one class has a linear relation between the output response and input light flux whereas the other class has a nonlinear relation between these quantities such that the slope of the curve obtained by plotting the logarithm of the output response against the logarithm of the input light flux is a constant γ which has a value of about 0.6.

(a) Linear vidicon

The transfer characteristic of the linear vidicon can be described by

$$Q_T = \theta.B.A.t_f \qquad (3.19)$$

where Q_T = the total change in target stored charge due to light input in coulombs.

θ = effective quantum efficiency in coulombs per photon.

B = input flux density in photons per second per square centimetre.

A = scanned area of target in square centimetres.

t_f = frame integration time in seconds.

Differentiating equation (3.19) with respect to input flux density gives

$$\frac{dQ_T}{dB} = \theta.A.t_f .$$

On substituting dB = pB where p is the contrast (assumed small), we see that

$$\Delta Q_T = \theta . A . t_f . pB = pQ_T \, . \qquad (3.20)$$

To detect this signal reliably (signal to noise ratio of 3:1) equation (3.18) gives $\Delta Q_T / t_f = 3i_t$ where i_t is the total noise current. Then from equation (3.20)

$$Q_T = 3i_t . t_f / p \, . \qquad (3.21)$$

(b) Non linear vidicon

The slope of the curve log Q_T plotted against log B is approximately a constant (denoted by γ) over the normal operating range of the vidicon,

i.e. $$\frac{d(\log Q_T)}{d(\log B)} = \gamma$$

$$\frac{\frac{1}{Q_T} . dQ_T}{\frac{1}{B} . dB} = \gamma \, .$$

On substituting dB = pB for a low contrast scene

$$\Delta Q_T = \gamma Q_T \frac{pB}{B} = p\gamma Q_T \, . \qquad (3.22)$$

The signal current from equation (3.18) is $i_1 = \Delta Q_T / t_f$. Allowing this to equal three times the noise current gives

$$\frac{p\gamma Q_T}{t_f} = 3i_t$$

$$\text{or} \quad Q_T = \frac{3 i_t t_f}{p\gamma}. \tag{3.23}$$

3.3.5 Limit of detectable contrast for vidicons

The vidicon target can support only a limited amount of charge and the change in this charge caused by input light must be kept to a small fraction of the total stored charge to avoid excessive nonlinearity (changing γ) at high light input levels and loss of resolution due to "beam bending" effects. If the maximum change in stored charge is $Q_{T(max)}$ it follows that

$$Q_{T(max)} = cV_{max}$$

where c is the target capacitance (2 nF typically) and V_{max} is the change in voltage when an element of the target is discharged by the scanning beam. As an example let V_{max} = 5V which ensures that for a typical target supply of 30V the response is still reasonably linear.

Then $Q_{T(max)} = 10$ nC. (3.24)

Sec. 3.3

The limit of detectable contrast $p_{(min)}$ for the linear vidicon is found from equations (3.21) and (3.24).

Thus $$Q_T = Q_{T(max)} = \frac{3i_t.t_f}{p(min)}$$

$$p_{(min)} = \frac{3i_t.t_f}{Q_{T(max)}} = \frac{3i_t.t_f}{10^{-8}} . \qquad (3.25)$$

Similarly the limit of detectable contrast for the non-linear vidicon follows from equations (3.23) and (3.24) viz.

$$p_{(min)} = \frac{3i_t.t_f}{\gamma \times 10^{-8}} . \qquad (3.26)$$

3.3.6 Cooled F.E.T. amplifier

The total noise current can be reduced by using cooled field effect transistor amplifiers. Two cases will be considered below.

(a) Germanium F.E.T. type TIXM12 cooled to 4 K

(b) Silicon F.E.T. type 2N3823 cooled to 78 K.

It has been shown by Elad and Nakamura (1967) that the mutual conductance of the germanium F.E.T. increases as the temperature is lowered right down to 4 K at which temperature the mutual conductance is about double the value at 290 K. The silicon F.E.T. also shows an increase in g_m as it is cooled down to 78 K after which the g_m

falls rapidly for lower temperatures. At 78 K the g_m of the silicon devices is about double that at 290 K. The characteristics of the F.E.T.'s are summarized below.

Type	Material	g_m 290 K	g_m 78 K	g_m 4 K	Input capac. + feedback capac.
TIXM12	Ge	5 000 20 000$\mu\Omega^{-1}$		10 000 40 000	19 pF
2N3823	Si	3 500 6 500$\mu\Omega^{-1}$	7 000 13 000		8 pF

The values which will be substituted into the noise terms of equation (3.13) are for the TIXM12, g_m = 20 000μ mhos at 4 K

C_T = 30 pF

and for the 2N3823, g_m = 10 000μ mhos at 78 K

C_T = 20 pF .

A capacitance of 5 pF is allowed for vidicon target capacitance and about 6 pF for wiring capacitance. It is assumed that a cascode input circuit is used so that Miller effect capacitance is negligible. The magnitude of f_1 is taken as 8 MHz and $\overline{v^2}$ is given by $\overline{v^2} = 4kT.\frac{2}{3}.\frac{1}{g_m}$ from equation (2.67) and relation $\overline{v^2} = \frac{\overline{i_t^2}}{g_m^2}$. On substituting these values for the TIXM12 the noise terms are:-

(1) $\overline{i_d^2}\, f_1 = 2qI_d f_1 = 0.25 \times 10^{-18}$A

Sec. 3.3

(2) $\overline{i_g^2}\ f_1 = 2qI_g f_1$ which is negligible as gate current is small at 4K.

(3) $\overline{i_s^2}\ f_1 = 4kTG_s f_1 = 0.014 \times 10^{-18}\ A^2$

(4) $\overline{v^2}G_s^2\ f_1$ which is negligible

(5) $\frac{\overline{v^2}C_T^2(2\pi)^2}{3} \times f_1^3 = \frac{4kT}{3} \times \frac{2}{3g_m} \times (2\pi)^2 \times C_T^2 \times f_1^3$

$= 0.11 \times 10^{-18}\ A^2.$

The total rms noise current for the G_e F.E.T. at 4 K is thus

$$i_t = 0.6 \text{ nA (rms)}. \qquad (3.27)$$

This noise value represents an improvement by a factor of about seven over the valve amplifier. The vidicon should, therefore, be capable of operating at a proportionately lower light input level or alternatively lower contrast scenes could be detected. However, at the lower light levels, the vidicon photoconductive lag may increase, so that the vidicon cannot respond as rapidly to fast changing scenes.

The noise terms for the silicon field effect transistor 2N3823 at 78 K are:-

(1) $\overline{i_d^2}\ f_1 = 2qI_d f_1 = 0.25 \times 10^{-18}\ A^2$

(2) $\overline{i_g^2}\ f_1 = 2qI_g f_1$ which is negligible as gate current is small

(3) $\overline{i_s^2}\, f_1 = 4kTG_s\, f_1 = 0.27 \times 10^{-18} A^2$

(4) $\overline{v^2} G_s^2\, f_1$ which is negligible

(5) $$\frac{\overline{v^2} C_T^2 (2\pi)^2}{3} \cdot f_1^3 = \frac{4kT}{3} \cdot \frac{2}{3g_m} \cdot (2\pi)^2 . C_T^2\, f_1^3$$

$$= 0.77 \times 10^{-18} A^2 .$$

The total rms noise current for the Si F.E.T. at 78 K is thus

$$i_t = 1.1 \text{ nA (rms)} . \qquad (3.28)$$

The noise current in this case is thus only about one quarter of that obtained with a typical valve amplifier.

Cooled F.E.T. amplifiers offer improved signal to noise ratio over valves and they have been used generally in recent years with cooled high resolution γ ray detectors at bandwidths up to about 1 mHz. (Refer Elad and Nakamura 1967).

The present author is not aware of any reported application of cooled F.E.T. amplifiers to wide band vidicon cameras; however, the possible improvement in this application is illustrated in the next section.

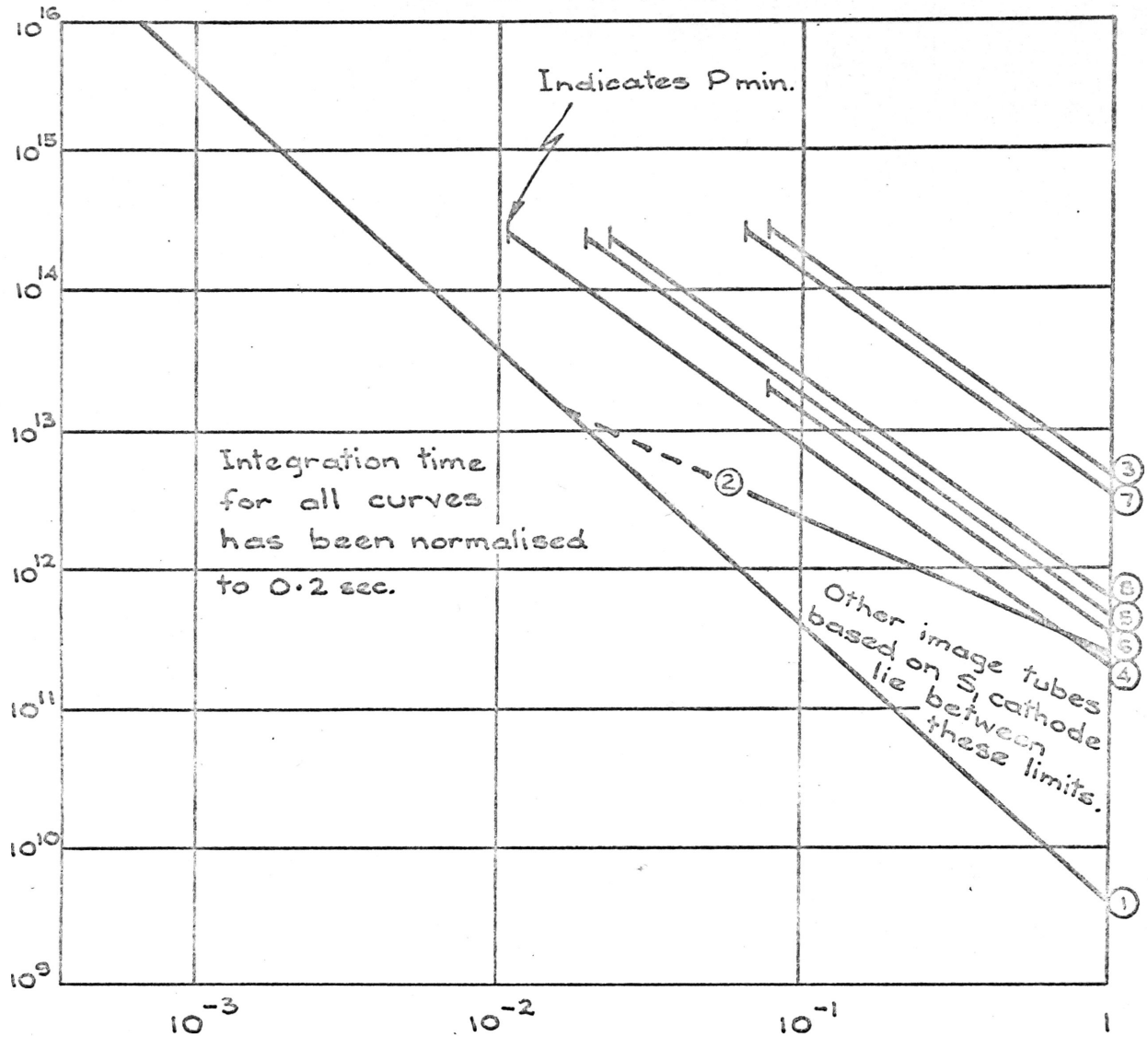

Graph N° :

① Perfect detector; $\eta = 10^{-3}$; $\lambda = 1083$ nm.

② Type 6914A image converter; $\lambda = 1083$ nm.

③ Type 2000 IR vidicon valve amplifier; $\lambda = 1083$ nm; $f_1 = 8$ MHz.

④ Type 2000 IR vidicon Ge F.E.T. amplifier; 4 K; $\lambda = 1083$ nm; $f_1 = 8$ MHz.

⑤ Type 2000 IR vidicon Si F.E.T. amplifier; 78 K; $\lambda = 1083$ nm; $f_1 = 8$ MHz.

⑥ Type 7735 A vidicon valve amplifier; $\lambda = 656$ nm; $f_1 = 8$ MHz.

⑦ Slow scan IR vidicon valve amplifier; $f_1 = 1{\cdot}6$ MHz; $t_f = 0{\cdot}2$ sec.

⑧ Slow scan type 2000 IR vidicon Ge F.E.T. amplifier; 4 K; $\lambda = 1083$ nm; $f_1 = 1{\cdot}6$ MHz; $t_f = 0{\cdot}2$ sec.

FIG. 3·4 FLUX-CONTRAST RELATIONS FOR VARIOUS IMAGING DEVICES

3.4 Comparison of Circuits and Devices.

In order to compare the relative merits of the various photon imaging devices the required number of incident photons per unit area per second Φ_T is plotted in Fig. 3.4 as a function of the corresponding detectable contrast p for each device.

The criterion adopted for reliable detection is that the amount of light comprising the input signal must be three times the light equivalent noise input for each device.

For the perfect detector this relation is easily calculated and is given by equation (3.5) which shows that the required light input is inversely proportional to the square of the contrast or $\Phi_T \propto \frac{1}{p^2}$.

The light equivalent noise input for the other devices tested is defined as that value obtained by the experimental method described in Chapter 4. The performance of these devices is limited by their characteristic noise level. The dependence of the required flux on the scene contrast is discussed in the following paragraphs.

In the case of the linear image converter or the linear vidicon the signal is derived from an amount of flux equal to $p\Phi_T$ where p is the contrast. This signal is compared to the characteristic noise source.

Sec. 3.4

$$\therefore \quad p\phi_T = \text{constant},$$

$$\phi_T \propto \frac{1}{p} .$$

In the case of the nonlinear vidicon the signal is derived from the change in target charge caused by the change in light flux $p\phi_T$. From equation (3.23)

$$Q_T \propto \frac{i_t t_f}{p} .$$

For the nonlinear vidicon

$$Q_T \propto \phi_T^{\gamma}$$

$$\phi_T \propto Q_T^{\frac{1}{\gamma}} \propto \left(\frac{i_t t_f}{p}\right)^{\frac{1}{\gamma}} \propto \left(\frac{i_t t_f}{p}\right)^{1.66}$$

for $\gamma = 0.6$.

Since the graph of ϕ_T versus p for a "perfect detector" provides a useful basis for comparison of other "real" devices, the first case considered is the "perfect detector".

3.4.1 Perfect detector (noiseless image converter)

Assuming the values

$\eta = 10^{-3}$ electrons per photon at $\lambda = 1083$ nm

$t_1 = 0.2$ s

$m = 10^5$ picture elements

for the perfect detector (a noiseless image converter with type S_1 cathode), and substituting in equation (3.5) we find

$$\phi_T = 4.5 \times 10^9/p^2.$$

This relationship is plotted on a log-log scale in Fig. 3.4 together with the graphs appropriate to other devices which are considered in the following sections.

3.4.2 "Real" image converter

It is shown in Chapter 4, Section 4.3, that the experimentally determined light equivalent noise input of a real image converter (type 6914A) is $\phi_T = 46 \times 10^9$ photons $cm^{-2}s^{-1}$. Increasing this input by a factor of three for the required minimum detectability gives a corresponding input flux required by the ("real") image converter of $\phi_T = 138 \times 10^9$ photons $cm^{-2}s^{-1}$.

The corresponding relation $\phi_T = 138 \times 10^9/p$ is plotted in the comparison graph of Fig. 3.4, and is labelled with the type number (6914A) of a particular image converter used in the experimental work.

3.4.3 Infrared vidicon

In this section three different circuits are considered. All are assumed to have 8 MHz bandwidth. They are:-

(a) I.R. vidicon with valve amplifier

(b) I.R. vidicon with Ge F.E.T. at 4 K

(c) I.R. vidicon with Si F.E.T. at 78 K

The light equivalent noise input for the valve amplifier is (from the experimental results of Chapter 4, Section 4.3.5) $\Phi_T = 1.7 \times 10^{12}$ photons $cm^{-2}s^{-1}$. For three times the light equivalent noise input, the flux required in each case is respectively:-

(a)' $\Phi_T = \frac{5 \times 10^{12}}{p^{1.66}}$ photons $cm^{-2}s^{-1}$.

(b)' $\Phi_T = \frac{5 \times 10^{12}}{(p \times 7)^{1.66}} = \frac{2 \times 10^{11}}{p^{1.66}}$ photons $cm^{-2}s^{-1}$.

(c)' $\Phi_T = \frac{5 \times 10^{12}}{(p \times 4)^{1.66}} = \frac{5 \times 10^{11}}{p^{1.66}}$ photons $cm^{-2}s^{-1}$.

where $\gamma = 0.6$. i.e. $\frac{1}{\gamma} = 1.66$.

In relations (b)' and (c)' it is assumed that the γ remains equal to 0.6 at the lower flux levels. The factors 7 and 4 in the denominators of (b)' and (c)' respectively are the noise reduction factors calculated in Section 3.3.6 for the F.E.T. circuits. The relations (a)', (b)', (c)' are also plotted in Fig. 3.4. The limiting detectable contrasts are calculated from equation (3.26) assuming an integration time of 0.2 s and are listed below. These limiting values (p_{min}) are also shown in Fig. 3.4.

Sec. 3.4

(a) For the valve $p_{min} = \dfrac{3 i_t t_f}{\gamma \times 10^{-8}}$

$= \dfrac{3 \times 4.1 \times 10^{-9}}{0.6 \times 10^{-8} \times 25} = 0,08$ contrast

(b) Ge F.E.T. $p_{min} = 0.011$ contrast

(c) Si F.E.T. $p_{min} = 0.02$ contrast.

3.4.4 Visible spectrum vidicon with valve amplifier

From the equation (4.12) the light equivalent noise input in this case at 656 nm is $\Phi_T = 125 \times 10^9$ photons-$cm^{-2}s^{-1}$. Three times this flux gives $\Phi_T = 3.75 \times 10^{11}$ photons $cm^{-2}s^{-1}$ and the corresponding flux-contrast relationship $\Phi_T = \dfrac{3.75 \times 10^{11}}{p^{1.66}}$ is plotted in Fig. 3.4.

3.4.5. Slow scanned vidicon.

The vidicon is, in principle, capable of long storage times. Thus slower scan rates permit, in principle, decreased bandwidth with consequent lower noise. The performance expected from an infrared vidicon with an integration time or frame scan time of 0.2 s is calculated below for the valve amplifier at 290 K and for the Ge F.E.T. amplifier at 4 K.

The new bandwidth = $8 \times \dfrac{1}{25} \times \dfrac{1}{0.2} = 1.6$ MHz. The noise level of the valve amplifier for 1.6 MHz bandwidth,

assuming all other parameters of equation (3.13) constant, is found by substituting 1.6 MHz for f_1 in equation (3.13) and summing the five noise terms. The resulting valve noise current is

$$\text{(valve) } i_t = 0.65 \text{ nA (rms)}. \qquad (3.29)$$

Similar calculations give for the noise current of the Ge F.E.T. amplifier at 4 K and 1.6 MHz bandwidth the magnitude

$$\text{(Ge F.E.T.) } i_t = 0.24 \text{ nA (rms)}. \qquad (3.30)$$

Three times the light equivalent noise input at 1083 nm is $3 \times 1.7 \times 10^{12}$ photons $cm^{-2}s^{-1}$ at the normal scan rate. Although the noise current is reduced by slow scanning the signal current is also reduced according to equation (3.17). If the γ of the tube is assumed constant ($\gamma = 0.6$), it follows that the light flux required for a scan time of 0.2 s equals, for the valve

$$\Phi_T = \frac{3 \times 1.7 \times 10^{12}}{\left[p\frac{4.1}{0.65} \times \frac{1}{5}\right]^{1.66}} = \frac{3.5 \times 10^{12}}{p^{1.66}} \text{ photons } cm^{-2}s^{-1}$$

and for the Ge F.E.T.

$$\Phi_T = \frac{3 \times 1.7 \times 10^{12}}{\left[p\frac{4.1}{0.24} \times \frac{1}{5}\right]^{1.66}} = \frac{0.68 \times 10^{12}}{p^{1.66}} \text{ photons } cm^{-2}s^{-1}.$$

The minimum contrast p(min) for each case is calculated by equation (3.26) and is 0.065 and 0.024 respectively.

These relations are plotted on Fig. 3.4.

3.4.6 Effects of spatial frequency response.

The flux-contrast relations derived above apply at low spatial frequencies when the resolution is not limited by the device considered. At high spatial frequencies both the minimum detectable contrast and the flux required to detect a scene of given contrast can be expected to increase in order to maintain a signal current from the vidicon, which is detectable above the fixed circuit noise.

This dependence upon spatial frequency is explained in the following paragraphs, and two numerical examples are given. The signal current i_1 from the vidicon target at low spatial frequencies is found from equations (3.18) and (3.22)

$$i_1 = \frac{\Delta Q_T}{t_f} = \frac{p\gamma Q_T}{t_f} .$$

For minimum detectable contrast p(min) this becomes

$$i_1 = \frac{p(\min)\,\gamma\, Q_T\ (\max)}{t_f}$$

where Q_T(max) is the maximum charge limitation of the vidicon target.

This current decreases at high spatial frequencies to the value of $i_1 . r$ where r is the relative amplitude of the contrast modulation response. Therefore, to maintain the signal current at its previous detectable level requires that the minimum detectable contrast p(min) be increased to $\frac{p(min)}{r}$.

Now consider the increase in flux required to detect a scene of given contrast at high spatial frequency. The signal current at high spatial frequency is given by

$$r\, i_1 = \frac{p \gamma Q_T\, r}{t_f} .$$

To restore this current to its detectable value i_1 requires that Q_T be increased to $\frac{Q_T}{r}$ for fixed contrast p. For the linear vidicion this means that the light flux would have to be increased by the factor $\frac{1}{r}$. For the non-linear vidicon $Q_T \propto (\Phi_T)^{\gamma}$ and in this case the light flux would have to be increased by the factor $\frac{1}{r^{(1/\gamma)}}$.

Example 1 (a) Find the input flux required to detect a scene of contrast 0.1 with a 7735A vidicon. λ = 656nm. Bandwidth = 8mHz. Find also the resolution obtained.

(b) What flux is required to resolve 300 TV lines?

Sec. 3.4

(a) Curve 6 of Fig. 3.4 applies to this case. ϕ_T is found to be 1.5×10^{13} photons/sq.cm /sec at p=0.1 The resolution obtained from the contrast modulation response of Fig. 4.17 is 125 T.V. lines.

(b) Fig. 4.17 shows that at 300 T.V. lines the contrast modulation response is reduced to ¼; therefore the flux required is given by $1.5 \times 10^{13} \times 4^{1.66} \simeq 1.5 \times 10^{14}$ photons/sq.cm /sec. Inspection of curve 6 shows that this exceeds the maximum flux allowed by target saturation and therefore this device cannot resolve a scene of contrast 0.1 with a resolution of 300 T.V. lines. (125 lines is about the limit.)

Example 2 Find the highest resolution obtainable with an infra red vidicon type 2000 under the following conditions:-

Scene contrast = 0.1 Silicon F.E.T. at 78K.

Bandwidth 8mHz. λ = 1083nm.

Curve 5 of Fig. 3.4 applies to this example. From this curve the maximum flux allowed by target saturation is 2×10^{14} photons/sq.cm /sec which is ten times greater than the flux required to detect the scene at low spatial frequencies. It is therefore possible to detect spatial frequencies out to the point where the contrast modulation response has fallen to $\frac{1}{10^{\gamma}} = \frac{1}{4}$.

From Fig. 4.18 the resolution obtained is 300 T.V. lines.

Ch.4

Chapter 4.

EXPERIMENTAL WORK.

4.1 Scope of Experimental Work

Laboratory measurements were carried out to determine values for circuit noise, light equivalent noise input and spatial frequency response which could be substituted into the appropriate theoretical equations derived in earlier parts of this thesis. The practical performances of the vidicon and image converter can then be assessed. The measurements are conveniently divided into three groups of measurements.

(i) Measurement of the electrical noise of a commercial vidicon camera and of the input capacitance and bandwidth of the circuit.

(ii) Measurement of the light equivalent noise input of an infrared vidicon, a visible spectrum vidicon, and a single stage infrared image converter.

(iii) Measurement of the spatial frequency response of an infrared vidicon and a visible spectrum vidicon.

Details of these measurements are given in the following sections.

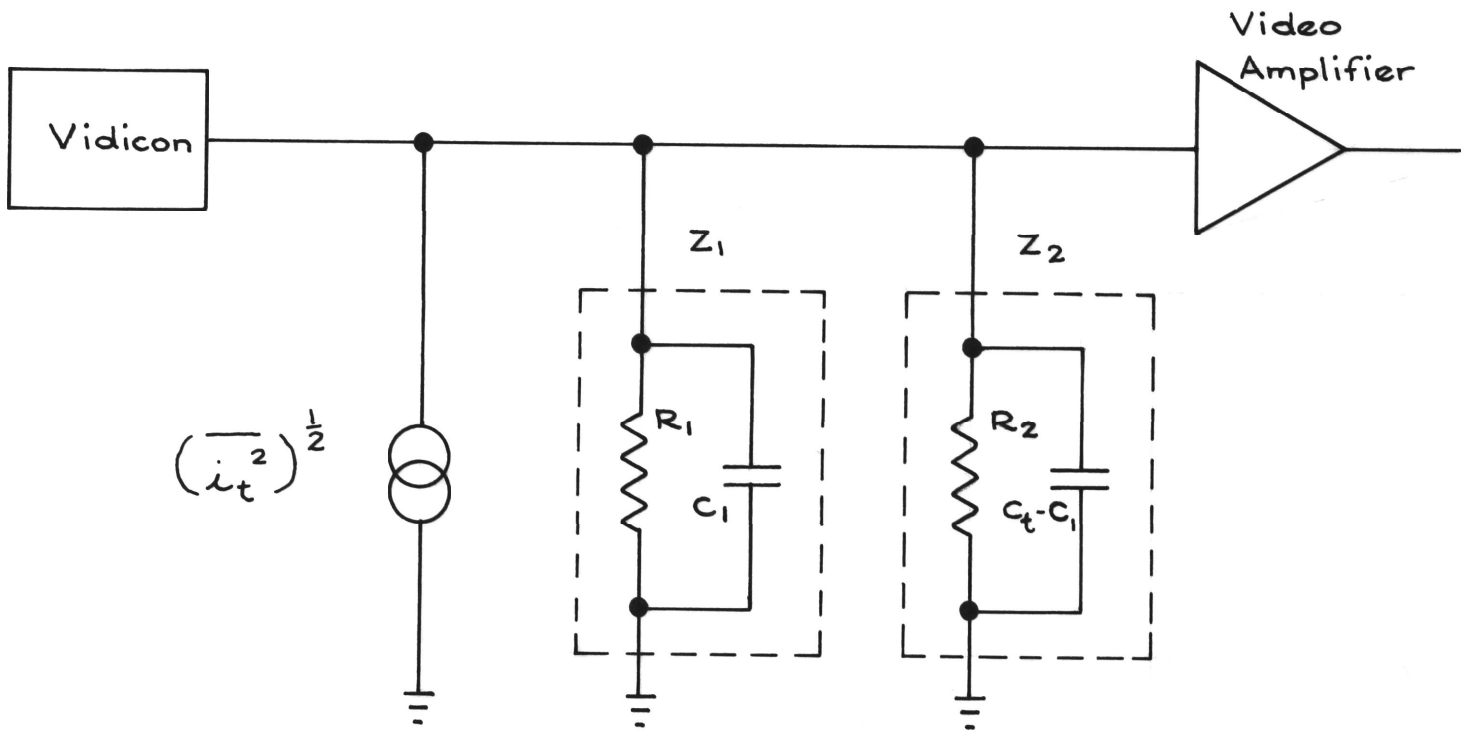

FIG. 4·1 VIDICON INPUT CIRCUIT

4.2 Measurement of Vidicon Circuit Noise

The noise current of the vidicon camera Type BG900, which has a valve input amplifier, was measured for a video bandwidth of 8 MHz. The following section (4.2.1) describes the experimental method used to measure this noise current and Section 4.2.2 gives the result of the measurement.

Section 4.2.3 describes the measurement and setting of the bandwidth to 8 MHz. Section 4.2.4 gives details of the measurement of input capacitance, which is required to correlate the experimental noise value to the theoretical value calculated from the noise theory given in Chapter 2.

4.2.1 Method of noise measurement

The method used to measure the electrical noise of the vidicon camera is illustrated in Fig. 4.1 and 4.2. Fig. 4.1 shows the essential (a.c.) input circuit of the vidicon and video amplifier with coupling and bypass capacitors of negligible reactance removed.

The equivalent root mean square noise current generator is shown as $\left(\overline{i_t^2}\right)^{\frac{1}{2}}$. The impedance Z_1 comprises a resistor R_1 and its self capacitance C_1. Z_2 consists of a resistor R_2 shunted by the total input circuit capacitance C_t minus C_1. Also R_1 = 220 kΩ and R_2 = 330 kΩ.

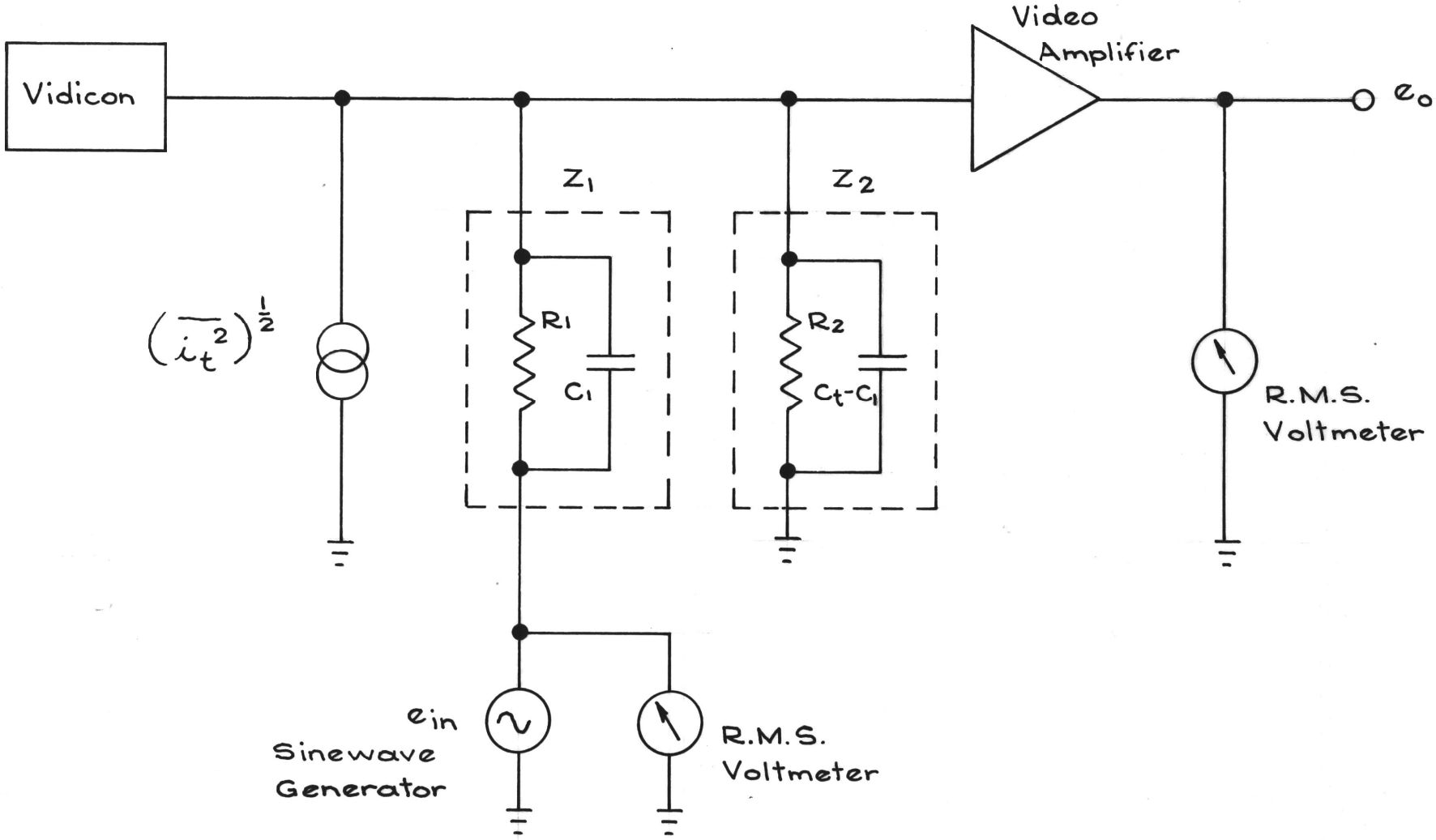

FIG. 4·2 CIRCUIT FOR NOISE MEASUREMENTS

Sec. 4.2

The noise measurement was made by feeding a sine wave voltage generator into the "earthy" end of R_1 (see Fig. 4.2). The voltage of this generator was increased from zero to e_{in} until the r.m.s. output voltage of the video amplifier increased by the factor $\sqrt{2}$. Because the signal generator and the random input noise are uncorrelated, it follows that the r.m.s. input noise current is then given by

$$\left(\overline{i_t^2}\right)^{\frac{1}{2}} = e_{in}/Z_1 . \qquad (4.1)$$

For sufficiently low frequencies, the shunt capacitor C_1 can be neglected and

$$\left(\overline{i_t^2}\right)^{\frac{1}{2}} = e_{in}/R_1 . \qquad (4.2)$$

Derivation of equation (4.2) follows simply by equating the voltage produced at the input grid by the noise current to the voltage produced at the input grid by the voltage e_{in}.

$$\left(\overline{i_t^2}\right)^{\frac{1}{2}} \cdot \frac{Z_1 Z_2}{Z_1 + Z_2} = e_{in} \cdot \frac{Z_2}{Z_1 + Z_2} .$$

$$\therefore \quad \left(\overline{i_t^2}\right)^{\frac{1}{2}} = e_{in}/Z_1 \quad \text{as required.}$$

4.2.2 Experimental results

The video amplifier normally contains synchronizing and blanking pulses and it was necessary to remove these

pulses before the random noise could be measured.

The bandwidth of the circuit was set to 8 MHz as described in the next section. The voltage required to increase the output noise by a factor of $\sqrt{2}$ was found to be $e_{in} = 1.3 \times 10^{-3}$V at 50 kHz. Then the r.m.s. noise current calculated from equation (4.2) is

$$\left(\overline{i_t^2}\right)^{\frac{1}{2}} = \frac{e_{in}}{R_1} = \frac{1.3 \times 10^{-3}}{220 \times 10^3} = 6 \times 10^{-9}\text{A}. \qquad (4.3)$$

Some of this noise is due to the second stage of the amplifier. In fact when the first valve was removed from the circuit the output noise voltage was reduced by the factor 0.5. Assuming no correlation between the first and second stage noise, the first stage noise alone can be found as follows. We have

$$\overline{i_1^2} + \overline{i_2^2} = (6 \times 10^{-9})^2\text{A}^2$$

and $$\overline{i_2^2} = (6 \times 10^{-9} \times 0.5)^2\text{A}^2 \ .$$

$$\therefore \quad \left(\overline{i_1^2}\right)^{\frac{1}{2}} = 5.2 \times 10^{-9}\text{A}.$$

The theoretically calculated value for the first stage noise is 4.1 nA which is reasonably close to the measured value (see equation (3.14)).

4.2.3 Bandwidth measurement

Before proceeding with the noise measurements, it was

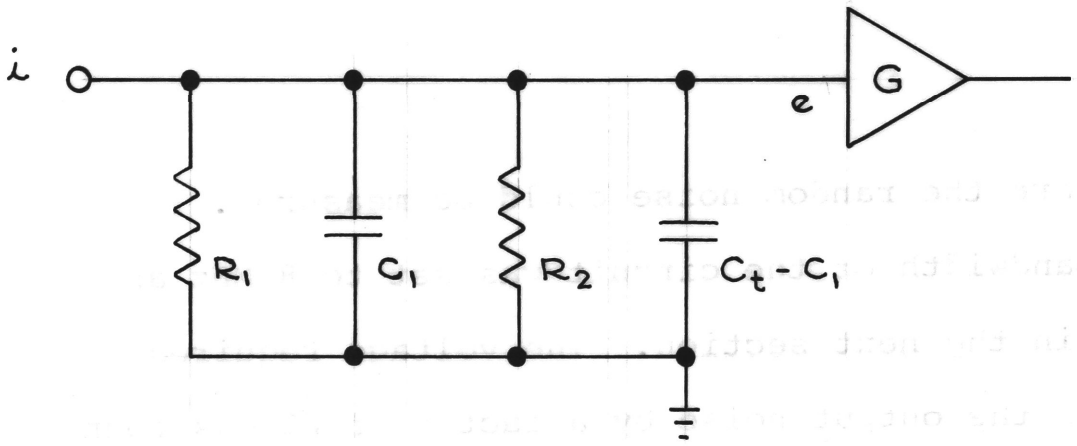

FIG. 4·3 VIDICON INPUT CIRCUIT

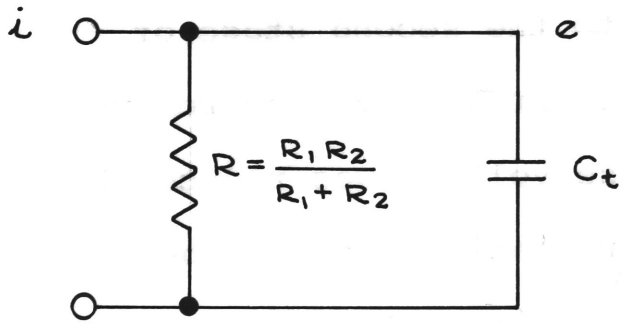

FIG. 4·4 INPUT CIRCUIT EQUIVALENT TO FIG. 4·3

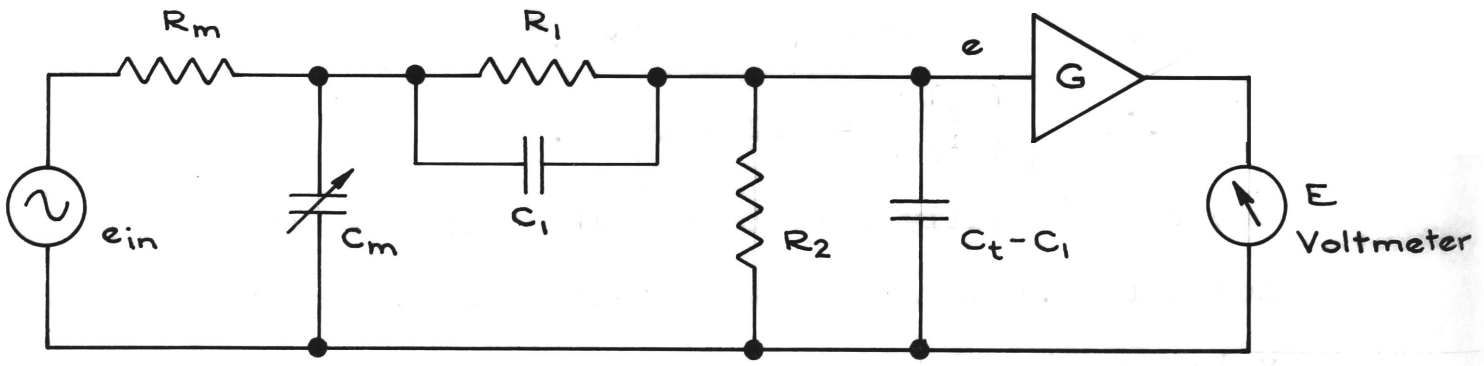

FIG. 4·5 CIRCUIT USED TO MEASURE BAND WIDTH

essential to measure the bandwidth of the video amplifier and to adjust this bandwidth to be within the range of the available measuring equipment.

The true r.m.s. voltmeter used has a bandwidth of 10 MHz and the bandwidth of the camera was adjusted to 8 MHz for all tests. There were difficulties in measuring the bandwidth due to the high impedance of the input circuit.

Fig. 4.3 shows the input circuit driven by a current source (e.g. the vidicon) and this is followed by the video amplifier with transfer function G.

The method of finding the overall frequency response with the aid of a voltage source at the input is shown in Figs. 4.4 and 4.5. Fig. 4.4 is an equivalent circuit of the input section of Fig. 4.3. Fig. 4.5 shows the circuit used to measure bandwidth.

A compensated probe was built and adjusted so that $R_m.C_m = R_1.C_1$ and $R_m << R_1$. The input voltage e_{in} was held constant over the range 20 kHz to 10 MHz and the frequency response taken by measuring the output voltage E of the video amplifier over this frequency range. The effective bandwidth was taken to be

$$B.W. = \int_0^\infty |E_0|^2 \, df \qquad (4.5)$$

where E_0 is normalized to equal unity at low frequencies. Graphical integration was used to evaluate the effective bandwidth from the frequency response and the latter was adjusted to give an effective bandwidth of 8 MHz. It remains to be shown that the input circuit of Fig. 4.5 gives the same frequency response as the circuit of Fig. 4.4.

The form of the frequency response for Fig. 4.4 can be written

$$e \propto (1 + j\omega RC_t)^{-1}. \tag{4.6}$$

Referring now to Fig. 4.5 and noting that $R_m C_m = R_1 C_1$ and $R_m \ll R_1$, we see that the network $R_1 C_1$, $R_2(C_t - C_1)$ presents negligible loading to the network $R_m C_m$. The voltage e is therefore given by

$$e = \frac{1}{1 + j\omega R_m C_m} \cdot \frac{\dfrac{R_2}{1 + j\omega(C_t - C_1)R_2}}{\dfrac{R_1}{1 + j\omega C_1 R_1} + \dfrac{R_2}{1 + j\omega(C_t - C_1)R_2}}$$

$$= \frac{1}{1 + j\omega C_m R_m} \cdot \frac{R_2}{R_2 + \dfrac{R_1\left(1 + j\omega(C_t - C_1)R_2\right)}{1 + j\omega C_1 R_1}} \cdot$$

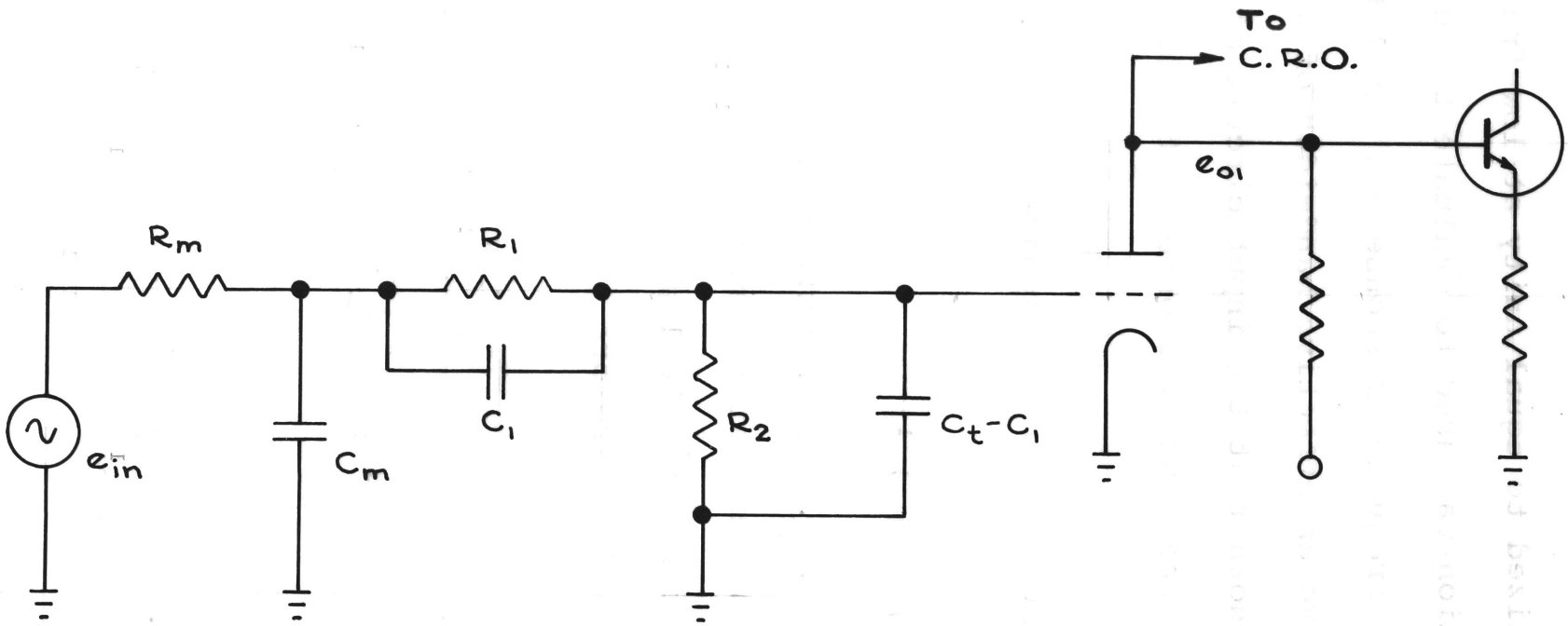

FIG. 4·6 CIRCUIT FOR MEASUREMENT OF INPUT CAPACITANCE

Sec. 4.2

Since $C_m R_m = R_1 C_1$, this becomes

$$e = \frac{R_2}{R_2 + j\omega C_1 R_1 R_2 + R_1 + j\omega (C_t - C_1) R_1 R_2}$$

$$= \frac{1}{\frac{R_1 + R_2}{R_2} + j\omega C_t R_1} \propto \frac{1}{1 + j\omega C_t \frac{R_1 R_2}{R_1 + R_2}}$$

$$\propto \frac{1}{1 + j\omega C_t R} \qquad \text{as required.}$$

4.2.4 Input capacitance

The input capacitance was obtained indirectly from the frequency response of the first stage as explained below.

The first stage of the video amplifier is a nuvistor triode valve which drives a transistor emitter follower as shown in Fig. 4.6. The probe described previously for bandwidth measurements was used to feed in an input voltage of variable frequency. The output voltage e_{01} of the first stage was measured by means of a C.R.O. The frequency response of the circuit is determined from the relationship $\omega = 2\pi f = (RC_t)^{-1}$, where f is the frequency at which the output voltage, e_{01}, is 3db down and RC_t is

Sec. 4.2

the input circuit time constant. Since we have in this case $R = R_1 R_2 / (R_1 + R_2) = 130\ k\Omega$ and since the measured value of f was 50 kHz, the input circuit capacitance is given by:-

$$C_t = (2\pi f R)^{-1} = 25\ pF.$$

This value was also found by an independent check using a capacitive divider measuring technique.

4.3 Measurement of Light Equivalent Noise Input

The light sources used for measurements of light equivalent noise input of the detectors are described in the following sections 4.3.1 to 4.3.4. The light equivalent noise input of an infrared vidicon and a single stage image converter were measured at 900 nm and the results extrapolated to 1083 nm.

Also the light equivalent noise input of a visible spectrum vidicon was measured at 700 nm and this result was extrapolated to 656 nm which is also a wavelength of interest in solar astronomy.

Details of these measurements are given in sections 4.3.5 to 4.3.7. These results are used in Chapter 3 to calculate the limiting performance expected of these devices.

4.3.1 Test light sources

Solid state gallium arsenide (Ga As) and gallium phosphide (Ga P) diode light sources were used throughout the measurement of light equivalent noise input. These light sources offered the advantage that no elaborate optical equipment or filters were required.

The method of measurement was to place the light source in direct contact with the vidicon or image converter face plate and then to vary the current through

the light source until the image of the light source appeared just detectable above the system noise. The light equivalent noise input can be found from a current input versus light output calibration of the light source. The light flux input per unit area can be calculated from the size of the image. It is emphasised here that these are not precise photometric measurements, but they are sufficiently accurate and reproducible to describe adequately the practical performance of the devices tested.

The solid state sources used emit radiation over a relatively narrow spectral bandwidth. These emission bands are sufficiently close to the wavelengths of interest to provide simply and directly the required performance information.

4.3.2 Characteristics of gallium arsenide light sources

The light source used for the infrared measurements was a gallium arsenide electro-luminescent diode - Hewlett-Packard type h.p.a. 4104. This source radiates in a narrow band at a wavelength of 900 nm when forward biased. The radiation may be switched on or off in a

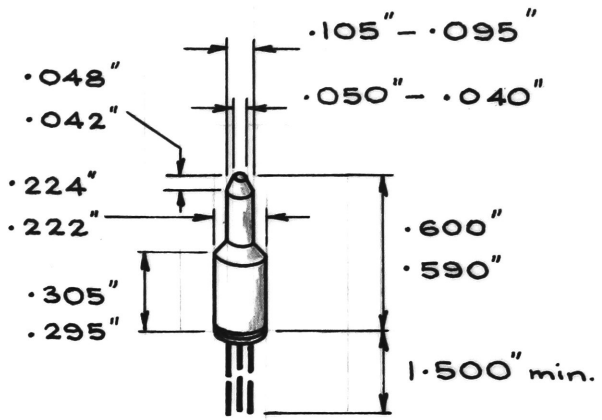

FIG. 4·7 DIMENSIONS OF GaAs SOURCE

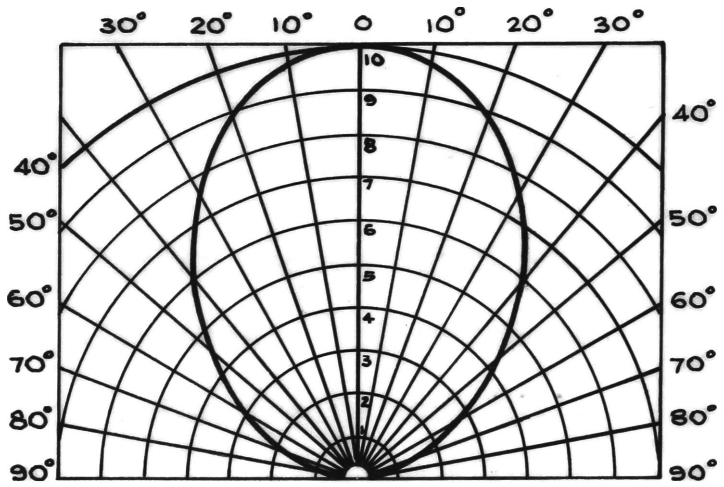

FIG. 4·9 RADIATION PATTERN OF GaAs SOURCE

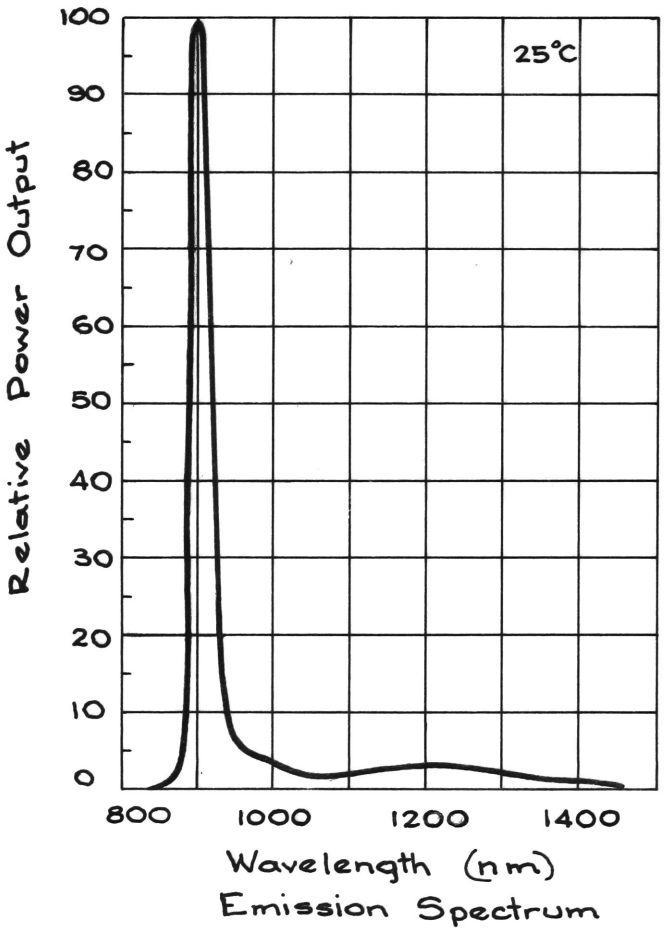

FIG. 4·8 EMISSION SPECTRUM OF GaAs SOURCE

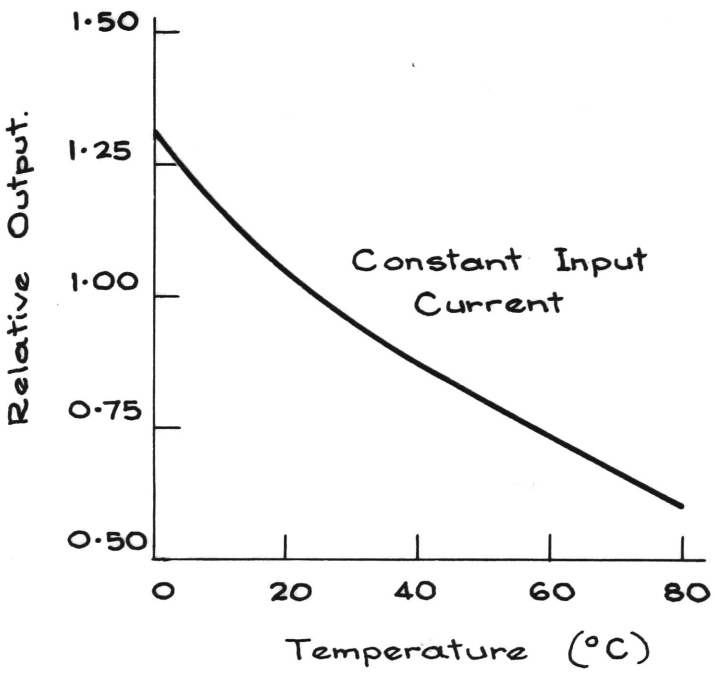

FIG. 4·10 TEMPERATURE DEPENDENCE OF OUTPUT OF GaAs SOURCE

few nanoseconds. The h.p.a. 4104 has a hermetrically sealed glass fiber optic light guide which places the emitting source optically on the end surface of the device.

The manufacturer's data states that the minimum and typical values of quantum emission efficiency at 2 mA forward current are 0.0005 and 0.001 photons per electron respectively. At 30 mA forward current the stated efficiencies at 0.001 (minimum) and 0.002 (typical) photons per electron. Other characteristics of the diode taken from the manufacturer's data are given in Figs. 4.7 to 4.10. Fig. 4.7 gives the geometrical dimensions of the device. The emission spectrum is given in Fig. 4.8 while Fig. 4.9 shows the polar diagram of the radiation. The light output versus temperature is shown in Fig. 4.10.

4.3.3 Calibration of gallium arsenide light source

In order to know the light output of the gallium arsenide source at any bias current, it is necessary to know the absolute output at a particular value of current and the relative output at all other values of current. The manufacturer's figure of 10^{-3} photons per electron at 2 mA has been accepted as the absolute

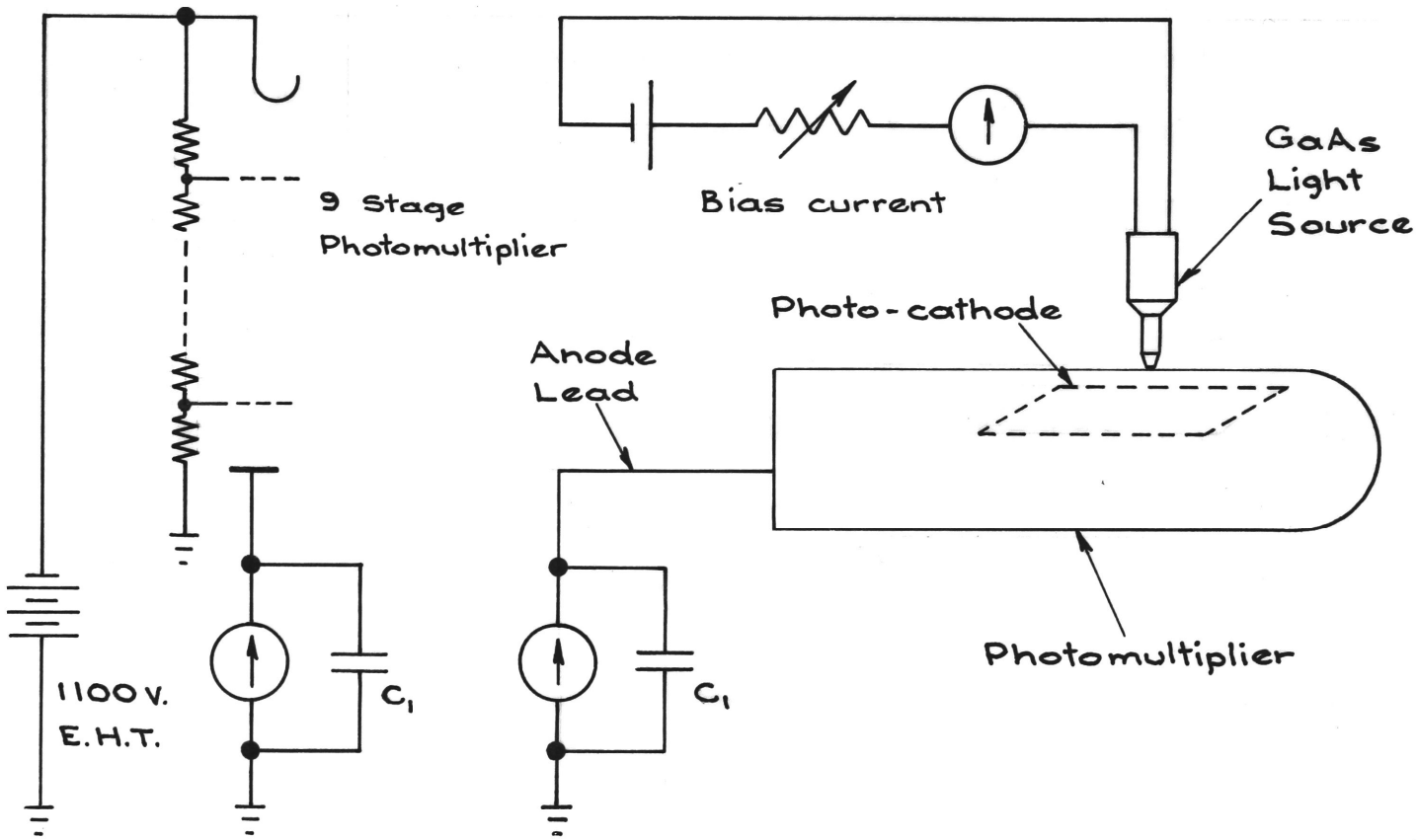

FIG. 4·11 CIRCUIT AND MECHANICAL ARRANGEMENT OF PHOTOMULTIPLIER USED FOR CALIBRATING LIGHT SOURCES

reference value of output throught this work.

Relative calibration was accomplished with the aid of a photomultiplier as shown in Fig. 4.11. The light source was pressed against the glass envelope of the photomultiplier via a film of silicone grease. The photomultiplier used was a H.T.V. type R-196 which is similar in construction to the R.C.A. type 931 but has a type S_1 cathode.

A stable power supply was set to 1100V and the photomultiplier anode current was read on an electrometer. Noise fluctuations of the anode current were reduced by connecting a polystrene dielectric capacitor (C_1 = 1μF) across the electrometer and by operating the apparatus in an air conditioned room at a controlled temperature of (21 ± 1)^{0}C. Measurements were taken after a stabilizing period of 24 hours. The photomultiplier is an excellent device for this type of comparative measurement because it has a linear response over a very large range of light intensity.

Table 4.1 gives the values obtained by the above method.

Sec. 4.3

The solid state light sources were used in particular configurations to supply light input to the vidicon and the image converter.

The light sources were calibrated in these particular configurations by using the same configurations in conjunction with the photomultiplier as described above.

Sec. 4.3

Table 4.1

Calibration of Ga As Source

Bias Current I_b	Anode Current I_a
3 mA	76 μA
2 "	42 "
1 "	16.5 "
0.5 "	5.9 "
0.4 "	4.2 "
0.25 "	2.1 "
0.1 "	0.46 "
75 μA	290 nA
50 "	160 "
40 "	120 "
30 "	75 "
25 "	62 "
20 "	52 "
15 "	44 "
10 "	37 "
5 "	34 "
0 "	32 "

Values of anode current (I_a) from Table 4.1 are plotted in the curve of Fig. 4.12.

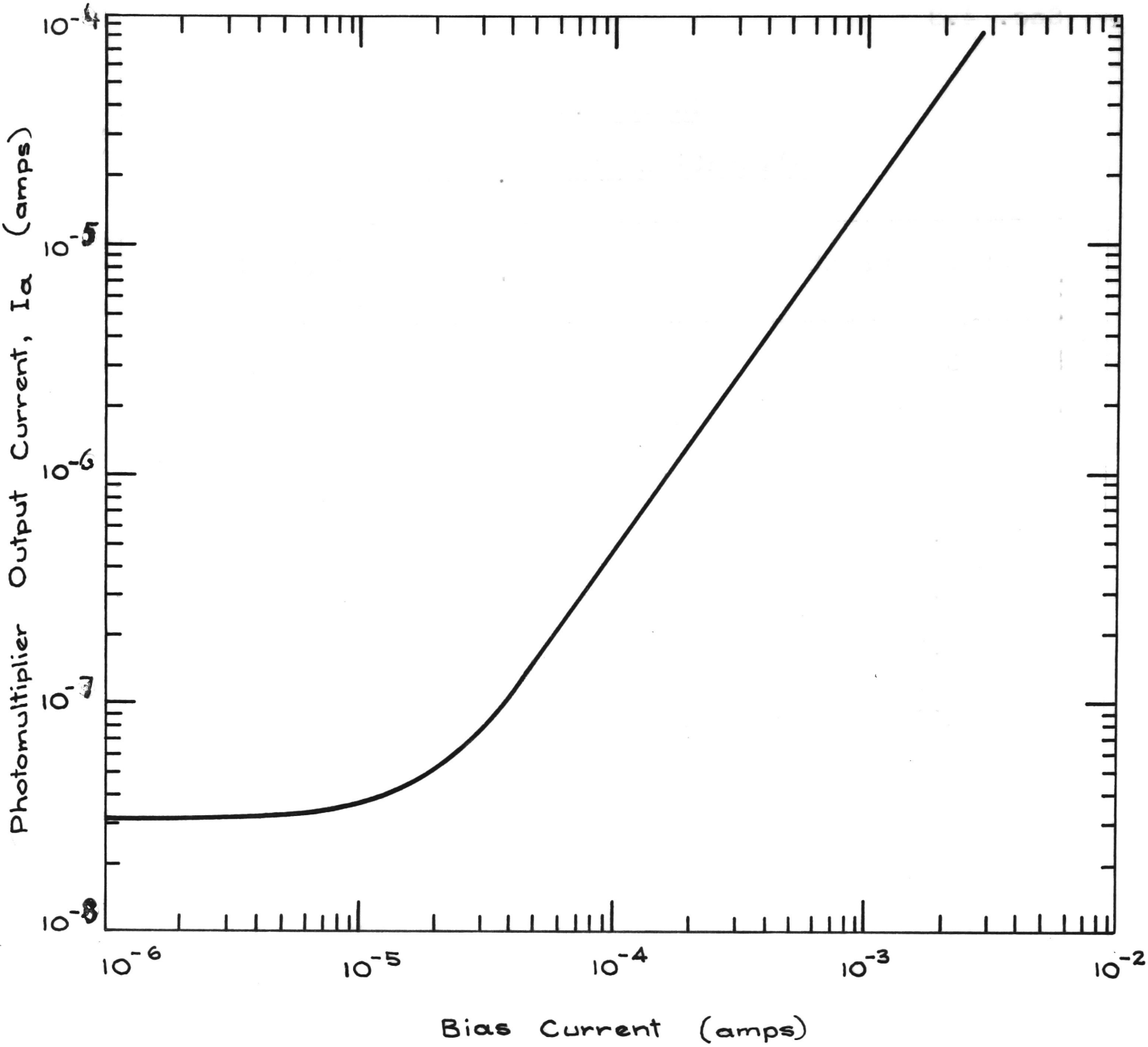

FIG. 4·12 RELATIVE OUTPUT OF GaAs LAMP AS A FUNCTION OF BIAS CURRENT

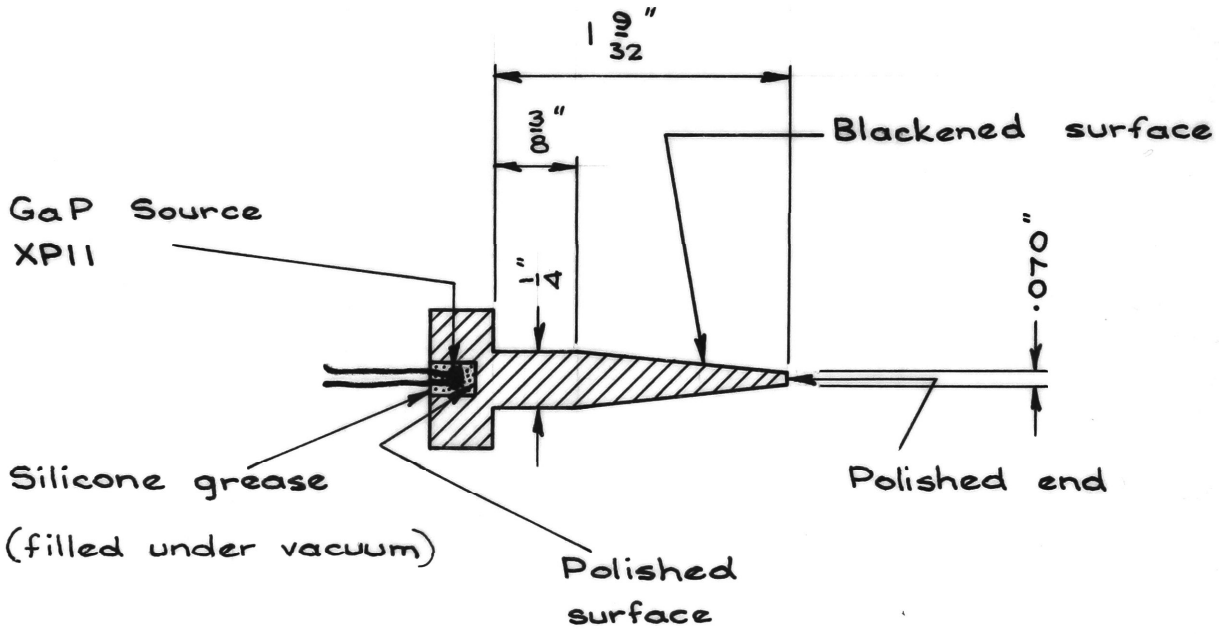

FIG. 4·13 Ga P LAMP AND LIGHT PIPE ASSEMBLY

4.3.4 Gallium phosphide light source

The gallium phosphide light source used was a Ferranti type XP11. Manufacturer's data states that this source radiates at a wavelength of 700 nm with a bandwidth at half peak of 70 nm.

To adapt the source for the proposed measurements, it was fixed into a perspex light guide as shown in Fig. 4.13. The light output from the gallium phosphide source was measured after each experiment by comparison with the gallium arsenide source using the photomultiplier calibration system of Fig. 4.11. First the output of the photomultiplier was measured with the gallium phosphide source in situ at a given current. The gallium arsenide source was then substituted for the gallium phosphide source and the bias current was adjusted for the same output from the photomultiplier, thus giving the light output from the gallium phosphide source at a given current in terms of a current through the gallium arsenide source.

It is assumed here that the quantum efficiency of the S_1 photocathode of the photomultiplier is the same at 700 nm and 900nm.

This assumption is justified by the experimental curves taken on five S_1 cathodes by Malkerbe, Tessier and Veron (1966). They show no change in spectral response at 700 nm and 900 nm expressed in milliamps per watt and therefore the quantum efficiency in electrons per photon would be higher at 700 nm by the factor 9/7 which has been ignored in this work.

The above response also agrees with the manufacturer's data; see for example R.C.A. data sheet 7102 5-65 Fig. 2.

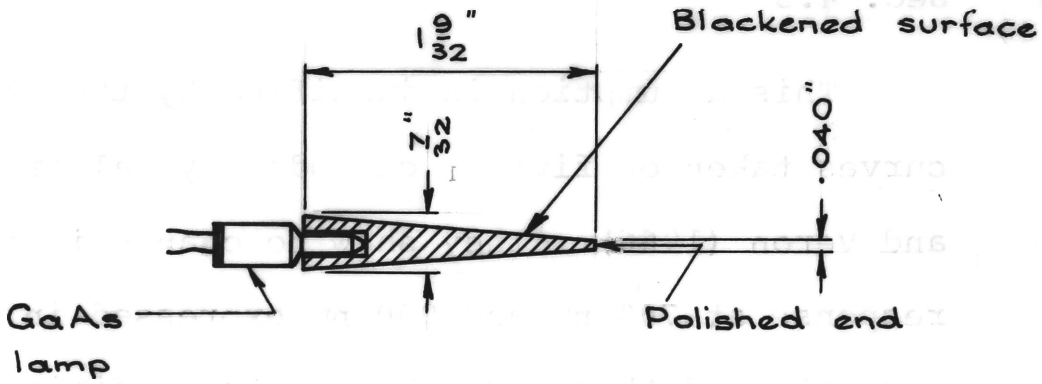

FIG. 4·14 GaAs LAMP AND LIGHT PIPE ASSEMBLY

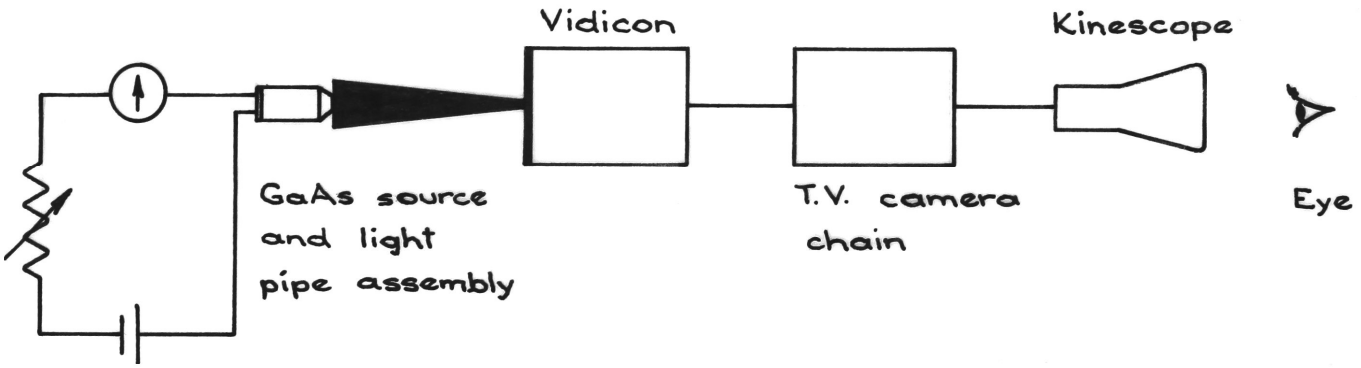

FIG. 4·15 ARRANGEMENT FOR MEASUREMENT OF LIGHT EQUIVALENT NOISE INPUT

4.3.5 Light equivalent noise input of infrared vidicon

For the infrared vidicon measurements an additional perspex light pipe shown in Fig. 4.14 was fitted to the source to confine the beam to a small solid angle. Fig. 4.15 shows the method used to measure the light equivalent noise input of the infrared vidicon at 900 nm.

The vidicon used was a G.M.B.H. type 2000 and it was operated in an EMI television camera type BG900. The Ga As light source with the additional light pipe was pressed into contact with the centre of the vidicon face plate using a thin film of silicone grease for optical coupling. Bandwidth of the camera was 8 MHz. The kinescope output was observed by eye with no ambient lighting. At the threshold of detection the camera controls; focus, beam current and target voltage and the monitor controls; contrast and brightness, were all adjusted for maximum detectivity of the image. The image on the kinescope screen appeared as a half inch diameter circle of uniform brightness. The kinescope scan amplitudes were adjusted to be 6 in. × 8 in. corresponding to a scanned target of 0.96 cm × 1.28 cm. The bias current through the Ga As source was then adjusted until the ½ in. diameter image could just be seen above the noise background. The current required was

250 μA. The amount of input light per sq. cm required to just detect the image in the noise background by the above method is defined here as the light equivalent noise input. A value of three times this amount of light is taken as the criterion for reliable detection. This measurement is independent of spot size under the following conditions. Firstly, the size of the image of the light spot on the final recording device must be sufficiently large so that its detection is unaffected by the spatial frequency response of the recording device. Secondly, the system is assumed to be limited by a fixed background noise which is much higher than photon noise anywhere in the system, including the final recording device.

Next the Ga As source, with the additional light pipe still attached, was transferred to the photomultiplier, (see Fig. 4.11) and the photomultiplier output current was measured with a bias current of 250 μA as described in Section 4.3.3. On removing the light pipe from the source, it was found that a current of 22 μA through the source produced the same photomultiplier output. The total light input can now be found from the curve of Fig. 4.12 and the efficiency of the source at one value of current.

Sec. 4.3

The efficiency of the source is taken as 10^{-3} photons per electron at 2 mA from the manufacturer's data. The input light flux Φ is found from the curve in Fig. 4.12 and the following equation,

$$\Phi = I_o n_e \theta_o (I_a/I_a) \text{ photons/second} \quad (4.7)$$

where I_o = reference bias current

n_e = the number of electrons per coulomb of charge

θ_o = the efficiency of the source at the bias current I_o in photons per electron

ΔI_a = change in photomultiplier anode current upon applying noise equivalent bias current

I_a = change in photomultiplier anode current upon applying a bias current of I_0.

On substituting the appropriate values given above viz.

$$I_0 = 2 \times 10^{-3} \text{ A}$$

$$n_e = 6 \times 10^{18}$$

$$\theta_0 = 10^{-3}$$

$$\Delta I_a = (57 - 32) \times 10^{-9} \text{A}$$

$$I_a = 42 \times 10^{-6} \text{ A}$$

in equation (4.7), we have

$$\phi = 7.2 \times 10^9 \text{ photons/second.} \qquad (4.8)$$

This quantity is the light equivalent noise input for an image of ½ in. diameter on a 6 in. × 8 in. screen. The light input required for the whole scene of area 48 in^2, (equivalent to approximately 1 cm^2 target area) is given by

$$\phi_t = 7.2 \times 10^9 \times 48 \times 4 \times 4/\pi = 1.7 \times 10^{12}$$

$$\text{photons cm}^{-2} \text{ s}^{-1}. \qquad (4.9)$$

There is no significant difference between the spectral response of the infrared vidicon at 900 nm and 1083 nm and therefore the above results are directly

applicable at 1083 nm.

4.3.6 Light equivalent noise input of visible spectrum vidicon

An R.C.A. vidicon type 7735 A was fitted into the camera and the light equivalent noise input was measured at 700 nm by use of the gallium phosphide source in the manner described in Section 4.3.5. The image formed on the kinescope screen appeared as a circle of 7/8 in. diameter. This circle appeared to have uniform brightness except for a small spot in the centre which had about twice the brightness of the rest of the circle. The area of the bright spot was so small that its contribution to the total flux could be neglected. The bias current required to just detect the image under optimum conditions of camera and monitor adjustment was 5 mA.

When the source was transferred to the photomultiplier, it was found that the equivalent input to the Ga As source was 13 μA. From Fig. 4.12 and equation (4.7) it is found that the light equivalent noise input equals

$$\phi = 2 \times 10^{-3} \times 6 \times 10^{18} \times 10^{-3} \times \frac{(4.1 - 3.2) \times 10^{-8}}{4.2 \times 10^{-5}}$$

$$= 2.5 \times 10^{9} \text{ photons } s^{-1}. \qquad (4.10)$$

The corresponding total flux required for the whole scan area is

$$\phi_t = 2.5 \times 10^{9} \times 48 \times \frac{4}{\pi} \times \frac{64}{49} = 2 \times 10^{11} \text{photons } cm^2 s^{-1}. \qquad (4.11)$$

This figure holds at 700nm. For operation at 656 nm a correction factor can be applied to account for the difference in vidicon response betweeen 656 nm and 700 nm. From R.C.A. data for the 7735A vidicon this factor equals 1.6 and therefore, the total flux required at 656 nm is given by

$$\Phi_T(656\text{ nm}) = 2 \times 10^{11}/1.6 = 0.125 \times 10^{12} \text{photons cm}^{-2}\text{s}^{-1}. \quad (4.12)$$

4.3.7 Light equivalent noise input of Image Converter

The light equivalent noise input of an image converter type 6914A was measured at 900 nm using the gallium arsenide source and a high tension supply of 12.5 kV. The image formed on the phosphor was a circle of 0.1 in. diameter and this was just detectable with a bias current of 5 μA through the light source.

Using Fig. 4.12 and equation (4.7), the light flux required to equal the noise is found to be

$$\Phi = 2 \times 10^{-3} \times 6 \times 10^{18} \times 10^{-3} \times \frac{(3.4 - 3.2) \times 10^{-8}}{4.2 \times 10^{-5}}$$

$$= 0.56 \times 10^{9} \text{ photons s}^{-1} \quad (4.13)$$

The total flux required for a whole scene area of 1 cm^2 at the cathode, allowing a factor 0.75 for the linear magnification of the 6914A, is

$$\Phi_t = 5.6 \times 10^8 \times \frac{4}{\pi} \times \frac{(0.75)^2}{(0.1 \times 2.54)^2} = 6.2 \times 10^9$$

photons $c\bar{m}^2 s^{-1}$. (4.14)

Extension of this result to 1083 nm requires a large correction factor due to the falling spectral response of the S_1 cathode. This factor taken from the average S_1 type cathode response curve given by Malherbe et alia (1966) is approximately 15. Thus the total flux required at 1083 nm is

$$\Phi_t \text{ (1083 nm)} = 15 \times 6.2 \times 10^9 = 9.2 \times 10^{10} \text{ photons } c\bar{m}^2 s^{-1}. \quad (4.15).$$

Because of the large spread in spectral response of the S_1 cathodes beyond 1000 nm shown by Malherbe, the above result should be used with caution. However, it is useful in that it shows that the image converter has a potential detectivity of about 18 times that of the infrared vidicon with a valve amplifier at a wavelength of 1083 nm.

The worst S_1 cathode measured by Malherbe shows a drop in quantum efficiency of 30 times from 900 nm to 1083 nm, and thus the result of equation (4.15) should be within a factor of two of the correct value.

It can, therefore, be concluded that image intensifiers which have lower background than the 6914A image converter offer the best performance at 1083 nm, despite the relatively low quantum efficiency of their type S_1 cathode.

4.4 Measurement of Vidicon Camera Spatial Frequency Response

As indicated in Section 1.2 the performance of an imaging device can be specified for low contrast scenes if both the spatial frequency response and the system noise are known.

Sections 4.4.1 to 4.4.3 below describe measurements taken of the spatial frequency response of the camera with the infrared vidicon and with the visible spectrum vidicon.

These measurements show the relative output current of the video amplifier as a function of input spatial frequency and they do not include any loss of resolution of the kinescope or the eye.

4.4.1 General method of measurement

The spatial frequency response of the vidicon camera was measured using an opaque test pattern of alternate black and white bars for the visible vidicon input signal and a glass test pattern of alternate black and transparent bars for the infrared vidicon.

The input signal from the test patterns was reflected light from normal laboratory lighting plus a tungsten floodlight in the first case and transmitted light from tungsten filament lamps operated well below normal brilliance behind a diffusing screen for the infrared

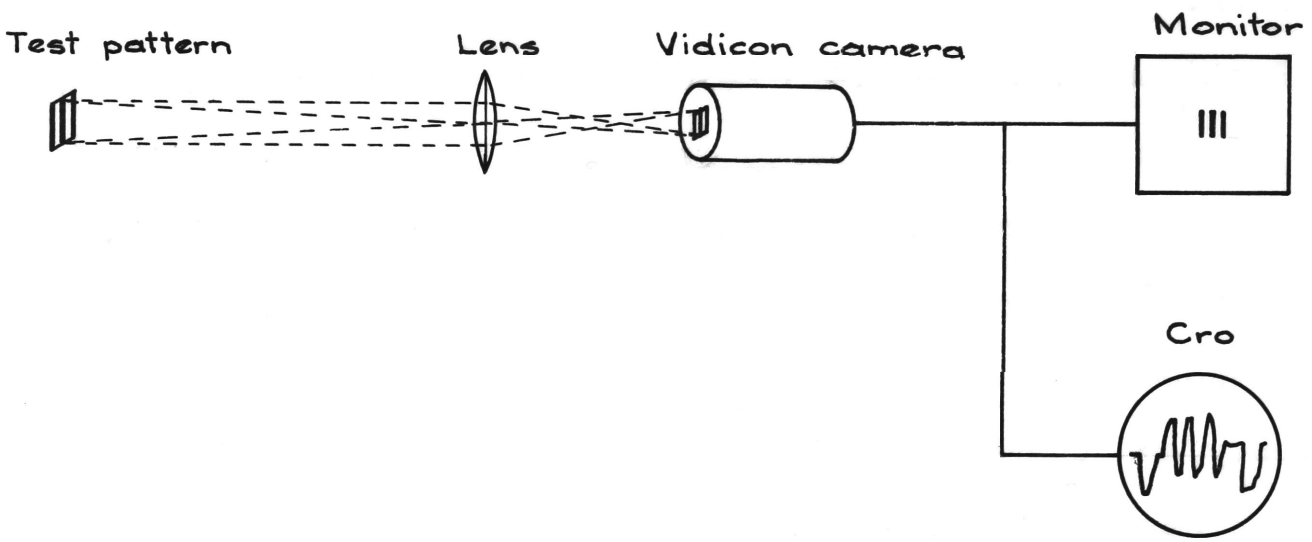

FIG. 4·16 ARRANGEMENT FOR MEASURING SPATIAL FREQUENCY RESPONSE OF VIDICON CAMERA

vidicon. Each test pattern contained a range of 28 spatial frequencies. The electrical output signal from the video amplifier was measured for variable input spatial frequency.

Fig. 4.16 shows the essential features of the apparatus. Each test pattern was placed in a fixed position relative to the vidicon and focussed on to the vidicon target to give an image near the centre of the monitor screen. All measurements were made within one inch of the centre of the monitor to ensure that only light rays close to the optical axis of the lens were utilised as the quality of the lens at 900 nm was unknown.

The spatial frequency was determined by the overall magnification of the system and the known lines per inch of the test patterns. The video output signal peak to peak amplitude corresponding to the scanned pattern was measured on a delayed sweep cathode ray oscilloscope which had its time base synchronized to view one horizontal line near the centre of the image.

4.4.2 Spatial frequency response with visible spectrum vidicon

The test pattern contained 28 charts numbered 1 to 28 with spatial frequency inversely proportional to chart

number. Chart number 28 contained 10 line pairs in ½ in. i.e. 20 lines per inch. The overall magnification measured between the test chart and the size of its image in the monitor was 3/2. Thus the number of lines per inch on the monitor $= 20 \times \frac{28}{\text{Chart number}} \times \frac{2}{3} = \frac{1120}{3} \times \frac{1}{\text{Chart number}}$. For an 8 in. scan the total number of lines n_t is given by $n_t = \frac{1120}{3} \times 8 \times \frac{1}{\text{Chart number}} = \frac{3000}{\text{Chart number}}$. Experimental results are tabulated in Table 4.2.

Table 4.2

Chart number	T.V. Lines (n_t)	P-P Video Output (Volts)	Relative Output
28	107	0.60	100
24	125	0.58	97
19	158	0.50	83
14	214	0.36	60
11	273	0.24	40
9	333	0.14	23

The r.m.s. noise output was 0.06 V. The final measurement is of the same order of magnitude as the noise. The spatial frequency response of Table 4.2 is plotted in Fig. 4.17.

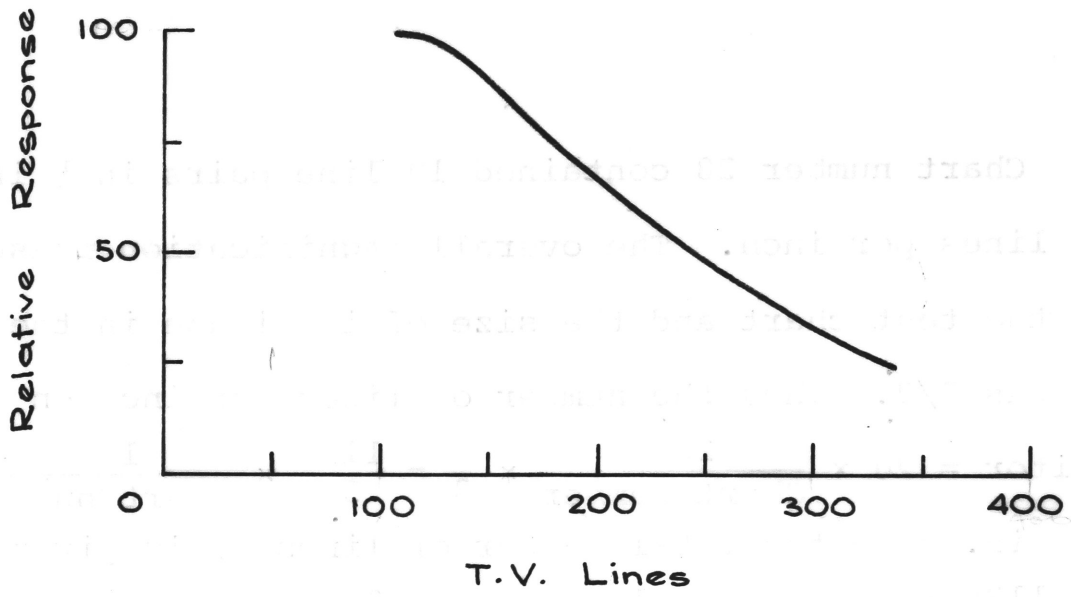

FIG. 4·17 SPATIAL FREQUENCY RESPONSE OF VISIBLE SPECTRUM VIDICON

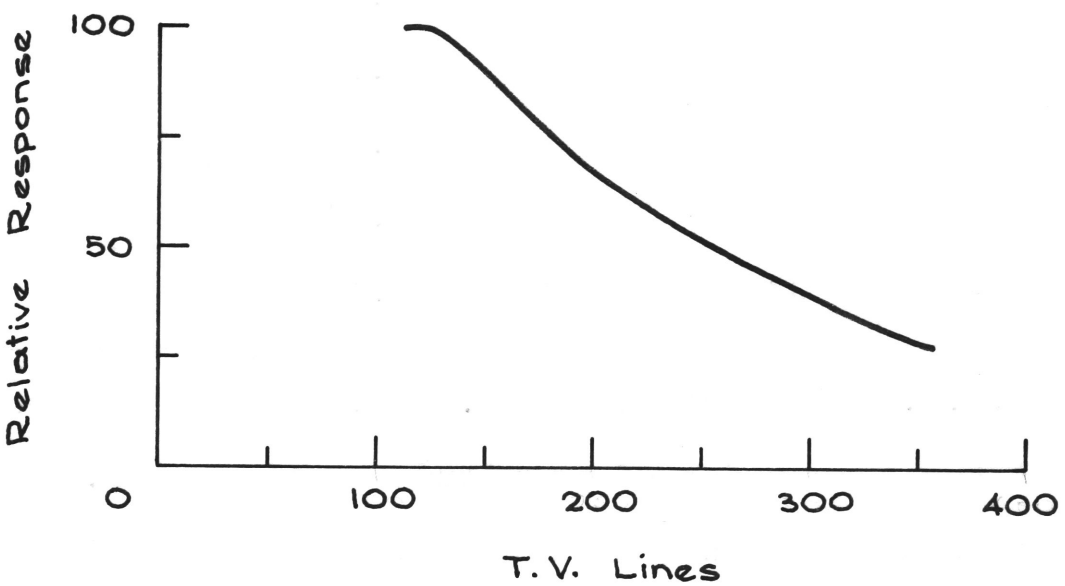

FIG. 4·18 SPATIAL FREQUENCY RESPONSE OF I R VIDICON

Sec. 4.4

4.4.3 Spatial frequency response with infrared vidicon

The apparatus was adjusted, with the infrared vidicon installed in the camera, so that chart No. 27 measured 13 lines per inch on the monitor or a total of 104 lines in the 8 in. scan. Experimental figures are given in Table 4.3 and these are plotted in Fig. 4.18.

Table 4.3

Chart number	T.V. Lines (n_t)	P-P Video Output (Volts)	Relative Output
27	104	0.40	100
22	127	0.40	100
17	166	0.32	80
12	235	0.24	60
9	315	0.16	40
8	356	0.10	25

The noise level at the output was 0.06 volts r.m.s. and the probable error in the last point is about ± 25 per cent.

Chapter 5 CONCLUSION

The results presented in Fig. 3.4 show that image tubes which are based upon photoelectric emission from a type S_1 cathode are potentially the best choice for imaging low contrast scenes at 1083 nm with short exposure times. Firstly they require less light than the vidicon for an acceptable signal to noise ratio and secondly the image tubes are capable of detecting very low contrast scenes because their photocathodes are linear over an extremely wide range of input light intensity whereas the limited dynamic range of the vidicon restricts the minimum detectable contrast to about 8 percent with a valve amplifier and to about 1 percent with a cooled F.E.T. amplifier for an integration time of $\frac{1}{5}$- seconds in each case.

There are a wide range of image tubes with S_1 cathodes in use or under development and the review paper by Livingstone (1967) gives an excellent description of these tubes. Probably the most perfect of these devices is the image tube of Lallemand, however, this tube has operational disadvantages as discussed by Livingstone. Cascade intensifier tubes are easy to use and although they are not as free from spurious response and distortion as

Lallemand's tube continued development should improve their performance.

For the application considered in this thesis, a suitable tube would be a two stage image intensifier with fibre optic coupling to a photographic plate, as this combination provides sufficient gain to preserve the photon statistics of the initial photocathode.

It is interesting to note from fig 3.4 that for scene contrasts less than 2 percent, the photon noise predominates over the noise level of all practical image tubes with S_1 cathodes. There is little point, therefore, in searching for a very low noise image intensifier for low contrast scenes. Because the noise level of image intensifier tubes is generally less than that of the image converter used in the experimental work, it can be concluded that the performance curves for all other image intensifier tubes with S_1 cathodes lie between curves 1 and 2 on Fig. 3.4.

Much of this thesis is concerned with the determination of the limitations of vidicons due to circuit noise and their limited dynamic range, and the performance expected of vidicons is described in Fig. 3.4 by curves 3 to 8. These curves show that the amount of light required by the vidicon approaches within a factor of 10 the amount required by image tubes for low contrast scenes only if cooled F.E.T. amplifiers are used.

The effects of slow scanning on the vidicon are calculated for two cases, and it is found in the case of a valve amplifier that only a small reduction in light input results, whereas in the case of a cooled F.E.T. amplifier, slow scanning actually increases the light required for a satisfactory image.

It can be concluded that slow scanning is not the best way to increase the integration time, and integrating by a photographic plate should give better results. A point of interest discussed in section 3.3.2 is that cooling the input resistor of a valve amplifier has little effect upon the signal to noise ratio except for low bandwidth systems which restrict the resolution far below the capabilities of the vidicon.

The wavelength of 656 nm is also of interest in solar observations, and curve 6 of Fig. 3.4 describes the flux contrast relations for a visible spectrum vidicon at this wavelength. This curve is in good agreement with the data presented by Weimer (1960) and De Hann (1960) and it provides verification of the validity of the experimental methods used in this work to assess the performance of both the visible and infrared vidicons.

BIBLIOGRAPHY.

Aldous W.H. 1961, Noise in Electron Devices (Chapman and Hall)

Bogner R.E. 1965, Electron. Engng. 444, 115

Cherry E.M. and Hooper, D.E. 1968, Amplifying Devices and Low Pass Amplifier Design. (John Wiley).

Crawford B. 1965, Communications Handbook Part 2 (Texas Instruments)

De Hann E.F. 1960, Adv. Electronics Electron Phys. (Academic Press) 12 291

Elad E and Nakamura M. 1967, University of California, Lawrence Radiation Lab. Report ULC.R.L., 17818.

Elad E. and Nakamura M. 1967, I.E.E.E. Transactions on Nuclear Science, N.S. 14, 1, 523.

Firor J. and Ziron H. 1962, Astrophys.J. 135, 122

Fisher R. 1964, Astrophys. J. 140, 1326

Friss H.T. 1944, Proc. I.R.E. 32, 419.

Gebel R.K.H. 1962, Adv. Electronics Electron Phys. (Academic Press) 16, 451.

Haus H.A. and Adler R.B. 1959, Circuit Theory of Linear Noisy Networks (John Wiley).

Krittman I.M. 1963, I.E.E.E. Transactions on Electron Devices EDlO 6, 404.

Livingstone W.C. 1967, Adv. Electronics Electron Phys. (Academic Press) 23, 347.

Lubszynski H.G. and Wardley J. 1963, I.E.E. Conference Report Series Number 5.

Malherbe A., Tessier M. and Veron S. 1966, Adv. Electronics Electron Phys. 22A, 493.

Montgomery H.C. 1952, Proc. I.R.E. 40, 1461.

North D.O. 1940 R.C.A. Review 4, 441.

Rindfleisch T. and Willingham D. 1966, Adv. Electronics Electron Phys. (Academic Press) 22A, 341.

Rose A. 1963 Concepts in Photoconductivity and Allied Problems (John Wiley).

Rothe H. and Dalke W. 1956, Proc. I.R.E. 44, 811.

Schade O.H. 1962, R.C.A. Electron Tube Division Report EM7752.

Schwartz R.T. and Friedland B. 1965, Linear Systems (McGraw-Hill).

Sevin L.J. 1965, Field Effect Transistors (McGraw-Hill).

Sommers H.S. 1963, J. Appl. Phys. 10, 2923.

Tandberg-Hanssen E., Curtis G.W. and Watson D.K. 1959, Astrophys. J. 126, 260.

Van der Ziel A. 1954, Noise (Prentice-Hall).

1958, Proc. I.R.E. 6, 1019.

1962, Proc. I.R.E. 3, 461.

Van der Ziel A. and Becking A. 1958, Proc. I.R.E. 6, 589.

Weimer P.K. 1960, Adv. Electronics Electron Phys. (Academic Press) 13, 387.